

FUNDAMENTAL STUDIES ON ULTRAFAST CHIRAL AND ACHIRAL SEPARATIONS
IN LIQUID CHROMATOGRAPHY AND SUB/SUPERCRITICAL FLUID
CHROMATOGRAPHY

by

CHANDAN LAXMAN BARHATE

Presented to the Faculty of the Graduate School of
The University of Texas at Arlington in Partial Fulfillment
of the Requirements
for the Degree of

DOCTOR OF PHILOSOPHY

THE UNIVERSITY OF TEXAS AT ARLINGTON

April 2017

Copyright © by Chandan L Barhate 2017

All Rights Reserved



I dedicate this dissertation to my parents, Malati Barhate, Laxman Barhate and my wife

Priyanka Narkhede

Acknowledgements

Looking back four years from now, I remember my determination to pursue doctoral studies in chemistry, which was one of my lifelong passions. In these four years, I encountered many individuals who are responsible for what I am today. I am taking this opportunity to thank them in my thesis. In my graduate work, the take home message is that there is no shortcut to success; hard work and determination are the key to success in life.

My mentor Prof. Daniel Armstrong deserves special thanks for believing in me and providing me an opportunity to work in his group. He is an accomplished scientist and I learned a lot from his courses and his approach towards doing state of the art research. He always welcomed new ideas and provided the best research culture in his laboratory. I appreciate that he was always available for advice. High quality research is not possible without collaboration. I am grateful to Dr. Christopher Welch (Merck), Dr. David Bell (Sigma, Millipore) and Dr. Terry Berger (SFC, Inc.) who provided excellent support in my research. My sincere appreciation is extended to Dr. Erik Regalado and Dr. M. Farooq Wahab of Merck and UTA respectively. It was a very nice experience working with all my co-authors and collaborators. I would like to acknowledge Dr. Umesh Jinwal for his useful educational advices. Ms. Barbara Smith's administrative and timely support was extremely valuable in my research. I also appreciate the constructive advices from my committee members.

My parents owe a special "thank you" who always stood by and encouraged me. Words cannot express my gratitude for all the sacrifices they made for me. My wife Priyanka was always behind me in good and difficult times. I appreciate her patience and support. My research would not have been possible if she were not present in my life. I will not forget the support from my sisters, Seema Mahajan and Deepa Waykole and brother-in-

laws Rajesh Mahajan and Hukumchand Waykole. Finally my dear friends Rahul Patil, Mohsen Talebi, Dyaneshwar Patil, Piyush Parkhey, Kumar Abhishek, Jayant Salvi, Siddharth Mistry and Avinash Veer will always be in my good memories and prayers.

April 17th ,2017

Chandan L. Barhate

ABSTRACT

FUNDAMENTAL STUDIES ON ULTRAFAST CHIRAL AND ACHIRAL SEPARATIONS IN LIQUID CHROMATOGRAPHY AND SUB/SUPERCRITICAL FLUID CHROMATOGRAPHY

Chandan L. Barhate, PhD

The University Of Texas at Arlington, 2017

Supervising Professor: Daniel W. Armstrong

This thesis is based on fundamental contributions in the field of ultrafast chiral and achiral separations using liquid and sub/supercritical fluid chromatography. The high efficiency sub-2 μm particles of narrow particle size distribution (NPSD) and 2.7 μm superficially porous particles (SPP) were used as a support for bonding various chiral selectors. The chiral selectors used in this thesis are teicoplanin (T), teicoplanin aglycone (TAG) and vancomycin (V) cyclofructan-6 derivatized isopropyl carbamate (CF6-P), cyclofructan-7 dimethylphenyl carbamate (CF7-DMP), tert-butyl carbomoylated quinine and hydroxypropyl- β cyclodextrin (HPRSP) . These high efficiency particles were packed in 0.5, 2.0, 3.0 and 5 cm long columns

As we enter the ultrafast chromatography regime various interesting phenomena manifest themselves which are usually not observed in routine chromatography. State of the art UHPLCs were shown to be insufficient for the narrow peaks obtained in the ultrafast chromatography in terms of extra-column volumes. Optimized instruments with reduced extra column volume, highest possible sampling frequencies and optimum digital filters were needed to preserve the "true" peak shape. Using short columns, chiral, achiral and shape selective separations were demonstrated in the sub-second to sub-minute range. Frictional heating was shown to be beneficial for both SPP and NPSD particles in chiral chromatography, unlike reversed phase chromatography. Additionally the instrumental idiosyncrasies of SFC are discussed such as the connection tubing diameter effect, noise

analysis of backpressure regulator and peak shape analysis (upsampling effects on peak shapes).

Real world applications of pharmaceuticals and intermediates were developed for reverse phase liquid chromatography (RPLC) and SFC mode for 50 compounds belonging to various classes. This research culminated by exploring two dimensional liquid chromatography (2D-LC). Multiple achiral × chiral and chiral × chiral 2D-LC examples (single and multiple heart-cutting, high-resolution sampling, and comprehensive) using ultrafast chiral chromatography in the second dimension were successfully applied to the separation and analysis of complex mixtures of closely related pharmaceuticals and synthetic intermediates, including chiral, achiral drugs, metabolites, constitutional isomers, stereoisomers, and organohalogenated species.

Table of Contents	
Acknowledgements.....	iv
Abstract.....	vi
Table of Contents.....	viii
List of Illustrations.....	xiii
List of Tables.....	xvii
Chapter	
1. Introduction	1
1.1 Ultrafast chromatography for high throughput analysis.....	1
1.2 Resolution equation	1
1.2.1 Approaches for enhancing separation efficiency in packed beds.....	2
1.2.2 Tuning selectivity of chromatographic support	3
1.3 Two dimensional liquid chromatography (2D-LC).....	5
1.4 Organization of dissertation	7
2. Gone in Seconds: Praxis, Performance, and Peculiarities of Ultrafast Chiral Liquid Chromatography with Superficially Porous Particles	8
2.1 Abstract.....	8
2.2 Introduction.....	8
2.3 Experimental.....	11
2.3.1 Materials	12
2.3.2 synthesis of stationary phases	12
2.3.3 Instrumentation	12
2.3.4 Axial Temperature gradient in mobile viscous frictional heating	13

2.4 Discussion	13
2.4.1 Effect of packing on columns used for ultrafast chiral LC ...	18
2.4.2 Detector sampling rates and response times	23
2.4.3 Extra column band broadening effects on ultrafast separations	25
2.4.3 Kinetic and thermal (frictional) considerations.	27
2.5 Conclusions	33
3. Ultrafast separation of fluorinated and desfluorinated pharmaceuticals using highly efficient and selective chiral selectors bonded to superficially porous particles	35
3.1 Abstract	35
3.2 Introduction	35
3.3 Reagents and materials	38
3.4 Instrumentation	38
3.5 Result and discussion	39
3.5.1 Performance comparison of different SPP bonded CSPs for separation of fluoro and desfluoro analogues	42
3.5.2 Optimization of separation factor	46
3.5.3 HPLC-ESI-MS studies	47
3.6 Conclusions	49
4. High efficiency, narrow particle size distribution, sub-2 μm based macrocyclic glycopeptide chiral stationary phases in HPLC and SFC	51
4.1 Abstract	51
4.2 Introduction	52
4.3 Experimental	54
4.3.1 Reagents and materials	54

4.3.2	Synthesis of stationary phases	55
4.3.2	UHPLC and SFC instrumentation	56
4.3.3	Measurement of axial temperature gradient	57
4.4	Results and discussion	57
4.4.1	Synthesis and loading	58
4.4.2	Observations on slurry packing sub 2- μ m particles	59
4.4.3	Performance comparison of different particle type CSPs	61
4.4.4	Applications of macrocyclic glycopeptide bonded 1.9 μ m NPSD particle based CSPs for rapid chiral separations in liquid chromatography	62
4.4.5	van Deemter analysis of sub 2- μ m CSPs	67
4.4.6	Supercritical fluid chromatography applications	71
4.6	Conclusions	73
5.	Instrumental Idiosyncrasies Affecting the Performance of Ultrafast Chiral and Achiral Sub/Supercritical Fluid Chromatography	75
5.1	Abstract	75
5.2	Introduction	76
5.3	Experimental section	78
5.4	Results and discussion	80
5.4.1	Representative ultrafast enantiomeric separation and instrument comparison	80
5.4.2	Ramification of the choice of connection tubings ultrafst SFC	84
5.4.3	Impact of backpressure regulator settings on ultrafast SFC chromatograms	89
5.4.4	Ultrafast peak shapes and the choice of digital filters in SFC	92

5.4.5 not all "Identical" sampling frequencies are created equal.....	94
5.5 Conclusion	97
6. Salient Sub-Second Separations	99
6.1 Abstract	99
6.2 Introduction	99
6.3 Experimental section	101
6.3.1 Materials.....	101
6.3.2 Stationary Phases	101
6.3.3 instrumentation	102
6.4 Results and Discussion	103
6.4.1 Preparation and characterization of short 0.5 cm x 0.46 cm i.d columns	104
6.4.2 Is the sampling frequency available for sub-second chromatography?	105
6.4.3 Hardware considerations in Sub-second chromatography	105
6.4.4 examples of Sub-second chromatography	107
7. Ultrafast chiral separations for high throughput enantiopurity analysis	114
7.1 Abstract	114
7.2 Introduction	114
7.3 experimental section	115
7.3.1 instruments	115
7.4 Results and disucssion	119
7.5 Conclusions	134
8. Ultrafast Chiral Chromatography as the Second Dimension in Two-Dimensional Liquid Chromatography Experiments	136

8.1 Abstract	136
8.2 Introduction	136
8.3 Experimental section	139
8.3.1 Instrumentation	139
8.3.2 Chemical and reagents	140
8.3.3 Stationary phases	140
8.3.3.1 Achiral	140
8.3.3.2 Chiral	141
8.4 Results and discussion	141
8.5 Conclusions	157
Chapter 9	158

List of Illustrations

Figure

1.1 Structures of chiral selectors utilized in this work.....	5
1.2 Schematics of one dimensional (1D) and two-dimensional liquid chromatography (2D-LC).	6
2.1 Enantiomeric separations of BINAM on CF6-P bonded to SPPs and FPPs	14
2.2 Representative ultrafast enantiomeric separations on each of 6 chiral stationary phases	17
2.3 Effect of detector sampling rate and response time on efficiency (N) and resolution (R_s) in ultrafast chromatographic separations	25
2.4 Optimization of Agilent 1290 UHPLC for ultrafast separations by replacing stock parts with low extra column volume alternatives	26
2.5 van Deemter plots for chiral and achiral analytes in polar organic mode, normal phase, and reversed phase on 2.7 μ m SPP CSPs	28
3.1 Performance comparison of SPP bonded selectors with commercially available columns	40
3.2 Constant mobile phase and retention time comparison of ciprofloxacin and desfluoro ciprofloxacin	41
3.3 Ultrafast separation of ezetimibe, ciprofloxacin, ofloxacin and their desfluoro analogues	44
3.4 Ultrafast separation of voriconazole and desfluoro voriconazole	46
3.5 HPLC-ESI MS of (A) ezetimibe and desfluoroezetimibe, (B) voriconazole and desfluorovoriconazole	49

4.1 Enantiomeric separation of propranolol, thalidomide and 5, 5-diphenyl-4 methyl-2-oxazolidone using constant mobile phase conditions on teicoplanin, vancomycin and teicoplanin aglycone bonded phases	62
4.2 Examples of ultrafast chiral separations on UHPLC (50 mm × 4.6 mm ID columns) with teicoplanin, vancomycin and teicoplanin aglycone bonded phases	66
4.3 Enantiomeric separation of propranolol using teicoplanin bonded phase	66
4.4 UHPLC van Deemter curves of 50 mm × 4.6 mm ID teicoplanin bonded columns packed with particles of different sizes	67
4.5 van Deemter plots for chiral analytes in polar organic and reversed phase mode on 1.9 µm- NPSD V and 1.9 µm NPSD T	70
4.6 Examples of ultrafast chiral separations on SFC teicoplanin and teicoplanin aglycone bonded phases	72
4.7 SFC van Deemter curves for the 50 mm × 4.6 mm ID teicoplanin bonded columns packed with particles of different sizes	73
5.1 Representative ultrafast chiral separations on SFC. Column: Teicoplanin bonded 1.9 µm NPSD silica	81
5.2. Enantiomeric separation of cis-4,5 diphenyl-2-oxazolidinone on optimized Jasco and Agilent SFC systems	84
5.3. Comparison of efficiencies for achiral (1,3 dinitrobenzene) and chiral probes (3-phenylphthalide) as a function of the tubing internal diameters	86
5.4 van Deemter curves of the first eluting enantiomer of 3-phenylphthalide. Column: 5 × 0.46 cm i.d.; teicoplanin bonded 1.9 µm NPSD silica	89
5.5 Effect of backpressure regulator setting on the dead time, retention time, and baseline noise in ultrafast SFC	92
5.6 Comparison of digital filters in Jasco SFC for a chiral probe (3-phenylphthalide)	94

5.7 Assessment of peak shapes on two detectors used in SFC (UV 2075 and XLC 3070 UV)	95
6.1. Computer simulation of a sub-second separation with RMS noise of ± 0.06 under a second in (A) time domain, (B) frequency domain via Fourier analysis	105
6.2. Demonstration of effect of extra column effect originating from short connection tubing	107
6.3. Sub-second chromatography on various stationary phases using 0.5×0.46 cm i.d. columns	108
6.4 Application of power transforms in sub-second chromatography of three components	112
7.1 Structures of 50 pharmaceuticals and intermediates	121
7.2 Scoring system. (a) Chiral RP-LC screening of 50 enantiomeric mixtures. (b) Chiral SFC screening of 50 enantiomeric mixtures	124
7.3 Ultrafast chiral separations of all mixtures by RP-LC (a) and SFC (b).	130
7.4 MISER chiral SFC for high-throughput enantiopurity analysis of an alcohol obtained from a ketone via enzymatic catalysis	132
8.1 Multiple heart-cutting 2D-LC analysis of warfarin and hydroxywarfarin stereoisomers	142
8.2 Optimization of loop filling (%) and column length in the second dimension for the separation of warfarin and hydroxywarfarin stereoisomers	146
8.3. (a) Comprehensive chiral \times chiral 2D-LC method for complete resolution of isomers of a synthetic intermediate	151
8.4. Single heart-cutting 2D-LC method for separation of complex mixture of closely related stereoisomers from an anti-HCV therapeutic	153

8.5. Multiple heart-cutting 2D-LC method for separation of complex mixture of fluorophenylacetic acid isomers	155
---	-----

List of Tables

2.1. Comparison of Theoretical Plates/Meter (N/m), Reduced Plate Height (h), and USP Tailing Factor Using a Standard Achiral Probe 1,3-Dinitrobenzene	16
2.2. Chromatographic Data for Optimized Ultrafast Chiral Separations on Six Different Chiral Stationary Phases (CSP) Bonded to 2.7 μm Superficially Porous Particles ..	18
3.1 Ultrafast separation of desfluoro impurities	45
3.2 Optimized separation factors of fluoro and desfluoro compounds	47
4.1. Physical and chemical characteristics of the silica particles used in this work	57
4.2 Fast chiral separations on 1.9 mm NPSD based columns.	63
4.3 Longitudinal temperature gradient as a function of flow rate.	69
5.1 Ultrafast chiral separations on 1.9 μm NPSD based columns	82
6.1 Sub-Second Screening for Achiral, Chiral in Various Chromatographic Modes	109
7.1 Chromatographic columns used for chiral screening	122
7.2 Estimation of fast chromatographic separation from selected screening conditions.....	125
7.3 Detailed chromatographic conditions of ultrafast chiral RP-LC methods	126
7.4 Detailed chromatographic conditions of ultrafast chiral SFC methods	128
7.5 Results from enzymatic catalysis screening by MISER chiral SFC	133

8.1 Repeatability of retention times, peak areas and R_s values for the 2D-LC method shown in figure 8.1	144
8.2 Injection, Column Volume Percent Loop Filled in Volume Units	145
8.3 R_s values and repeatability of injections of warfarin, 6 and 8-hydroxywarfarins on 2 and 5 cm chiral columns at different sampling time and loop filling % in the second dimension	148
8.4 Repeatability of retention times, peak areas and R_s values for the 2D-LC method shown in figure 8.3	150
8.5 Repeatability of retention times, peak areas and R_s values for the 2D-LC method shown in figure 8.4	151
8.5. Multiple heart-cutting 2D-LC method for separation of complex mixture of fluorophenylacetic acid isomers	154
8.6 Repeatability of retention times, peak areas and R_s values for the 2D-LC method shown in figure 8.5	156

Chapter 1

Introduction

1.1 Ultrafast chromatography for high throughput analysis

More than four decades ago, Csaba Horvath expressed the value of fast chromatography by showing separation of four ribonucleosides in four minutes using a 151.7 x 0.1 mm i.d. column packed with pellicular particles.¹ Since then, separation scientists have made constant efforts in improving the speed of chromatographic analysis. Tremendous improvements in reverse phase achiral chromatography have been made where separating more than 7 compounds under 24 s have become a routine.² Given the fact that more than 90 % of the drugs contain chiral mixtures, there is a need to come up with reliable high speed analytical procedures. Additionally, enantiomeric analysis is often required to support stereochemical research in synthetic chemistry and bioanalytical research.³ The focus of this thesis is to overcome speed limitations in chiral and achiral chromatography guided by the fundamental understanding of chromatographic principles.

1.2 The Resolution Equation

The fundamental resolution equation serves as a guideline in any mode of chromatography.⁴

$$R_s = \left(\frac{\sqrt{N}}{4}\right) \left(\frac{\alpha - 1}{\alpha}\right) \left(\frac{k_2}{1 + k_2}\right) \quad (1)$$

Where R_s is the resolution between the critical pair, N is the peak efficiency, k is the retention factor and α is the selectivity of the two analytes on a given stationary phase. As can be seen from eq. 1, the chromatographic resolution is dependent on three factors namely, efficiency, selectivity, and the retention factor of the analytes. In

order to obtain the same resolution for a rapid separation we need to increase the N while maintaining the same or better selectivity.

1.2.1 Approaches for enhancing separation efficiency in packed beds

The chromatographic efficiency (N) can be defined as given in equation 2

$$N = \left(\frac{t_r}{\sigma}\right)^2 \quad (2)$$

Where t_r is retention time and σ is the standard deviation in time. It can be shown that at the van Deemter minimum the efficiency is inversely proportional to the particle diameter. A direct consequence of this relationship is that smaller particles are required for maintaining the same efficiency of a long column packed with traditional 5 μm particles. These particles will serve as a support for bonding the chiral selectors. One of the interesting unsettled debates in high efficiency chromatography is the role of particle size distribution (PSD) of the packing material. Four decades ago, Halasz was of the opinion that the width of sieve fraction of silica does not affect the chromatographic efficiency as long as the deviation from the arithmetic mean is smaller than 40%.⁵ This was an empirical observation with large diameter particles (50-200 μm).⁵ On the other hand, Desmet showed a linear correlation between the standard deviation of the particle diameter and reduced plate height with <5 μm FPPs.⁶ This question was investigated theoretically and experimentally by Gritti et al. using the recently introduced 1.9 μm narrow particle size distribution fully porous silica (FPP) particles, which are commercially available under the trade name of Titan (Supelco).^{7,8} These silica particles have a narrow particle size distribution (e.g. <10% RSD) and the column efficiencies are unusually high; for instance, producing an intrinsic reduced plate height of 1.7 in narrow bore columns, such narrow diameters known to pose challenges during the slurry packing process.⁷ All previous studies on the effect of particle size distribution and the use of Titan silica have only

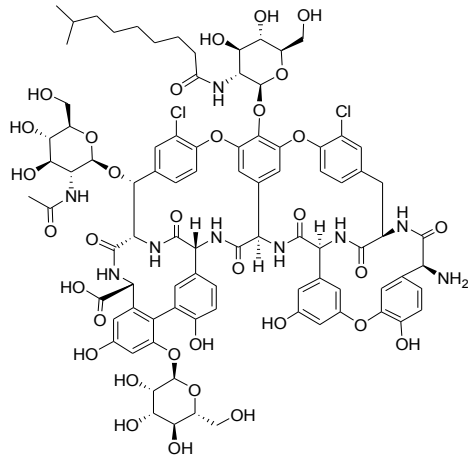
considered achiral (C-18) stationary phases. Besides, FPP silica supports, the emerging superficially porous particles (SPPs) were proven to produce highly efficient, i.e. over 200,000 plates/m, chiral columns with a variety of brush type chiral selectors including macrocyclic glycopeptides.

1.2.2 Tuning selectivity of chromatographic supports

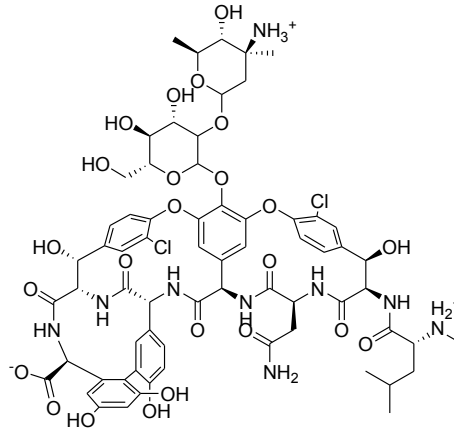
Selectivity (α) in chromatography can be defined in as

$$\alpha = \frac{k_2}{k_1} \quad (3)$$

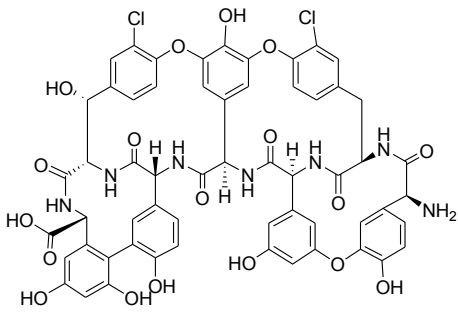
It is the ratio of the retention factors for two chromatographic peaks. In 1994 macrocyclic antibiotics (glycopeptides) were developed as versatile stationary phases for acidic, basic and neutral chiral molecules.⁹ The hydrolytically stable macrocyclic bonded phases could be used in the normal phase, reverse phase and polar organic modes, and with SFC to produce baseline separations of a wide variety of compounds.¹⁰ Today the majority of all enantioselective separations of amino acid and small peptide analytes are done on columns that employ either a teicoplanin or teicoplanin aglycone (TAG) based chiral selectors.¹¹ In 2009, new chiral selectors known as cyclofructans were introduced.¹² One of the advantages of these chiral selector molecules when immobilized on silica is that not only can they separate enantiomers but they also produce superior separations for some achiral molecules.¹³⁻¹⁵ In this work a variety of chiral selectors as shown in Figure 1.1, were bonded to perform high efficiency chiral and achiral separations.



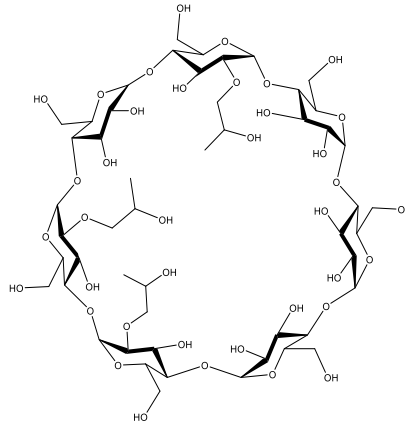
a) Teicoplanin



b) Vancomycin



c) Teicoplanin aglycone



d) Hydroxypropyl- β -cyclodextrin

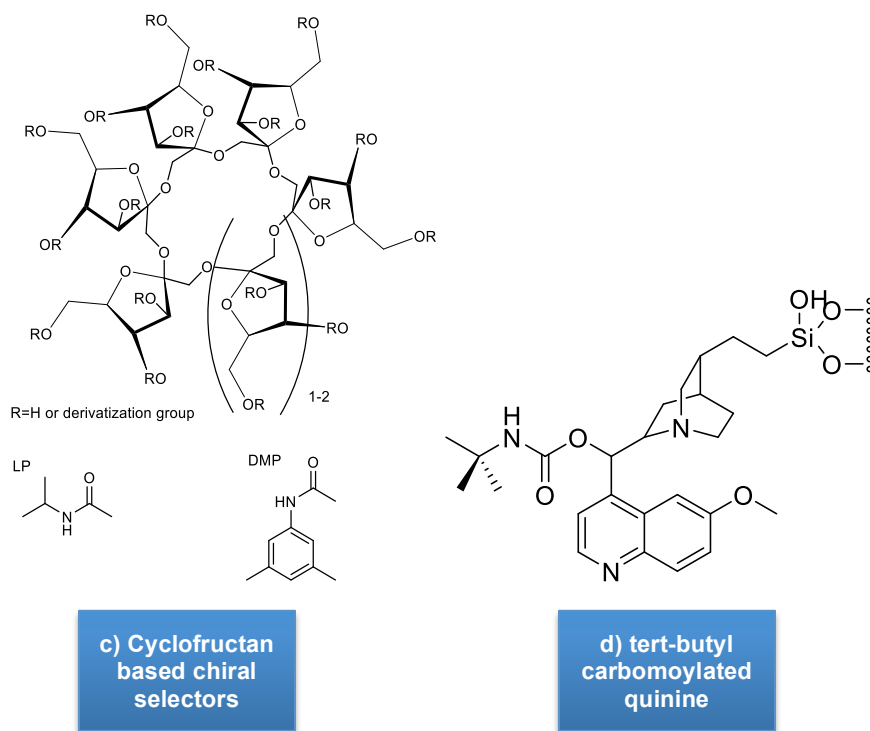


Figure 1.1 Structures of chiral selectors utilized in this work

1.3 Two dimensional liquid chromatography (2D-LC)

The chromatographic separation of complex mixtures and closely related species is one of the most difficult tasks in pharmaceutical and biomedical research. The chromatographic efficiency of existing columns is not adequate to handle such complex mixtures. Figure 1.2 compares the schematic differences of between standard HPLC and a two-dimensional set up. The main differences are the utilization of two pumps, two columns and two detectors and associated sample storage valves. It is preferred that the selectivities of two columns be orthogonal to utilize most of the space available in two dimensions. Complex separations can be performed in one dimensions where the peak capacities increase either as (n_1+n_2)

in heart cut and $n1 \times n2$ in comprehensive 2D-LC), where n is the peak capacity.^{16,17} Recent years have seen a rapid growth in the use of multidimensional chromatography for the study of complex mixtures, with two-dimensional (2D) chromatography is emerging as a valuable tool for pharmaceutical, biomedical research, and other disciplines.¹⁸⁻²⁵

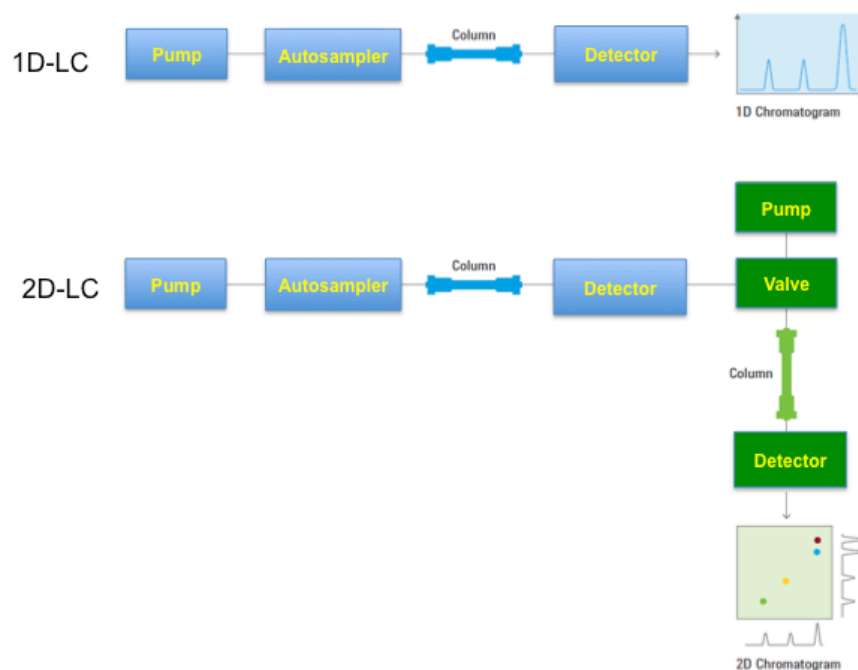


Figure 1.2 Schematics of one dimensional (1D) and two dimensional liquid chromatography (2D-LC)

Achiral–chiral two-dimensional chromatographic analysis has been known for decades; for example, enantioselective bioanalysis from the 1980s often employed column switching, where serum proteins or other interfering components are removed by a first-dimension separation, with a heart cut of the desired component of interest passing to a second-dimension separation employing a chiral stationary phase (CSP) column. However, the relatively slow speed of chiral separations has

limited the use of chiral stationary phases (CSPs) as the second dimension in 2D-LC, especially in the comprehensive mode. Herein we report an investigation into the use of ultrafast chiral chromatography as a second dimension for 2D chromatographic separations.

1.4 Organization of Dissertation

This dissertation focuses primarily on fundamental studies of ultrafast chiral and achiral separations in UHPLC, 2D-LC and SFC. Chapter 2 addresses the synthesis of superficially porous particle based chiral stationary phases and some theoretical aspects ultrafast chiral separations. Chapter 3 addresses the application of SPPs based chiral columns for ultrafast separations of pharmaceutically important compounds with very similar structures, namely fluoro and desfluoro analogs. Chapter 4 is based on systematic studies on the synthesis and packing studies of high efficiency, narrow particle size distribution chiral columns and their applications. In Chapter 5 we examine SFC ultrafast chiral separations, and explain the counterintuitive effects of connection tubings and the nature digital filters in SFC. Chapter 6 is based on separations in the sub-second regime. Practical and theoretical challenges of very fast chromatography will be addressed. In chapter 7, real life applications of ultrafast enantioseparations with important pharmaceuticals and synthetic intermediates are shown. Chapter 8 is based on the analysis of complex mixtures and closely related species by two-dimensional liquid chromatography using ultrafast methods in the second dimension. Chapter 9 concludes the thesis with a summary and future outlook.

Chapter 2

Gone in Seconds: Praxis, Performance, and Peculiarities of Ultrafast Chiral Liquid Chromatography with Superficially Porous Particles

2.1 Abstract

A variety of brush-type chiral stationary phases (CSPs) were developed using superficially porous particles (SPPs). Given their high efficiencies and relatively low backpressures, columns containing these particles were particularly advantageous for ultrafast “chiral” separations in the 4–40 s range. Further, they were used in all mobile phase modes and with high flow rates and pressures to separate over 60 pairs of enantiomers. When operating under these conditions, both instrumentation and column packing must be modified or optimized so as not to limit separation performance and quality. Further, frictional heating results in axial thermal gradients of up to 16 °C and radial temperature gradients up to 8 °C, which can produce interesting secondary effects in enantiomeric separations. It is shown that the kinetic behavior of various CSPs can differ from one another as much as they differ from the well-studied C18 reversed phase media. Three additional interesting aspects of this work are (a) the first kinetic evidence of two different chiral recognition mechanisms, (b) a demonstration of increased efficiencies at higher flow rates for specific separations, and (c) the lowest reduced plate height yet reported for a CSP.

2.2 Introduction

For much of 3 decades, the development and study of chromatographic enantiomeric separations have been dominated by investigations focused on selectivity. This is not surprising given the unique position of chiral separations in chromatography where conventional strategies used for all other molecules are completely ineffective for enantiomers. Hence, the highest impact studies involved conceiving, understanding, and

optimizing the use of new and better chiral selectors.^{12,26-44} Numerous thermodynamic and mechanistic studies as well as evaluations of solvent and additive effects continue even today.^{11,45-47} As the field of “chiral separations” has matured, it has focused on other, more typical chromatographic concerns including speed, efficiency, and kinetic effects. While “chiral separations” are ultimately affected by the same parameters as achiral separations, they can have some idiosyncrasies (*vide infra*) as compared to the most extensively studied systems which typically involve reversed phase liquid chromatography on C18 or analogous stationary phases. The demand for fast and efficient achiral separations provided the impetus for researchers to explore new avenues to increase throughput of chiral screening and analysis. Welch et al. first used multiparallel chiral screening and method development systems that provided method development times of ~1 h.⁴⁸ Hamman et al. used supercritical fluid chromatography (SFC) at high flow rates, short columns, and a gradient to obtain a 2.5 min screening method.⁴⁹ Shortly after, Ai and co-workers developed a bonded sub-1 μm mesoporous silica based cyclodextrin chiral column and published a few 1–6 min enantiomeric separations.⁵⁰ Concurrently, Gasparrini et al. studied a bonded brush-type (π -complex) phase using sub-2 μm fully porous particles (FPPs) and demonstrated a few normal phase enantiomeric separations in the 15–40 s range.⁵¹⁻⁵³ More recently, superficially porous particles (SPPs) for achiral separations have allowed for column efficiencies comparable to sub-2 μm FPPs while using conventional HPLCs and column hardware.^{54,55} There have been numerous empirical and theoretical comparisons of these approaches when used in a reversed phase (C18) format.⁵⁶⁻⁵⁸ SPPs are able to decrease all contributions to band broadening (i.e., longitudinal diffusion, eddy dispersion, and stationary phase mass transfer contributions).⁵⁸ Initially it was thought that better packing of SPPs was due to their having narrower particle size distributions than FPPs, but it was

later shown that better packing homogeneity across the column (i.e., from wall to center of the bed) is largely responsible for the decreased eddy dispersion contribution.^{59,60} Since, SPP columns are generally better packed than FPP columns, they can yield reduced plate heights of 1.3–1.5 for columns packed with conventional achiral stationary phases, whereas FPP based columns typically have reduced plate heights greater than 2.0.⁵⁶ Also, the shell thickness of SPPs leads to a shorter trans-particle path length which can decrease mass transfer contributions to band broadening for large molecules with small diffusion coefficients and smaller molecules that have slow adsorption– desorption kinetics.^{54,61,62} This is particularly important at higher flow rates. The possible benefits of SPPs in other important but more specialized areas of LC are less explored. Chankvetadze compared a polysaccharide based chiral selector coated on FPPs and SPPs in both nano-LC and HPLC.^{63,64} In the latter, an obvious decrease in enantiomeric selectivity was noted for the SPP based material. Gritti and Guiochon's theoretical treatment of the same polysaccharide based chiral selector indicated that a 10% gain in resolution (R_s) could be possible due to the decreased plate heights afforded by the SPPs.⁶⁵ However, this estimated value was based on an assumption that the SPP based polysaccharide column would have a similar enantiomeric selectivity value as the analogous FPP based column which, as noted, has not been obtainable to date. Most recently, Spudeit et al. presented the first successful and practical SPP CSP.⁶² This work showed that brush-type chiral selectors (i.e., isopropylcarbamated cyclofructan 6) have a higher chiral selector load (per surface area). This plus the observed increase in column efficiency for the SPP based CSP resulted in improved enantiomeric separations, while maintaining the same enantiomeric selectivity as FPP based CSPs.⁶² Further, the SPP CSP maintained this performance with 50– 75% lower retentions. When comparing constant retention modes, the R_s values obtained using the SPP column were far greater

than the FPP columns. It was also noted that as flow rates increased (e.g., to 3 mL/min), the resolution per analysis time greatly improved for the SPP column (by 18–67%) meaning that high-throughput screening would benefit from such columns.⁶² In this work, a broad range of analyte types and polarities including pharmaceuticals, catalysts, peptides, amino acids, primary amines, and biaryls among others were baseline separated on a variety of SPP brush type CSPs that are very effective for ultrafast chiral separations (~4–40 s range). It is demonstrated that they can be performed in any mobile phase conditions or mode, i.e., reversed phase, normal phase, polar organic, and HILIC. Finally, the practice of ultrafast chiral LC often produces interesting and unusual consequences that must be recognized, dealt with, and/or properly understood for optimal performance.

2.3 Experimental

2.3.1 Materials

All HPLC solvents and reagents for reactions were purchased from Sigma-Aldrich (St. Louis, MO). Cyclo- fructan-6 (CF6) and cyclofructan-7 (CF7) derivatized with isopropyl carbamate and dimethylphenyl carbamate groups, respectively, were synthesized by AZYP LLC (Arlington, TX). The 2.7 μm superficially porous silica particles with a surface area of 120 m^2/g and pore size of 120 \AA were provided by Agilent Technologies (Wilmington, DE). The core is 1.7 μm in diameter and the surrounding shell thickness is 0.5 μm . The fully porous 2.1 and 3 μm silica particles were purchased from Daiso (Tokyo, Japan) and Glantreo (Cork, Ireland), respectively. The 2.1 μm fully porous particles have a surface area of 479 m^2/g and pore size of 91 \AA , whereas the 3 μm fully porous particles have a surface area of 300 m^2/g and pore size of 100 \AA . Tröger's bases were obtained as indicated in the literature.⁶⁶ All solvent mixtures are given in (v/v).

2.3.2 Synthesis of Stationary Phases.

All reactions were carried out in anhydrous solvents under a dry argon atmosphere. The synthetic procedures for the six stationary phases employed in this work have already been published.^{12,32,38,41,67} The first chiral stationary phases explored were cyclofructan based as they have recently proven to be unique chiral selectors.^{12,68-73} The cyclofructan-6 derivatized isopropyl carbamate (CF6-P) and cyclofructan-7 dimethyl-phenyl carbamate (CF7-DMP) were bonded to silica particles under anhydrous conditions as described previously.¹² The 2-hydroxypropyl- β -cyclodextrin bonded silica (CD-HP) was synthesized via a proprietary bonding procedure.^{32,67} Macro-cyclic antibiotics vancomycin, teicoplanin, and teicoplanin aglycone were covalently attached to silica surface as described by Armstrong et al.^{38,41} Each of the above chiral selectors were bonded to 2.7 μm SPPs. The 2.1 and 3 μm fully porous particles were functionalized with CF6-P.

Each stationary phase was slurry packed with a pneumatically driven Haskel pump (DSTV-122) into 10 cm \times 0.46 cm i.d., 5 cm \times 0.46 cm i.d., and 3 cm \times 0.46 cm i.d. stainless steel columns (IDEX Health and Science, Oak Harbor, WA). Commercial LARIHC CF6-P, LARIHC CF7-DMP, Chirobiotic V, Chirobiotic T, Chirobiotic TAG, and Cyclobond I 2000 HP-RSP columns (fully porous 5 μm particles, 25 cm \times 0.46 cm i.d.) which were used for comparative purposes were provided by AZYP LLC, Astec, and Supelco/Sigma-Aldrich.

2.3.3 Instrumentation

All ultrafast separations were performed on an Agilent 1290 Infinity series UHPLC system (Agilent Technologies, Santa Clara, CA) equipped with a quaternary pump, an auto-sampler, and a diode array detector. Routine separations were performed on an Agilent 1260 HPLC equipped with a quaternary pump, an auto-sampler, and a diode array detector. An inlet filter was installed between the pump outlet and the auto-sampler

injection valve to prevent clogging of 75 μm tubings. For fast separations, the data collection rate was set at 160 Hz with a response time of 0.016 s, unless otherwise stated. The thermostated column compartment and the column switching 6-port valve were bypassed to minimize the length of connection tubings. The instrument was further optimized to reduce extra-column effects by using an ultralow dispersion kit from Agilent (P/N 5067-5189). The kit consists of an ultralow dispersion needle and needle seat, two 75 μm i.d. stainless steel connection tubings, and a detector flow cell with a volume standard deviation $V(\sigma)$ of 0.6 μL . Alternatively, 75 μm i.d. polyether ether ketone (PEEK) nanoViper connection tubings (Thermo Fisher Scientific, MA) were also employed. The instrument was controlled by OpenLAB CDS ChemStation software (Rev. C.01.06 [61], Agilent Technologies 2001–2014) in Microsoft Windows 8.1 (see the Supporting Information for the calculation of peak parameters). The reported percentages of mobile phases (m.p.) are listed as volume/volume (v/v).

2.3.4 Axial Temperature Gradient in Mobile Viscous Frictional Heating.

The effect of viscous frictional heating of the mobile phases in the SPP columns was studied by wrapping the column in an insulating sheet (at room temperature) and inserting a Mastech thermocouple MS8222H (Pittsburgh, PA) inside the column outlet with the help of a screw cap. The flow rate was varied and the resulting temperature was monitored after 10 min of equilibration.

2.4 Discussion

Figure 1A provides comparisons of different particle size fully porous particles (FPPs) and superficially porous particles (SPPs) which have the same bonded chiral selector (via the same chemistry) and with the same mobile phase.

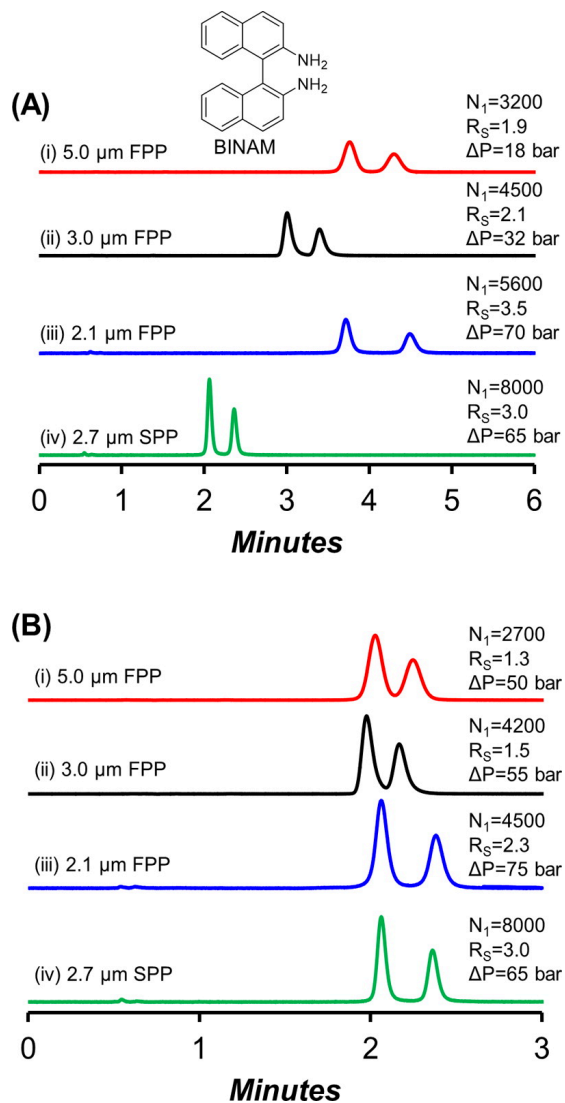


Figure 2.1 Enantiomeric separations of BINAM on CF6-P bonded to SPPs and FPPs at 1.0 mL/min, $T_{col} = 25\text{ }^{\circ}\text{C}$. All columns were 5 cm \times 0.46 cm in dimensions. (A) Constant MP mode, MP = 92:8 heptane-ethanol. (B) Constant retention mode, MP = (i) 82:18 heptane-ethanol, (ii) 85:15 heptane-ethanol, (iii) 82:18 heptane-ethanol, and (iv) 92:8 heptane-ethanol.

These chromatograms were generated using conventional HPLCs with conventional

conditions and column sizes (i.e., 1.0 mL/min flow rate and 5 cm × 0.46 cm i.d. columns). Clearly using the same mobile phase, the SPP-based CSP provided both the greatest efficiency and shortest analysis time as compared to all FPPs, including the 2.1 μm particles (Figure 2.1A). However, according to Gritti and Guiochon, a better comparison of such columns is realized when resolutions (R_S) are compared at constant retention (Figure 2.1B).⁶⁵ They also indicated that a SPP's core to particle diameter ratio (ρ) can be related to its gain in resolution. Specifically ρ values between 0.5 and 0.95 at constant retention factor (k) can slightly improve the resolution. Interestingly, recent work on a brush-type CSP showed a resolution increase of 20%.⁶² In Figure 1B, the increase in resolution of the SPP-CSP over both 3 and 2.1 μm FPPs is ~30%, which is quite impressive. The SPP-CSP used here had a ρ value of 0.63 (see Experimental Section), which is within the optimal range (vide supra).⁶⁵ A direct comparison of the efficiencies, reduced plate heights, and tailing factors of current commercial columns (5 μm particles) and the analogous CSPs on 2.7 μm SPPs is given in Table 1. The 3– 4 fold increase in efficiencies is impressive but not totally unexpected given the smaller SPP particle diameter. However, the reduced plate heights of the SPPs also are up to 2 times smaller and with comparable or better peak symmetries. The reduced plate height (h) of 1.6 for the CF7-DMP SPP is the smallest reported for any CSP on any particle to date. Given these results, it is clear that SPP based CSPs should be particularly advantageous for ultrafast chiral separations.

Table 2.1. Comparison of Theoretical Plates/Meter (N/m), Reduced Plate Height (h), and USP Tailing Factor Using a Standard Achiral Probe 1,3-Dinitrobenzene with 70:30 Heptane–Ethanol at Reduced Velocity of 4.5 (1 mL/min for 2.7 μm SPP, 0.6 mL/min for 5 μm FPP)

Stationary phase	N/m ^a	h	Tailing factor ^b
<i>Stationary phases bonded to 2.7 μm SPP</i>			
CF6-P ^c	172,000	2.2	1.1
CF7-DMP ^d	221,000	1.6	1.2
teicoplanin ^d	165,000	2.3	1.0
teicoplanin aglycone ^c	133,000	2.8	1.3
vancomycin ^d	173,000	2.1	0.9
hydroxypropyl-β-cyclodextrin ^d	181,000	2.0	1.4
<i>Commercial columns packed with 5.0 μm FPP (25 x 0.46 cm)</i>			
LARIHC CF6-P	70,000	2.9	1.1
LARIHC CF7-DMP	59,000	3.4	1.2
Chirobiotic-T	54,000	3.7	0.9
Chirobiotic-TAG	50,000	4.0	1.1
Chirobiotic-V	57,000	3.5	0.9
Cyclobond I 2000 HP-RSP	37,000	5.4	1.1

^a N/m calculated by half height method. ^b USP tailing factor $T = W_{0.05} / 2f$, where $W_{0.05}$ = peak width at 5% peak height and f = distance from the leading edge of the peak to the peak maximum at 5% peak height. ^c Dimensions of these columns were 10 cm × 0.46 cm. ^d Dimensions of these columns were 5 cm × 0.46 cm.

In the literature, the current accepted time limit for being labeled as an ultrafast chromatographic separation seems to be ~1 min.^{74,75} This is probably a reasonable choice since typical HPLC autoinjectors cycle at ~1 injection per min (or down to 0.5 min for UHPLC). Hence in ultrafast LC, the chromatographic separations can be completed more quickly than new samples can be injected (by conventional injection devices). Figure 2.1 and Table 2.1 show over 60 such baseline enantiomeric separations. The table covers a wide structural variety of enantiomers. Most separations are <40 s and almost a quarter of those are on the order of 10 or fewer seconds. Furthermore, these are accomplished in all mobile phase modes, i.e., normal phase, reversed phase, and

polar organic modes and on a variety of bonded CSPs. Theoretically, we could screen ~90 to 360 chiral analytes per hour which could use less solvent than any other current method. However, this is restricted to ~60 to, at most, 120 samples/hour because of instrumental autoinjector limitations. Certainly, this is neither the first nor the only example of chromatographic potential being limited by instrumental deficiencies.^{74,76} Indeed, as discussed in the following paragraphs, the separations shown in Figure 2.2 and listed in Table 2.2 cannot be achieved under standard HPLC conditions used for Figure 2.1.

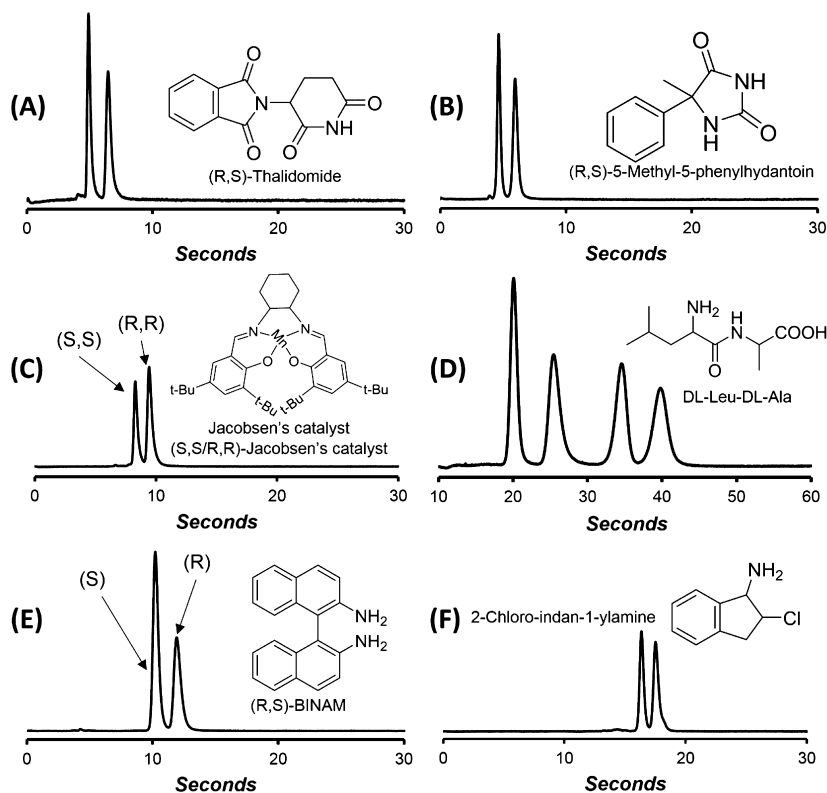


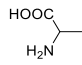
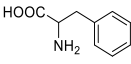
Figure 2.2 Representative ultrafast enantiomeric separations on each of 6 chiral stationary phases: (A) vancomycin SPP (3 cm × 0.46 cm), MP = methanol, 4.95 mL/min,

$T_{\text{col}} = 60\text{ }^{\circ}\text{C}$; (B) teicoplanin aglycone SPP (3 cm \times 0.46 cm), MP = methanol, 4.70 mL/min, $T_{\text{col}} = 60\text{ }^{\circ}\text{C}$; (C) hydroxylpropyl- β -cyclodextrin SPP (5 cm \times 0.46 cm), MP = 97:3:0.3:0.2 acetonitrile-methanol-TFA-TEA, 4.75 mL/min, $T_{\text{col}} = 60\text{ }^{\circ}\text{C}$; (D) teicoplanin SPP (3 cm \times 0.46 cm), MP = 40:60 water-methanol, 3.00 mL/min, $T_{\text{col}} = 22\text{ }^{\circ}\text{C}$; (E) CF7-DMP SPP (3 cm \times 0.46 cm), MP = 90:10 heptane-ethanol, 4.80 mL/min, $T_{\text{col}} = 22\text{ }^{\circ}\text{C}$; (F) CF6-P SPP (10 cm \times 0.46 cm), MP = 70:30:0.3:0.2 acetonitrile-methanol-TFA-TEA, 4.50 mL/min, $T_{\text{col}} = 22\text{ }^{\circ}\text{C}$.

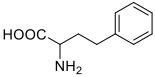
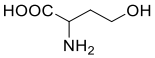
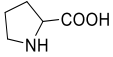
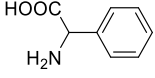
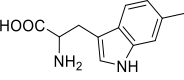
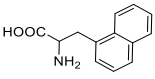
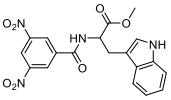
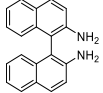
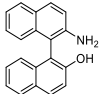
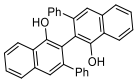
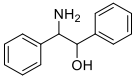
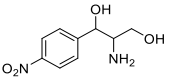
2.4.1 Effect of Packing on Columns Used for Ultrafast Chiral LC.

Accomplishing ultrafast separations in HPLC generally requires higher flow rates, higher pressures, and shorter columns. Consequently, both the column packing quality and permeability are important. Commercial packing procedures are usually trade secrets. When packing identical columns with different slurry solvents, it was found that the use of a “well dispersed” slurry produced columns of $>2.3\times$ higher efficiencies and slightly different permeability according to Darcy’s law.

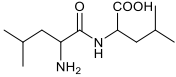
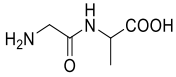
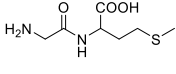
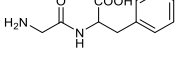
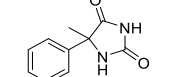
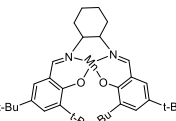
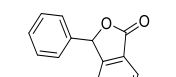
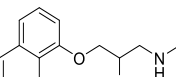
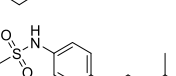
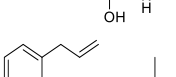
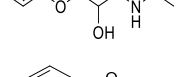
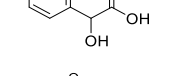
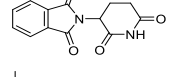
Table 2.2 Chromatographic Data for Optimized Ultrafast Chiral Separations on Six Different Chiral Stationary Phases (CSP) Bonded to 2.7 μm Superficially Porous Particles

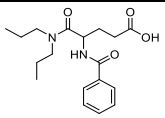
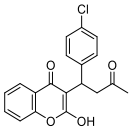
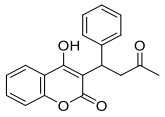
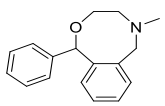
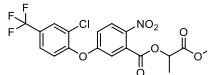
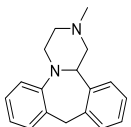
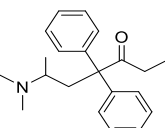
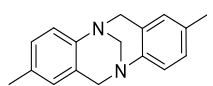
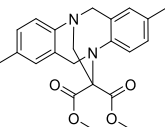
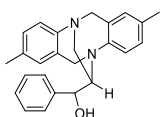
#	Analyte	Structure	CSP ^b	mobile phase; flow rate	t_{R_1} sec	t_{R_2} sec	R_S^1
1	Alanine		T	25:75 water:MeOH; 3.1 mL/min	12	18	3.2
			TAG	70:30 water:MeOH; 2.5 mL/min	10	13	2.2
2	Phenylalanin e		T	25:75 water:MeOH; 2.5 mL/min	15	21	2.2
			TAG	40:60 water:MeOH; 2.5 mL/min	15	22	2.1

#	Analyte	Structure	CSP ^b	mobile phase; flow rate	t _{R1} sec	t _{R2} sec	R _S ¹
3	4-Chlorophenyl alanine		TAG	40:60 water:MeOH; 2.5 mL/min	17	26	1.9
4	Threonine		T	10:90 water:MeOH; 2.9 mL/min	13	17	1.6
			TAG	25:75 water:MeOH; 2.5 mL/min	11	15	2.6
5	Methionine		T	90:10 water:MeOH; 3.7 mL/min	8	9	1.5
			TAG	90:10 water:MeOH; 3.3 mL/min	9	12	2.3
6	Valine		T	25:75 water:MeOH; 2.5 mL/min	10	15	2.6
			TAG	90:10 water:MeOH; 2.2 mL/min	11	14	1.6
7	Norvaline		T	80:20 water:MeOH; 3.0 mL/min	8	10	1.5
			TAG	80:20 water:MeOH; 3.0 mL/min	8	13	2.1
8	Leucine		T	10:90 water:MeOH; 2.9 mL/min	13	23	3.2
			TAG	90:10 water:EtOH; 3.0 mL/min	9	12	1.9
9	Isoleucine		T	60:40 water:MeOH; 2.5 mL/min	11	14	1.7
			TAG	90:10 water:MeOH; 2.5 mL/min	11	14	1.6
10	Norleucine		T	60:40 water:MeOH; 2.5 mL/min	11	15	2.3
			TAG	60:40 water:MeOH; 2.5 mL/min	13	17	1.7
11	Tyrosine		T	25:75 water:MeOH; 2.5 mL/min	14	18	2.0
			TAG	60:40 water:MeOH; 2.5 mL/min	13	18	1.7
12	m-Tyrosine		T	90:10 water:EtOH; 3.7 mL/min	9	12	1.9
			TAG	99:1 water:MeOH; 3.7 mL/min	10	31	2.5
13	o-Tyrosine		TAG	15:85 water:MeOH; 3.0 mL/min	16	23	1.6

#	Analyte	Structure	CSP ^b	mobile phase; flow rate	t _{R1} sec	t _{R2} sec	R _S ¹
14	Homophenyl alanine		T	90:10 water:MeOH; 3.5 mL/min	12	18	2.7
			TAG	60:40 water:MeOH; 2.2 mL/min	17	39	3.1
15	Homoserine		TAG	50:50 water:MeOH; 2.5 mL/min	10	13	1.5
16	Proline		T	90:10 water:MeOH; 3.7 mL/min	8	13	3.6
			TAG	90:10 water:MeOH; 3.0 mL/min	10	17	2.5
17	2- Phenylglycin e		T	90:10 water:MeOH; 3.5 mL/min	9	15	3.3
			TAG	30:70 water:MeOH; 2.7 mL/min	7	14	3.7
18	6-methyl- Tryptophan		T	25:75 water:MeOH; 2.5 mL/min	17	23	1.9
19	3-(1- Naphthyl)alan ine		T	25:75 water:MeOH; 2.5 mL/min	19	26	1.8
20	3,5-DNB- Tryptophan methyl ester		CF7- DMP	70:30:0.1 heptane:EtOH:TFA, 3.0 mL/min	38	44	1.9
21	BINAM		CF7- DMP	90:10 heptane:EtOH, 4.8 mL/min	10	12	1.9
22	NOBIN		CF7- DMP	98:2 heptane:EtOH, 4.5 mL/min	17	22	2.5
23	Vanol		CF6- P ^c	98.5:1.5 heptane:EtOH, 3.5 mL/min	29	33	1.7
24	(1R,2S/1S,2R) 2-Amino-1,2- diphenyletha nol		CF6- P ^d	70:30:0.3:0.2 ACN:MeOH:TFA:TEA, 4.0 mL/min	18	20	1.8
25	(1S,2S/1R,2R) 2-Amino-1- (4- nitrophenyl)- 1,3- propanediol		CF6- P ^d	80:20:0.3:0.2 ACN:MeOH:TFA:TEA, 4.0 mL/min	28	30	1.6

#	Analyte	Structure	CSP ^b	mobile phase; flow rate	t _{R1} sec	t _{R2} sec	R _S ¹
26	2,4-Dichloro- α-phenethylamine		CF6- p ^c	90:10:0.3:0.2 ACN:MeOH:TFA:TEA, 5.0 mL/min	12	14	1.8
27	2-Chloro- indan-1- ylamine hydrochlorid e		CF6- p ^c	90:10:0.3:0.2 ACN:MeOH:TFA:TEA, 4.5 mL/min	12	14	1.6
28	1(1- naphthyl)eth ylamine (1S,2S/1R,2R)		CF6- p ^d	80:20:0.3:0.2 ACN:MeOH:TFA:TEA, 4.5 mL/min	23	25	1.9
29	trans-1- Amino-2- indanol		CF6- p ^c	92:8:0.3:0.2 ACN:MeOH:TFA:TEA, 5.0 mL/min	20	26	1.8
30	α- Ethylbenzyla mine		CF6- p ^d	80:20:0.3:0.2 ACN:MeOH:TFA:TEA, 4.0 mL/min	30	32	1.6
31	1-biphenyl-4- yl- ethylamine		CF6- p ^d	80:20:0.3:0.2 ACN:MeOH:TFA:TEA, 3.0 mL/min	38	40	1.5
32	Norphenylep hrine hydrochlorid e		CF6- p ^d	75:25:0.3:0.2 ACN:MeOH:TFA:TEA, 3.7 mL/min	36	39	1.5
33	Normetanep hrine hydrochlorid e (1S,2S/1R,2R)		CF6- p ^d	75:25:0.3:0.2 ACN:MeOH:TFA:TEA, 3.6 mL/min	34	37	1.5
34	(1S,2S/1R,2R) 2-Amino-1- (4- nitrophenyl)- 1,3- propanediol		CF6- p ^d	80:20:0.3:0.2 ACN:MeOH:TFA:TEA, 4.0 mL/min	28	30	1.6
35	Tryptophano l		CF6- p ^d	80:20:0.3:0.2 ACN:MeOH:TFA:TEA, 4.0 mL/min	27	30	1.5
36	DL-Ala-DL- Ala ^c		T	40:60 water:MeOH, 3.3 mL/min	18	26	2.5
37	DL-Leu-DL- Ala ^c		T	40:60 water:MeOH, 3.0 mL/min	20	25	2.4

#	Analyte	Structure	CSP ^b	mobile phase; flow rate	t _{R1} sec	t _{R2} sec	R _S ¹
38	DL-Leu-DL-Leu ^e		T	40:60 water:MeOH, 3.3 mL/min	18	27	2.5
39	Gly-DL-Ala		T	40:60 water:MeOH, 3.3 mL/min	20	49	5.8
40	Gly-DL-Met		T	40:60 water:MeOH, 3.3 mL/min	19	55	6.4
41	Gly-DL-Phe		T	40:60 water:MeOH, 3.3 mL/min	21	49	5.0
42	5-Methyl-5-phenylhydantoin		T ^f TAG ^f V	MeOH, 4.7 mL/min MeOH, 4.7 mL/min 90:10 1% TEAA pH 7:ACN, 3.0 mL/min	5 5 15	5 6 17	1.5 2.4 1.7
43	Jacobsen's catalyst		CD-HP ^{c,f}	97:3:0.3:0.2 ACN:MeOH:TFA:TEA, 4.75 mL/min	8	9	1.8
44	3-Phenylphthalide		T	50:50 1% TEAA pH 4.1:MeOH, 2.6 mL/min	15	20	1.9
45	Propranolol		T	70:30:0.3:0.2 ACN:MeOH:AA:TEA, 4.0 mL/min	29	33	1.6
46	Sotalol		T ^c	60:40:0.3:0.2 ACN:MeOH:AA:TEA, 4.0 mL/min	20	22	1.5
47	Alprenolol		T ^c	65:35:0.3:0.2 ACN:MeOH:AA:TEA, 4.0 mL/min	21	24	1.5
48	Mandelic Acid		T	50:50 1% TEAA pH 4.1:MeOH, 2.4 mL/min	6	8	1.9
49	Thalidomide		V ^f	MeOH, 4.95 mL/min	5	6	2.7
50	Nicardipine		V	100:0.1 mM MeOH:NH ₄ TFA, 1.0 mL/min	29	34	1.7

#	Analyte	Structure	CSP ^b	mobile phase; flow rate	t _{R1} sec	t _{R2} sec	R _S ¹
51	Proglumide		V	80:20 1% TEAA pH 4.1:ACN, 4.0 mL/min	15	18	1.5
52	Coumachlor		V	80:20 1% TEAA pH 4.1:ACN, 4.5 mL/min	30	38	1.7
53	Warfarin		V	85:15 1% TEAA pH 4.1:ACN, 4.0 mL/min	29	36	1.5
54	Nefopam		CD- HP ^c	65:35 20 mM NH ₄ OAc:ACN, 2.5 mL/min	35	40	2.1
55	Lactofen		CF7- DMP ^c	98:2:0.1 heptane:IPA:TFA, 2.0 mL/min	31	34	1.8
56	Mianserin		V	100:0.15:0.05 MeOH:AA:TEA, 4.0 mL/min	15	19	1.7
57	Methadone		CD- HP ^c	78:22 0.1% AA in water:ACN, 3.7 mL/min	26	30	1.6
58	Tröger's base		CF7- DMP ^c	70:30 heptane:EtOH, 2.5 mL/min	18	20	1.8
59	<i>Ethano</i> - bridged Tröger's base 1		CD- HP ^c	57:43 20 mM NH ₄ OAc pH 4.1:EtOH, 1.3 mL/min	31	38	1.6
60	<i>Ethano</i> - bridged Tröger's base 2		CD- HP ^c	55:45 20 mM NH ₄ OAc pH 4.1:ACN, 2.0 mL/min	24	28	1.6

2.4.2 Detector Sampling Rates and Response Times.

The detector sampling rate (a.k.a. sampling frequency, data acquisition frequency or rate,

etc.) and the detector response time become increasingly important for rapidly eluting analytes and highly efficient separations as demonstrated with SPPs. Under certain circumstances, peak shapes, peak width, and baseline noise can vary considerably as a result of detector settings. There is some debate as to the exact cause and nature of these effects.⁷⁷ We will address this debate in a subsequent communication but will only present the empirical results, as it impacts enantiomeric separations herein. Figure 2.3 shows the effect of detector sampling rate and response time (for an Agilent 1290 UHPLC) on the efficiency (N), resolution (R_s), and baseline noise for six ultrafast enantiomeric separations performed under otherwise identical conditions. Note that with Agilent ChemStation software, the detector sampling rate and response times are coupled and the operator cannot independently change or “unpair” these two parameters. The observed effects are the combined result of these two parameters. At the lowest sampling rate and longest response time (bottom curve, Figure 2.3), the separation is not discernible, the apparent efficiency and resolution is poor, but there is little baseline noise. The separation parameters improve tremendously as the sampling rate increases and the coupled time constant decreases up to about the 80 Hz curve. Concurrently the noise level increases (see 80 × zoom in Figure 3). The default setting on this instrument is 2.5 Hz. It should be noted that with other instruments (Dionex and Shimadzu, for example) the operator can independently set these detector settings which could relate in an array of unwanted or suboptimal combinations.

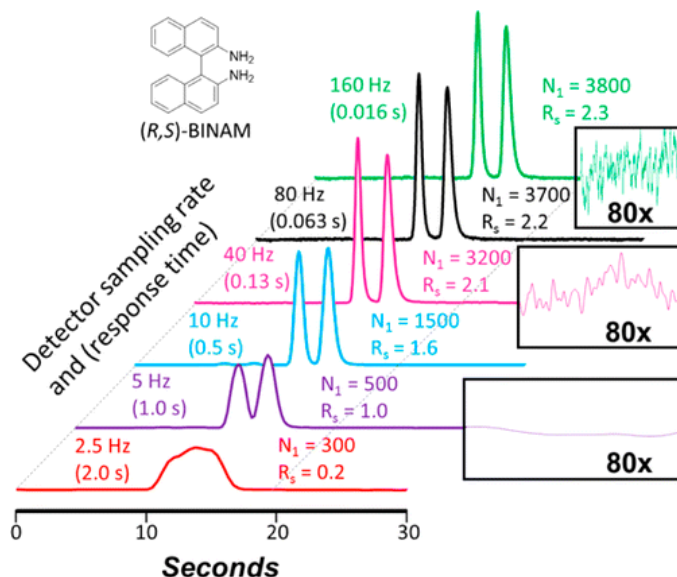


Figure 2.3 Effect of detector sampling rate and response time on efficiency (N) and resolution (R_s) in ultrafast chromatographic separations. BINAM analyzed on CF7-DMP SPP (3 cm \times 0.46 cm), MP = 90:10 heptane–ethanol, 4.0 mL/min, $T_{col} = 22\text{ }^\circ\text{C}$; 1 Hz = 1 s^{-1} .

It is apparent that to maintain high efficiency and good resolution when doing ultrafast separations that detector coupled sampling rates should be ≥ 40 Hz and response time ≤ 0.13 s (Figure 2.3). For enantiomeric separations < 10 s, even higher rates and lower times are needed. If one is simply screening samples and concentration is not a factor, the choice of detector settings are straightforward (e.g., 80 or 160 Hz). However, if one is examining either very low amounts of an analyte or enantiomeric purities, the higher baseline noise (top curve in Figure 2.3) can obscure low level enantiomeric impurities (e.g., $< 1\%$ and especially $< 0.1\%$) and decrease the accuracy and precision of the measurement.

2.4.3 Extra Column Band Broadening Effects on Ultrafast Separations.

It is well established that extra column band broadening is a concern when using short and/or narrow-bore columns that often are packed with smaller diameter particles, as in UHPLC.⁷⁸ In this regard, chiral separations are no different, especially when doing ultrafast separations where it is essential to maintain high efficiencies. Figure 2.4 illustrates this assessment. A “stock” UHPLC was tested (top chromatogram, Figure 2.4) and then the “extra column parts” of the instrument were replaced with smaller volume versions. Using the variance (σ^2) calculated from second moment analysis, intrinsic column efficiencies were calculated in each case, reflecting the true column efficiency of 4750 plates for a 20 s separation (see the Supporting Information). The σ^2 was also calculated using the relationship $\sigma_{ratio}^2 = \sigma_{system}^2 / \sigma_{column+system}^2$. As can be seen, a complete system optimization produced a decrease in the extra column variance ratio from 26% to 3% and this resulted in an ultrafast enantiomeric separation that went from ~71000 plates/m and a resolution of 1.4 to ~94 000 plates/m and a resolution of 1.7.

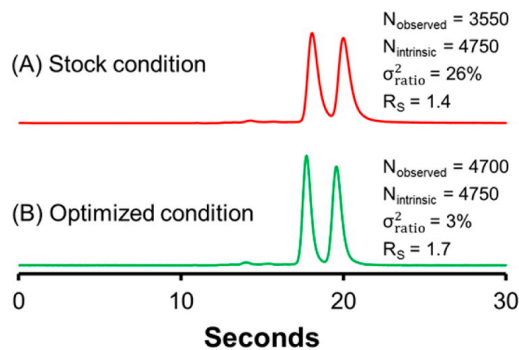


Figure 2.4 Optimization of Agilent 1290 UHPLC for ultrafast separations by replacing stock parts with low extra column volume alternatives. Tröger’s base analyzed on CF7-DMP SPP (5 cm × 0.46 cm), MP = 70:30 heptane–ethanol, 2.5 mL/min, $T_{col} = 22\text{ }^{\circ}\text{C}$.

Percent extra column contribution is expressed as $\sigma_{ratio}^2 = \sigma_{system}^2 / \sigma_{column+system}^2$. (A)

Stock condition: stock injection needle and needle seat, 254 μm i.d. connection tubing (22 cm total) with IDEX 10-32 finger tight fittings, and a 1.0 μL detector flow cell. (B)

Optimized conditions: ultralow dispersion needle and needle seat, 75 μm i.d. nanoViper connection tubing (22 cm total), 0.6 μL detector flow cell.

2.4.4 Kinetic and Thermal (Frictional) Considerations.

Both the general topic of column efficiency and the more specific issue of frictional heating have been considered for columns containing small particles (e.g., $<2 \mu\text{m}$ diameter) and for narrow bore columns.⁷⁹ Most of these studies focused on reversed phase C18 based column formats.⁸⁰⁻⁸⁴ There are few kinetic studies on small particle and SPP chiral stationary phases (CSPs) and none on the effect of frictional heating on these CSPs.⁶³⁻⁶⁵ As stated previously, CSPs are subject to the same thermodynamic and kinetic constraints as other column types. However, the manifestation of these kinetic terms can differ as much from one CSP to another as they do from conventional C18 or silica gel stationary phases. Likewise, the effect of frictional heating and column temperature gradients has been evaluated and discussed for C18 reversed phase columns.^{80,82,84} For SPP-based CSPs, differences as well as any peculiarities can be revealed by any of the related kinetic plots (van Deemter, reduced van Deemter, or Knox).⁷⁹ For the purpose of this discussion, we will use the standard Giddings' coupled van Deemter equation of:

$$H = \frac{B}{u} + C_S u + C u_{SM} + \left(\frac{1}{A} + \frac{1}{C_S u} \right)^{-1} \quad (4)$$

where H is the height equivalent to a theoretical plate, A is the eddy dispersion term, B is

the longitudinal diffusion term, C_S is stationary phase mass transfer, C_{SM} is mass transfer in the stagnant mobile phase (sometime treated as “short range” eddy dispersion), C_M is the moving mobile phase mass transfer term, and u is the linear velocity (m/s) of the mobile phase.⁸⁵

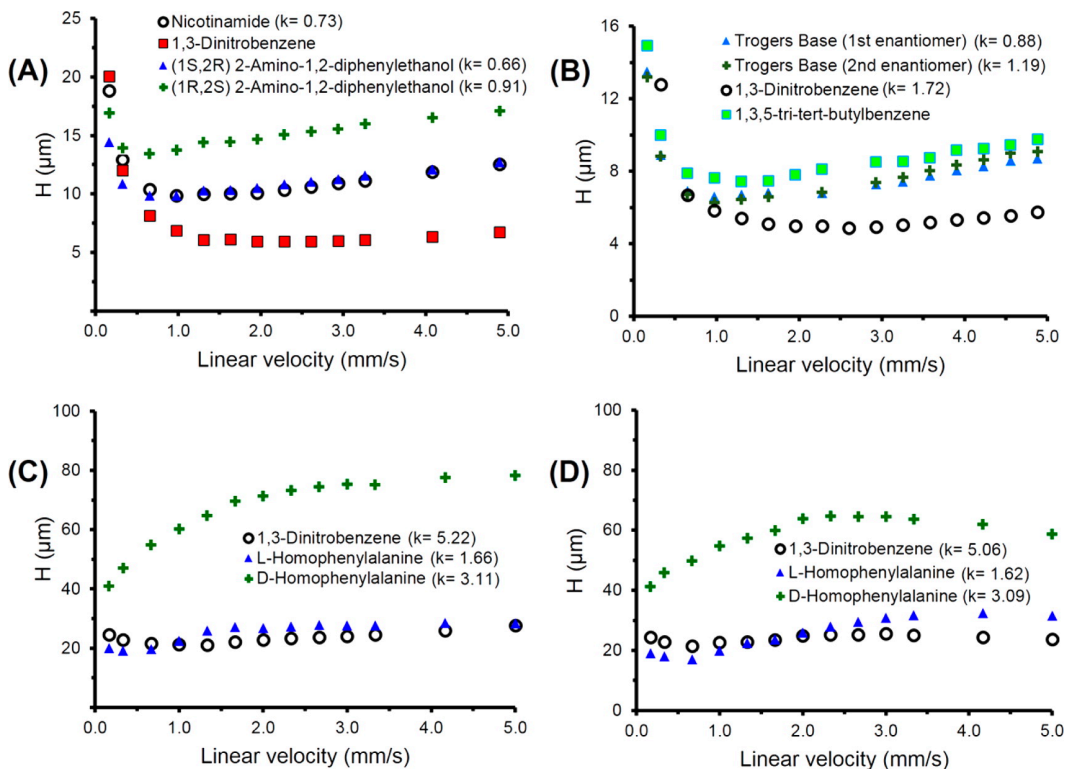


Figure 2.5 van Deemter plots for chiral and achiral analytes in polar organic mode, normal phase, and reversed phase on 2.7 μm SPP CSPs. (A) CF6-P SPP (10 cm \times 0.46 cm i.d.), MP = 80:20:0.3:0.2 acetonitrile–methanol–TFA–TEA, $T_{\text{col}} = 25\text{ }^{\circ}\text{C}$ (thermostated). (B) CF7-DMP SPP (10 cm \times 0.46 cm), MP = 90:10 heptane–ethanol, $T_{\text{col}} = 25\text{ }^{\circ}\text{C}$ (thermostated). (C) Teicoplanin bonded SPP (5 cm \times 0.46 cm), MP = 90:10 water–methanol, $T_{\text{col}} = 25\text{ }^{\circ}\text{C}$ (thermostated). (D) $T_{\text{col}} = 22\text{ }^{\circ}\text{C}$ (not thermostated), other conditions were identical to part C.

Figure 2.5 shows four unique sets of van Deemter plots done in the (A) polar organic mode, (B) normal phase mode, and (C and D) in the reversed phase mode under two different temperature conditions. Each set of curves contains one pair of enantiomers and at least one achiral test molecule. The experimental conditions are given in the legend. The solvent temperature at the column outlet was measured at different linear velocities and mobile phase modes (see the Experimental Section and Supporting Information). The “polar organic” plots in Figure 5A indicate what some would consider to be a normal “well behaved” system. The achiral void volume marker (1,3-dinitrobenzene) has the lowest H at all linear velocities above ~0.5 mm/s and the flattest rise at higher velocities. The least retained (first eluted) enantiomer and a retained achiral analyte (nicotinamide) had almost identical efficiencies at all linear velocities and similar, slightly greater slopes at higher linear velocities. The most retained enantiomer is generally thought to have the greatest resistance to stationary phase mass transfer as it is subject to a greater number of associative stereochemical interactions and often reorientation of the enantiomer.^{45,86} This appears to be so as the H_{\min} is at a slightly lower linear velocity for the second enantiomer compared to the first enantiomer and the achiral probe, indicating an increase in the C_s term.

Figure 2.5B shows the analogous plots for the enantiomers of Tröger’s base as well as retained and unretained achiral probe molecules in the normal phase mode. The relative kinetic behaviors of these molecules are quite different than those in Figure 2.5A. The plots of the enantiomers are almost identical at all linear velocities. However, this behavior is believed to be related to two different things, one of which relates to the stereochemical recognition mechanism while the other is related to general column properties. The similar kinetic behaviors of the two enantiomers indicate that chiral recognition is likely due to the presence of repulsive (steric) interactions rather than

multiple associative interactions with one of the enantiomers. For example, the minimum 3-point of interaction needed for chiral recognition could come from one associative interaction plus 2 steric interactions with one of the enantiomers. The only requirement of this model is that the total energy of association be greater than that of the combined steric repulsive interactions. Such systems have been proposed previously, but this is the first time kinetic data has been used to support such a scenario.^{45,86}

Also important is the relative behavior of the retained and unretained achiral analytes in Figure 2.5B which is opposite to that in Figure 2.5A. The unretained void volume marker (1,3,5- tri-tert-butylbenzene) has worst efficiency at all linear velocities but a flatter rise than the enantiomers at higher linear velocities. The retained achiral molecule (1,3- dinitrobenzene) exhibited the highest efficiency at all linear velocities and had the flattest rise at higher linear velocities. This type of behavior has been reported previously in a few instances for well packed, high efficiency columns.^{78,87} The van Deemter curves in Figure 2.5B were produced using a standard HPLC with a conventional injector, tubings, column compartment, and detector flow cell. When the extra column effects were minimized (Figure 2.4), the observed efficiencies of the 1,3,5-tri-tert-butylbenzene and 1,3- dinitrobenzene were nearly identical. This clearly illustrates the pronounced effects of extra column band broadening on observed efficiencies in such van Deemter curves. Indeed, the highest efficiency column (CF7-DMP with a reduced plate height ($h = 1.6$)) was chosen for this example in an ultrafast format. Clearly under these conditions, one must be aware at all times of extra column effects and how they can generate apparent anomalous behaviors.⁷⁹

Figure 2.5C,D is for the same reversed phase enantiomeric separation and the same retained achiral analyte (1,3- dinitrobenzene). The only difference in these two series of experiments was that the column in Figure 2.5C was in a thermostated, temperature

controlled, “still air device” set at 25 °C, while for Figure 2.5D the column was in ambient conditions (22 °C). It is well-known that teicoplanin chiral selectors strongly and selectively bind D-amino acid enantiomers and that this leads to greater resistance to mass transfer and broader peaks. This is confirmed by the upper plots for the more retained D-homophenylalanine in Figure 2.5C,D. Indeed no H minima vs linear velocity can be identified from these plots and the efficiencies are lower than those in the other mobile phase modes. It should be noted that such efficiencies can be greatly improved by judicious use of specific additives, but that is not the subject of this work. As in the polar organic mode, the curves for the first eluted (least retained) enantiomer and the achiral retained analyte (1,3-dinitrobenzene) are quite similar to one another and both show minima in the 0.5–1 mm/s region.

Perhaps the most striking aspect of these plots is the trend shown in Figure 5D. At linear velocities higher than ~2.5 mm/ s, the efficiencies of both enantiomers and 1,3-dinitrobenzene begin to improve significantly. This effect is most pronounced for the more retained D-homophenylalanine. It is well documented that two types of temperature gradients develop (axial and radial) when there is significant frictional heating.^{80,82,84,88} Eluents with the heat capacity and density of mobile phases used in Figure 5 (acetonitrile, heptane, and water) and operating pressures above 300 bar can easily generate axial temperature differentials of 10 °C.⁸⁴ In fact, when the flow averaged temperature was measured at the column outlet at various linear velocities in three different modes, the axial temperature differences ranged from 11 to 16 °C. This axial variation in fast separations does not contribute to an increase in peak width. On the other hand, the peak efficiency is significantly affected by radial temperature gradients which change local viscosities, velocity profiles, and diffusion coefficients of analytes. A first order “approximation” of the maximum radial temperature difference ΔT_R which can

develop between the column center and the column wall is given by

$$\Delta T_R = \frac{u \left(\frac{dP}{dz} \right) R^2}{4\lambda_{rad}} \quad (5)$$

where u is the superficial flow velocity in m/s (obtained by dividing the volumetric flow rate by the total cross sectional area of the column), dP/dz the change in pressure in the direction of the column axis (z) per unit length in N/m³, R the column radius in m, and λ_{rad} is the approximate thermal conductivity of the mobile phase in the radial direction in W/m °C. (65)

For example, in the normal phase mode (Figure 2.5B), the thermal conductivity of the heptane-ethanol mixture is approximately 0.13 W/m°C. At low linear velocities, (1.67 mm/s or 1 mL/min, $\Delta P = 80$ bar), the magnitude of the maximum radial temperature difference is 1 °C; however, as the linear velocity is increased to 5 mm/s (3 mL/min), the pressure drop is significant (250 bar), and the calculated maximal radial temperature gradient is 8 °C. Note that eq 1 is generally used for first order approximations, it has been shown that the calculated radial temperature gradients can overestimate the observed radial gradients because it ignores the compressibility of the eluent. Consequently the actual energy generated in the column is reduced by a factor of 2/3. On the other hand, as in Figure 2.5D, when a water-rich mobile phase is in use (thermal conductivity of 0.55 W/m°C), a linear velocity of 1.67 mm/s (1 mL/min) generated a back pressure of 112 bar due to higher viscosity. The calculated value of ΔT_R is only 1 °C, and at higher linear velocities, e.g., 5 mm/s (3 mL/min), a radial temperature difference of only 4 °C is developed. Also note that the axial temperature difference in Figure 2.5B,D was similar (~12 °C). However, the data used in Figure 2.5B was from a thermostated column (walls ~25 °C) while Figure 2.5D was not thermostated. Though, since heptane (Figure

2.5B) is far more compressible than water (Figure 2.5D), the energy produced is reduced by $2/3$. However, it is clear from Figure 2.5D, that there are other factors, as in some chiral separations when resistance to mass transfer effects are more pronounced. In these interesting cases, such as a high thermal conductivity water rich mobile phase, the gain in efficiency from an improvement in mass transfer at higher axial temperature gradients is enough to visibly counter any smaller losses in efficiency due to radial temperature gradients and eddy dispersion. This possibility was noted early on by Halašz⁸⁴ and is apparent in Figure 2.5D. See the Supporting Information for detailed temperature measurements and calculations.

2.5 Conclusions

The results of this study, indicate that (1) SPPs are advantageous for ultrafast and high efficiency chiral separations, (2) enantiomeric separations on the order of few seconds are now feasible in all mobile phases with bonded brush type CSPs, (3) kinetic behaviors can sometimes be used to shed light on chiral recognition mechanisms, (4) CSPs can show quite different kinetic profiles from each other and from achiral systems, (5) ultrafast chiral separations require optimized detection and minimization of extra column effects, (6) frictional heating effects must be accounted for in ultrafast separations as they can manifest themselves in disparate ways and to different degrees for various CSPs and mobile phase modes, (7) efficiencies and separation speeds for chiral analytes can now exceed those in capillary electrophoresis. Also it is feasible to expect that (8) SPPs may be advantageous for preparative separations when their high efficiencies, faster analyses times, and reduced solvent consumption compensate for lower chiral selector loading, (9) ultrafast SPP-CSPs may be attractive as the second dimension in 2D-LC because of their greater selectivity and orthogonality to conventional achiral stationary phases, and (10) real-time monitoring of product formation in asymmetric synthesis is possible with

ultrafast chiral separations.

Chapter 3

Ultrafast separation of fluorinated and desfluorinated pharmaceuticals using highly efficient and selective chiral selectors bonded to superficially porous particles

3.1 Abstract

The separation of fluorinated active pharmaceutical ingredients (APIs) from their desfluoro analogs is a challenging analytical task due to their structural similarity. In this work, fluorine containing APIs and their corresponding desfluorinated impurities were separated on five new 2.7 μm superficially porous particles (SPPs) functionalized with bonded chiral selectors. The unique shape selectivity of bonded macrocyclic glycopeptides and oligosaccharides was utilized to separate seven pairs of fluoro/desfluoro APIs resulting in some unprecedented selectivity values. For example, SPP bonded isopropyl cyclofructan 6 yielded a selectivity of 2.73 for voriconazole and desfluoro voriconazole. Further, the SPP based columns allowed for rapid separations ranging from 9 to 55 s with very high efficiencies ranging from 45,000 to 70,000 plates/m (at high flow rates) in both reversed phase and polar organic modes. Chromatographic separation and detection by HPLC-ESI-MS was demonstrated using ezetimibe and voriconazole and their desfluorinated impurities. Among the tested phases, SPP hydroxypropyl- β -cyclodextrin separated the most fluorinated and desfluorinated analogs with baseline resolution.

3.2 Introduction

Medicinal chemists frequently alter the chemical structure of natural products to produce new active pharmaceutical ingredients (APIs) with modified biological activity. This strategy often reduces side effects while increasing bioavailability.⁸⁹ One of the common strategies to increase the biological activity and bioavailability of an API is to incorporate fluorine atom(s) in the drug's structure which in turn increases the lipophilic character of

the API.^{90,91} Approximately, one fifth of all Food and Drug Administration (FDA) approved drugs, which are available in the market, contain at least one fluorine atom.^{92,93} During the synthesis of fluorinated pharmaceuticals, desfluoro impurities are often generated by hydrodehalogenation from palladium coupling or catalytic hydrogenation reactions.⁹⁴ These impurities can contaminate the API with the desfluoro analogue and persist throughout purification steps. Recently, Atici and Karlıg a reported that desfluoro ezetimibe, which is one of the impurities generated during the synthesis of the plasma cholesterol lowering drug ezetimibe, was observed consistently in the range of 0.05–0.15% in the final product.⁹⁵ Since fluorine and hydrogen have similar sizes and electronic structures, chromatography using ordinary C18 chemistries is often unable to separate these desfluorinated impurities causing them to co-elute with the major product of interest.

To date, only a few publications directly address the separation of fluorinated and desfluorinated mixture.⁹⁵⁻¹⁰⁰ Impurities in the fluorinated drug atorvastatin were separated on a C18 column using reverse phase (RP) gradient elution with THF as the organic modifier.⁹⁶ The typical retention time was 30 min for atorvastatin and desfluorinated atorvastatin. Alternatively, Turco et al. showed detection and quantification of desfluorinated impurities in casopitant mesylate using ¹⁹F NMR and LC–MS.⁹⁷ The authors utilized HPLC coupled with ESI-MS and the typical retention time for separation was approximately 4–6 min using RP mode. In 2015, Welch et al. performed a comprehensive study of 132 mobile phase and column combinations for the separation of 8 fluorinated APIs and their desfluoro analogues.⁹⁸ The authors found that perfluorinated stationary phases produced the best separations in most cases. Sub- 2µm fully porous perfluoro phenyl (PFP) columns were used to achieve separation times in the range of

1.5–4 min. The authors also showed the compatibility of the perfluorinated stationary phase using UHPLC coupled with high resolution electrospray ionization mass spectrometry.⁹⁹ Recently, Regalado et al. used 16 fluorinated stationary phases and showed faster separations ranging from 0.4 to 5 min and selectivity values in the range of 1.07–1.75.¹⁰⁰ For a comprehensive review on fluorinated stationary phases the readers can consult references.^{101,102}

It was recognized in the early 1980s that macrocyclic oligosaccharides bonded on silica can not only act as chiral phases but they also possess excellent shape selectivity for diastereomers and structural isomers.^{13,14,103-108} The authors separated hundreds of achiral compounds from their isomers using hydrolytically stable α -cyclodextrin bonded columns. Using the same column chemistry, nicotine and thirteen structurally related compounds were separated.¹⁰⁸ In 1994, macrocyclic glycopeptides such as vancomycin, teicoplanin, and teicoplanin aglycone were introduced as chiral selectors and it was shown that these chiral selectors have good selectivity for amino acids, β -blockers and heterocyclic compounds.^{9,109,110} In addition these chiral selectors were advantageous in separating diastereomers and large peptides.^{111,112} When the same chiral selectors were bonded to 2.7 μm superficially porous particles (SPPs), similar separations could be achieved under 30 s.^{62,113,114} Recently, more than 60 such ultrafast high resolution separations were shown in short 3–5 cm columns.^{113,115} Such fast separations are highly advantageous for drug screening where hundreds of pharmacologically active compounds have to be evaluated.

In this work the unique selectivity of vancomycin, teicoplanin, cyclofructan, and hydroxypropyl- β -cyclodextrin bonded on 2.7 μm SPPs was evaluated for the separation of fluorinated and desfluorinated compound mixtures. Given the unusual selectivity of the

above mentioned stationary phases, it is logical to test the capability of these columns for ultrafast separation of fluorinated drugs and their desfluorinated impurities. To best of our knowledge this is first example where chiral selectors bonded to SPP supports are employed for the separation of desfluoro impurities from fluorinated APIs.

3.3 Reagents and materials

Methanol (MeOH), ethanol (EtOH), acetonitrile (ACN), triethylamine (TEA), trifluoroacetic acid (TFA) and ammonium acetate (NH₄ OAc) were purchased from Sigma–Aldrich (St. Louis, MO, USA). All solvents utilized for separation purpose were HPLC grade or better. Ultrapure water was obtained from Milli-Q water purification system (Millipore, Billerica, MA, USA). Atorvastatin sodium, desfluoro atorvastatin sodium, voriconazole, desfluoro voriconazole, paroxetine, desfluoro paroxetine, ciprofloxacin, desfluoro ciprofloxacin, ofloxacin, desfluoro ofloxacin, aprepitant, desfluoro aprepitant (structures shown in Fig. 1), were purchased from Molcan Corporation (Ontario, Canada). The 2.7 μm superficially porous silica particles with an inner core diameter of 1.7 μm and surrounding shell thickness of 0.5 μm were provided by Agilent Technologies (Wilmington, DE). These silica particles have a surface area of 120 m²/g and pore size of 120 Å. Vancomycin SPP (5cm and 10 cm × 0.46 cm), teicoplanin SPP (5 cm × 0.46 cm), cyclofructan (CF 6) SPP (15cm×0.46cm), isopropyl bonded cyclofructan (CF6-P) SPP (10 cm × 0.46 cm) and hydroxyl-β-cyclodextrin (RSP) SPP (5 cm × 0.46 cm) chiral columns utilized in these studies were provided by AZYP LLC (Arlington, TX, USA). The commercial Chirobiotic V (10 cm × 0.46 cm) column used for comparative purposes was obtained from Supelco (Sigma–Aldrich).

3.4 Instrumentation

A 1290 UHPLC system from Agilent technologies, Santa Clara, CA was used for all

ultrafast separations. The instrument was equipped with an autosampler (G4226A), quaternary pump (G4204A) and a diode array detector (G4212A). For ultrafast separations, it was necessary to achieve low volume dispersion to reduce extra column effects by using 0.075 mm i.d. connection tubing (Agilent Technologies, USA) and an ultralow dispersion kit (Agilent, P/N 5067-5189). This kit includes two stainless steel capillary (0.075 mm × 220 mm and 0.075 mm × 340 mm) and low dispersion needle seat assembly (P/N G4226-87020). To minimize peak broadening from detection electronics, highest possible sampling frequency 160 Hz and shortest response time 0.016 s were used. The instrument was controlled by OpenLAB CDS ChemStation software (Rev. C.01.06 [61], Agilent Technologies 2001–2014) in Microsoft Windows 8.1. Before performing separations all solvents were degassed using sonication under vacuum. Reverse phase chiral HPLC-ESI-MS experiments were performed on Shimadzu LCMS 2020 system (Shimadzu Corporation, Kyoto, Japan) with two LC-20AD pumps, SIL-20AC autosampler, CBM-20A HPLC system controller, SPD-M20A photo-diode array detector and LCMS 2020 mass spectrophotometer. The ESI-MS was a single quadrupole mass analyzer. The software to control the mass spectrometer was Shimadzu LabSolutio LCMS 5.1.

3.5 Results and discussion

The drugs selected for these studies are FDA approved APIs and are commercially available (Fig. 3.1). All drugs are fluorine containing molecules and their corresponding hydrogen containing analog is referred to as their desfluoro impurity. Separation of these desfluoro impurities is very challenging considering the drug and its desfluoro analogue have very similar structures. In order to achieve ultrafast separations while maintaining baseline resolution between the drug and the impurity, the combination of ultrahigh

efficiency superficially porous supports and the unique selectivity of chiral macrocyclic glycopeptides or oligosaccharides were used to great effect.

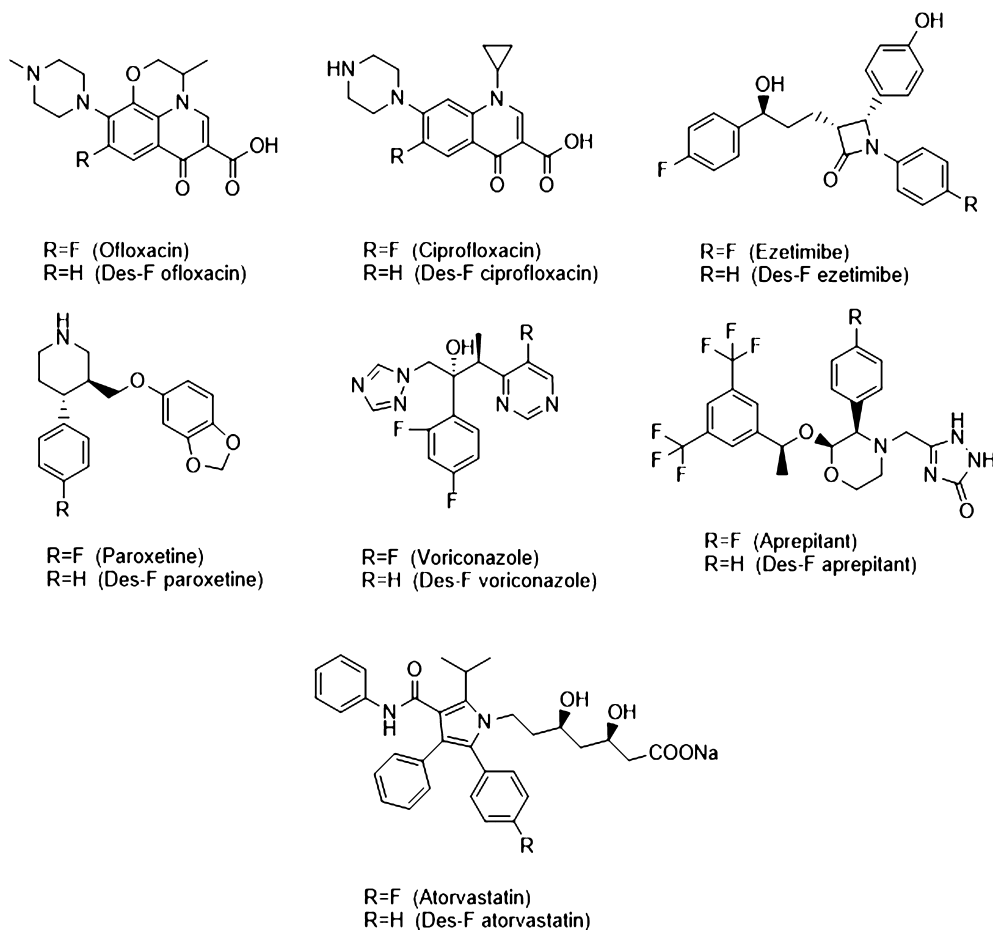


Fig. 6. Closely related fluoro and desfluoro compounds.

3.1 Performance comparison of SPP bonded selectors with commercially available columns

The state of art oligosaccharide and glycopeptide chiral stationary phases (CSPs) utilize 5 μm fully porous silica particles. Fig. 3.2 provides a comparison of a commercially available 5 μm Chirobiotic V column with the vancomycin SPP column. In Fig. 3.2A the same mobile phase and flow rates were used whereas in Fig. 3.2B mobile phase for the

Chirobiotic V column was adjusted to achieve the same retention time as the vancomycin SPP column. Better peak shapes were observed with the vancomycin SPP column compared to the Chirobiotic V column in both cases. The USP tailing factor was 1.9 with the vancomycin SPP column compared to 2.4 and 2.1 (at constant mobile phase and constant retention time, respectively) with the Chirobiotic V column. Interestingly, a 4× increase in plate count and a resolution increase from 1.4 to 1.8 was observed for the vancomycin SPP column compared to commercially available column of the same length at constant mobile phase (see Fig. 3.2A). The increase in resolution on the SPP column is due to the high efficiency of the SPPs rather than selectivity, because the same selectivity was observed for both vancomycin columns under constant mobile phase conditions.

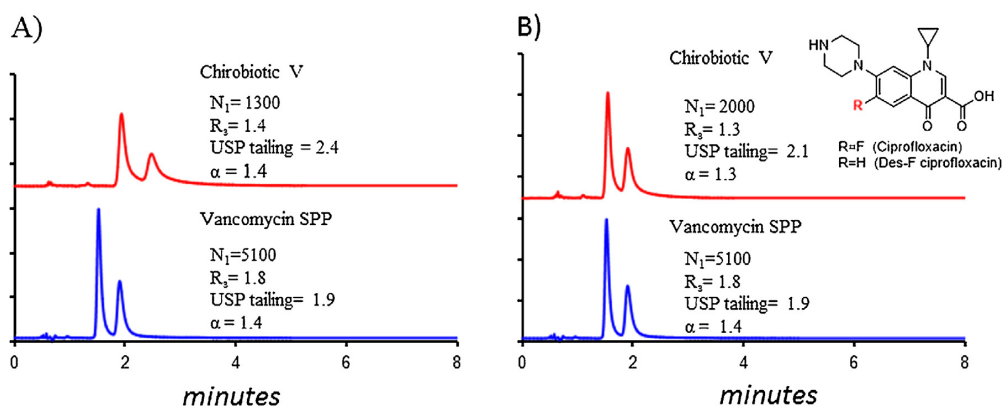


Fig.3.2 (A) Constant mobile phase comparison of ciprofloxacin and desfluoro ciprofloxacin. Columns are 10cm×0.46cm in dimension. MP: 90:10:0.3:0.2ACN:MeOH:AA: TEA, flow rate 2.0 mL/min. (B) Constant retention time comparison of ciprofloxacin and desfluoro ciprofloxacin. MP for vancomycin SPP column: 90:10:0.3:0.2 ACN:MeOH:AA:TEA, flow rate 2.0 mL/min, MP for Chirobiotic V column: 87:13:0.3:0.2

ACN:MeOH:AA:TEA, flow rate 2.0 mL/min.

3.5.1 Performance comparison of different SPP bonded CSPs for separation of fluoro and desfluoro analogues

Considering the equivalent selectivity and higher efficiencies of the SPP based stationary phases compared to the FPP based commercial columns, the potential for using the SPP based stationary phases for ultrafast separations was evaluated. Examples of highly selective and efficient ultrafast separations of fluoro APIs and their hydrogen containing structural analogs using hydroxylpropyl- β -cyclodextrin and CF6 SPP columns are shown in Fig. 3.3. The efficiencies of these high flow rate separations ranged from 45,000 to 70,000 plates/m. For example, ezetimibe and desfluoro ezetimibe were separated in under a minute and had a plate count of 50,000 plates/m with a resolution of 2.8 and a selectivity (α) of 1.59. An α of 1.59 is the highest selectivity obtained for these analogues to date when compared to previous studies.¹⁰⁰ Ciprofloxacin and desfluoro ciprofloxacin were separated with baseline resolution of 4.1 in 55 s and ofloxacin and desfluoro ofloxacin were separated with baseline resolution of 2.8 in 40 s.

Table 3.1 shows the optimized, ultrafast, separation results for the seven APIs and their desfluoro impurities. All separations were obtained in the polar organic mode except the ezetimibe and aprepitant mixtures which were separated in the reverse phase mode. The majority of separations were obtained under a minute with resolutions ranging from 1.2 to 4.3. The aprepitant and atorvastatin mixture was the most difficult to separate and it was only separated on the RSP and CF6 SPP columns respectively. Interestingly, desfluoro aprepitant eluted before the fluorinated API, whereas in all other fluoro and desfluoro mixtures, the fluoro analogues eluted first. In order to further evaluate the unique

selectivities of the various CSPs tested here, the separation of voriconazole and desfluoro vorinoconazole was compared for each column. Fig. 3.4 shows representative ultrafast separations of voriconazole and desfluoro voriconazole on macrocyclic glycopeptide (vancomycin, teicoplanin) and macrocyclic oligosaccharide (CF6-P, CF6, hydroxypropyl- β -cyclodextrin) SPP CSP columns. The separation time of voriconazole and desfluoro voriconazole in Fig. 3.4 ranges from 9 to 29 s. The separations were achieved in the polar organic mode with flow rates ranging from 3 to 5 mL/min which resulted in baseline separation on each column. All SPP stationary phases in this study provided selectivities ($\alpha_s = k_2 / k_1$) of more than 2.10 for voriconazole and desfluoro voriconazole which are the highest α_s values reported to date. Previous studies obtained a maximum selectivity of 1.60 with a C18 column.¹⁰⁰ Column efficiencies ranged from 70,000 to 95,000 plates/m. The fastest separation of the voriconazole and desfluoro voriconazole mixture was obtained with the vancomycin bonded SPP column with baseline resolution of 1.6 and a selectivity of 2.62 at 5 mL/min. All ultrafast separations shown in Fig. 3.4 are obtained in less than 30 s. The two cyclofructan based columns would also have allowed for baseline separations in \sim 10 s if shorter columns (5 cm) had been available.

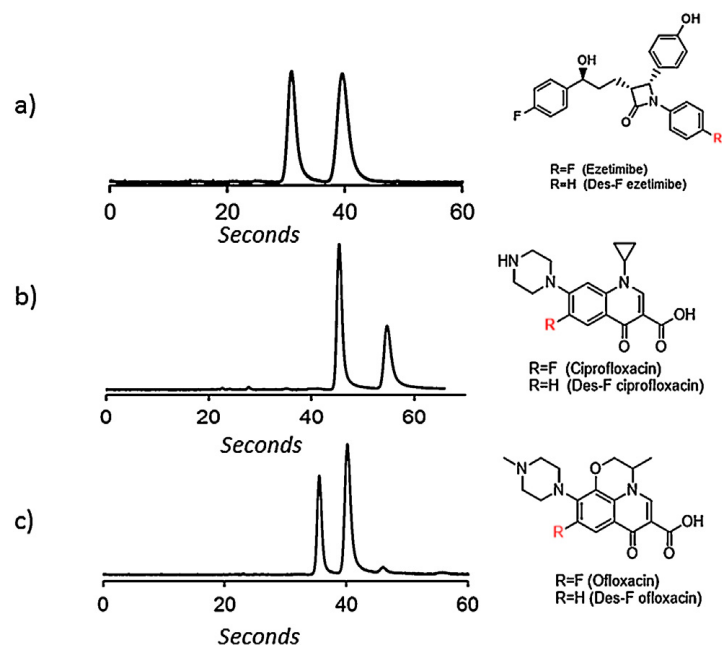


Fig. 3.3 Ultrafast separation of ezetimibe, ciprofloxacin, ofloxacin and their desfluoro analogues on (A) hydroxylpropyl- β -cyclodextrin SPP (5cm \times 0.46cm) column, MP: 50:50 5 mM NH₄OAc pH 4.0: MeOH, flow rate 2.0 mL/min. (B) CF6 SPP (15 cm \times 0.46 cm) column, MP: 90:10:0.3:0.2 ACN:MeOH:TFA:TEA, flow rate 4.5mL/min. (C) CF6 SPP (15cm \times 0.46cm) column, MP: 90:10:0.3:0.2 ACN:MeOH:TFATEA, flow rate 4.5 mL/min.

Table 3.1 Ultrafast separation of desfluoro impurities

Mixtures	Column ^a	Mobile phase	Flow rate (mL/min)	t ₁ (s)	t ₂ (s)	(R _s)	(α)
Ofloxacin and Desfluoro ofloxacin	A	95:5:0.3:02 ACN/MeOH/TFA/TEA	4.00	37	47	2.1	1.35
	B	90:10:0.3:02 ACN/MeOH/TFA/TEA	3.00	28	34	2.1	1.34
	C	90:10:0.3:02 ACN/MeOH/TFA/TEA	4.50	36	40	2.8	1.32
Ciprofloxacin and Desfluoro ciprofloxacin	A	95:5:0.3:02 ACN/MeOH/TFA/TEA	4.00	37	47	2.9	1.46
	B	97:3:0.3:02 ACN/MeOH/TFA/TEA	3.00	27	33	2.6	1.36
	C	90:10:0.3:02 ACN/MeOH/TFA/TEA	4.50	45	55	4.1	1.39
	D	90:10:0.3:02 ACN/MeOH/TFA/TEA	4.40	22	28	2.2	1.42
Ezetimibe and Desfluoro ezetimibe	B	50:50 5 mM NH ₄ OAc pH 4.0 :MeOH	2.00	31	40	2.8	1.59
Paroxetine and Desfluoro paroxetine	B	97:3:0.3:02 ACN/MeOH/TFA/TEA	2.00	41	45	1.3	1.11
Voriconazole and Desfluoro voriconazole	A	95:5:0.3:02 ACN/MeOH/TFA/TEA	4.00	18	22	3.8	2.28
	B	95:5:0.3:02 ACN/MeOH/TFA/TEA	3.00	12	14	1.9	2.72
	C	90:10:0.3:02 ACN/MeOH/TFA/TEA	4.50	25	29	4.3	2.15
	D	90:10:0.3:02 ACN/MeOH/TFA/TEA	5.00	7	9	1.6	2.62
	E	90:10:0.3:02 ACN/MeOH/TFA/TEA	5.00	8	11	1.6	2.69
Aprepitant and Desfluoro aprepitant	B	80:20 20mM NH ₄ OAc :EtOH	2.20	43	50	1.2	1.23
Atorvastatin and Desfluoro atorvastatin	C	98:2:0.3:02 ACN/MeOH/TFA/TEA	2.00	170	186	1.4	1.13

^a (A) 10 cm × 0.46 cm column packed with CF6-P SPP. (B) 5 cm × 0.46 cm column packed with hydroxylpropyl-β-cyclodextrin SPP. (C) 15 cm × 0.46 cm column packed with CF6 SPP. (D) 5 cm × 0.46 cm column packed with vancomycin SPP. (E) 5 cm × 0.46 cm column packed with teicoplanin SPP. These are recommended conditions for LC with UV detection.

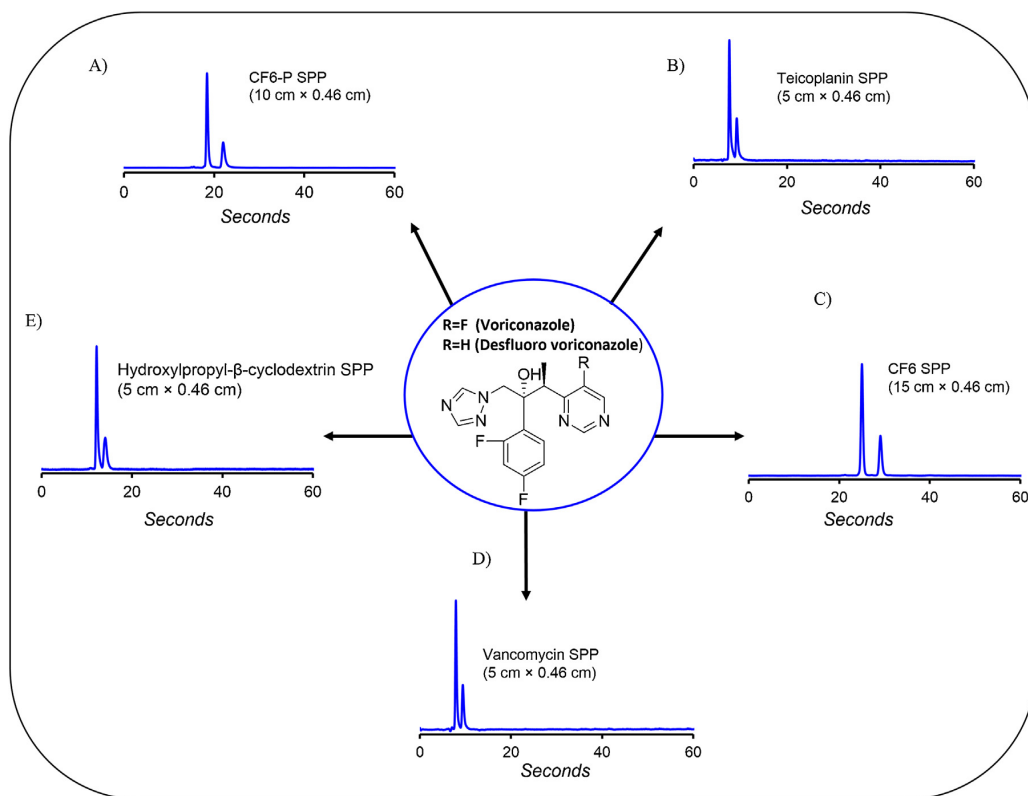


Fig. 3.4 Ultrafast separation of voriconazole and desfluoro voriconazole on (A) MP: 95:5:0.3:0.2 ACN:MeOH:TFA:TEA, flow rate 4.0mL/min. (B) MP: 85:15:0.3:0.2 ACN:MeOH:TFA:TEA, flow rate 5.0 mL/min. (C) MP: 90:10:0.3:0.2 ACN:MeOH:TFA:TEA, flow rate 4.5 mL/min. (D) MP: 90:10:0.3:0.2 ACN:MeOH:TFA:TEA, flow rate 5.0 mL/min. (E) MP: 95:5:0.3:0.2 ACN:MeOH:TFA:TEA, flow rate 3.0 mL/min.

3.5.2 Optimization of separation factor

The ultrafast separations shown in Table 3.1 were performed using strong mobile phase conditions to elute the analytes rapidly. An effect of this rapid elution is a diminution of the k' values. Hence mobile phase conditions were also optimized to achieve larger selectivity factors. For this purpose ciprofloxacin, ofloxacin and voriconazole were

selected with their desfluorinated analogs. The stationary phase used was CF6-P SPP (10 cm × 0.46 cm column). It has been demonstrated that by increasing length of the alcohol chain (for example ethanol to 1-butanol) can enhance the selectivity of the CSP. Similarly in the case of voriconazole and desfluoro voriconazole separation changing the alcohol modifier from methanol to 2-propanol the selectivity increased from 2.28 to 2.73. For ciprofloxacin and desfluoro ciprofloxacin selectivity factor increased from 1.46 to 1.58 and for ofloxacin and desfluoro ofloxacin increase from 1.35 to 1.42 was observed (see Table 3.2).

Table 3.2 Optimized separation factors of fluoro and desfluoro compounds

Mixtures	Column ^a	Mobile phase	Flow rate (mL/min)	t ₁ (min)	t ₂ (min)	Selectivity (α)
Voriconazole and Desfluoro voriconazole	A	99:1:0.3:02 ACN/IPA/TFA/TEA	2.00	0.71	1.04	2.73
Ciprofloxacin and Desfluoro ciprofloxacin	A	99:1:0.3:02 ACN/IPA/TFA/TEA	2.00	2.91	4.29	1.58
Ofloxacin and Desfluoro ofloxacin	A	99:1:0.3:02 ACN/IPA/TFA/TEA	2.00	1.44	1.83	1.42

Table 3.1 emphasized high speed separations using SPP based stationary phases. Selectivities in Table 3.1 range from 1.13 to 2.72. According to previous studies by Regalado et al. the highest selectivity for these compounds was 1.60 obtained for voriconazole and desfluoro voriconazole using a C18 column. In this work, all SPP chiral columns yielded selectivity factors greater than 2.1 and highest selectivity factor of 2.72 was achieved on hydroxypropyl-β-cyclodextrin SPP column while maintaining ultrafast conditions for voriconazole and desfluoro voriconazole. Similarly two more compound mixtures, ezetimibe, desfluoro ezetimibe and aprepitant, desfluoro aprepitant yielded optimized separation factors of 1.59 and 1.23, respectively which are higher than results previously reported.

3.5.3 HPLC-ESI-MS studies

Mass spectrometry is an important tool to identify potential impurities based on mass. Previous work utilized a PFP column with gradient elution for the separation of halogenated pharmaceuticals and their dehalogenated impurities by mass spectroscopy. In this work, the RSP SPP (5cm×0.46cm i.d.) column was used under isocratic conditions as an example of the currently developed method's MS compatibility. Mobile phases consisting of 5 mM ammonium acetate, pH 4.0-MeOH produced good separation and resolution of desfluoro impurities (Fig. 3.5) of ezetimibe and voriconazole. Fig. 3.5A MS results indicated that the fluoro containing ezetimibe eluted before its desfluoro impurity. For, voriconazole the EIC of m/z 350 corresponding to molecular ion $[M + H]^+$ eluted first and later the desfluoro analogue eluted with a m/z 332 (18 Da less).

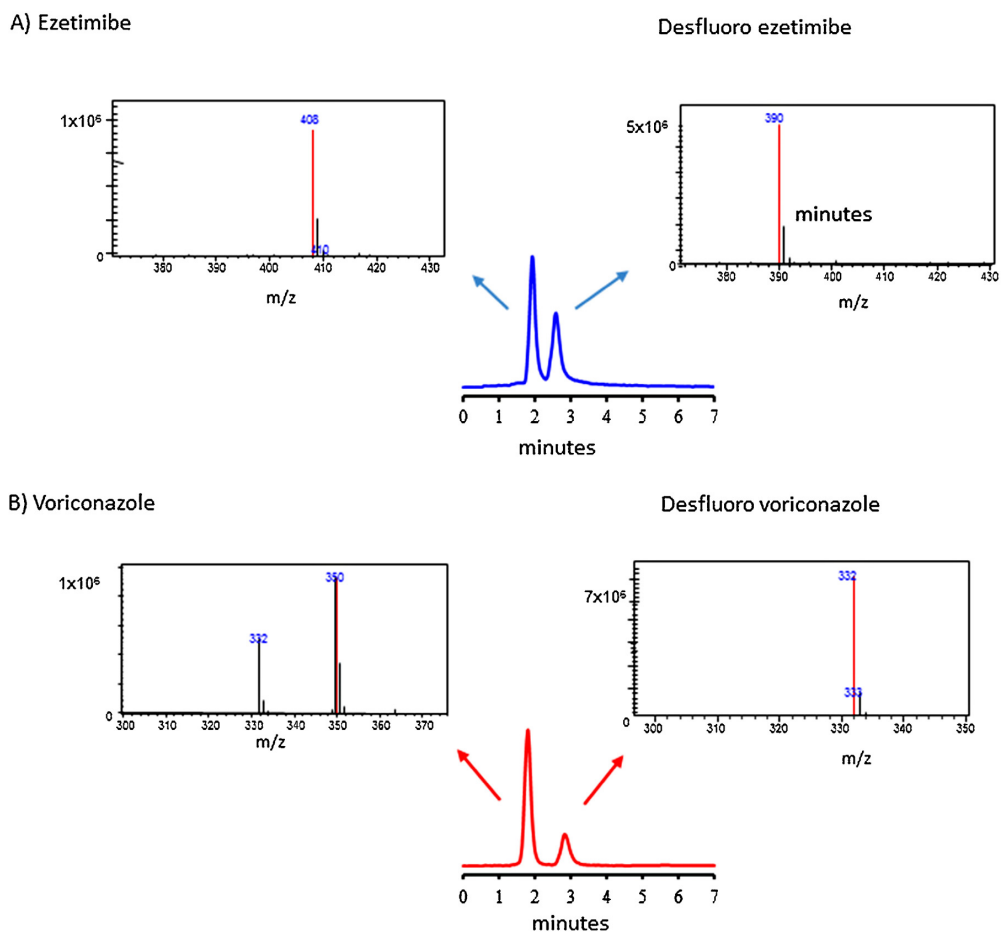


Fig. 3.5 HPLC-ESI MS of (A) ezetimibe and desfluoro ezetimibe, (B) voriconazole and desfluorovoriconazole, MP: 50:50 5 mM NH₄OAc pH4.0: MeOH, flowrate: 0.7mL/min. Injection volume: 1 μ L. Analytes concentration ranges from 0.1 to 0.5 mg/mL.

3.6. Conclusions

The separation of fluorinated and desfluorinated compounds can be challenging due to their structural similarity. Hydroxypropyl- β -cyclodextrin bonded to SPPs provided the maximum number of ultrafast separations. The mobile phases employed were compatible with standard photodiode array detection as well as electrospray ionization mass

spectrometry. Comparison of SPP bonded chiral stationary phases with commercially available ones showed better resolution and higher efficiencies for the SPP based columns. Several separations showed selectivity values better than any previously reported separations on fluororous phases.

Chapter 4

High efficiency, narrow particle size distribution, sub-2 μm based macrocyclic glycopeptide chiral stationary phases in HPLC and SFC

4.1 Abstract

State of the art chiral chromatography still employs 3–5 μm bonded or immobilized chiral selectors in 10–25 cm columns. With the availability of 1.9 μm narrow particle size distribution (NPSD) silica, it is now possible to make ever shorter, high efficiency columns practical for sub-minute chiral separations. Three macrocyclic glycopeptides (teicoplanin, teicoplanin aglycone, and vancomycin) were bonded onto 1.9 μm NPSD particles. Such packed columns had ~80% lower backpressure as compared to polydisperse (PD) 1.7 μm silica materials when using the same mobile phase. The decreased backpressure allowed for diminution of frictional heating and allowed for the use of the 1.9 μm NPSD particle based columns at high flow rates. The 1.9 μm NPSD particle based columns showed up to 190,000 plates m^{-1} for chiral molecules and 210,000 plates m^{-1} for achiral probes. Representative enantiomeric separations are shown for wide classes of compounds, including different types of amino acids, β -blockers, and pharmaceutically important heterocyclic compounds such as oxazolidinones. Applications in three liquid chromatography modes, namely, reversed phase, polar organic mode and normal phase chiral separations were shown with resolution values ranging from 1.5 to 5.7. Additionally, the same columns were used with supercritical fluid chromatography (SFC) for ultrafast separations.

4.2 Introduction

Silica particles bonded or coated with chiral selectors are considered state of art materials for separating enantiomers in chromatography. These stationary phases are utilized in high performance liquid chromatography (HPLC) and super/subcritical fluid chromatography (SFC). In the last four decades, the field of enantiomeric separations has progressed from something that was once considered difficult to do, to an essential, mature technique in pharmaceutical, bioanalytical, and synthetic organic laboratories. Currently, there are no chiral stationary phases that can separate all classes of chiral molecules. For these reasons, researchers engaged in stationary phase development have extensively focussed on synthesizing chiral selectors, which have high selectivity for various classes of enantiomers.^{9,12,116-120} With the advent of high-throughput screening methods, the role of chromatographic efficiency cannot be overemphasized. Yet, only recently did the importance of high efficiency chiral separations become a focus in chiral column development in liquid chromatography^{52,62,113,114,121-123} as well as supercritical fluid chromatography^{124,125}. High theoretical plate numbers, when coupled with chiral selectors having broad enantiomeric selectivity, allows chromatographers to develop rapid HPLC separations for screening processes with short columns.

A number of new approaches have been adapted to achieve high efficiency chiral separations. For instance, Guillarme et al. used chiral derivatizing reagents before performing diastereomer separations on 1.7 μm C-18 silica for β -blockers.¹²¹ Alternatively, chiral additives such as cyclodextrins have been used in the mobile phase with small particle achiral columns.¹²⁶ The most promising strategy for fast and high efficiency enantiomeric separations is to immobilize a chiral selector on a high efficiency silica support (small particles or core-shell particles).^{52,113,114} With the production of <5 μm fully porous particles (FFPs) and superficially porous particles (SPPs), significant

improvements have been made in ultrafast high efficiency chiral chromatography using liquid or super/subcritical mobile phases.^{52,62,113,114,127,128} Recently, Ai et al. employed sub 1- μm silica particles bonded with β -cyclodextrin to separate six compounds under 7 min [18].⁵⁰ Such columns afforded 49,500–73,700 plates m^{-1} under optimized conditions. Similarly, Gasparrini and co-workers bonded a pi-complex brush type chiral selector on 1.7 μm FPPs and showed few ultrafast separations ranging from 15 to 80 s obtained in the normal phase mode [10].⁵² Besides, FPP silica supports, the emerging SPPs were proven to produce highly efficient, *i.e.* over 200,000 plates m^{-1} , chiral columns with a variety of brush type chiral selectors including macrocyclic glycopeptides.^{62,113,114} Surprisingly, in a recent report, when a macrocyclic glycopeptide (teicoplanin) was bonded onto 1.7 μm SPPs with a very small particle size distribution, very low plate counts (21,400 plates m^{-1}) were observed, although the reasons for this low efficiency were not clear.¹²⁸

One of the interesting “unsettled debates” in high efficiency chromatography is the role of particle size distribution (PSD) of the packing material. Four decades ago, Halasz was of the opinion that the width of sieve fraction of silica does not affect the chromatographic efficiency as long as the deviation from the arithmetic mean is smaller than 40%.⁵ This was an empirical observation with large particle diameters (50–200 μm).⁵ On the other hand, Desmet showed a linear correlation between the standard deviation of the particle diameter and reduced plate height with $<5 \mu\text{m}$ FPPs.⁶ This debate was investigated theoretically and experimentally by Gritti using the recently introduced 1.9 μm Titan particles.^{7,8} These silica particles have a very narrow particle size distribution (e.g. $<10\%$ RSD) and column efficiencies are unusually high; for instance producing an intrinsic reduced plate height of 1.7 in narrow bore columns, which are known to pose challenges

during the packing process.⁷ All previous studies on the effect of particle size distribution and the use of Titan silica have only considered achiral (C-18) stationary phases.

In this work, we explore the potential advantages of using narrow particle size distribution (NPSD) silica for chiral chromatography with broad selectivity bonded macrocyclic glycopeptides. The slurry packing behavior and chromatographic performance of the NPSD particles were compared with commercially available 1.7 μm polydisperse (PD) silica. A broad range of analyte classes including β -blockers, amino acids, and heterocyclic compounds were rapidly baseline separated (separation time ≤ 1 min). It was shown that the macrocyclic glycopeptide bonded sub-2 μm particles can be used in all types of reversed phase, normal phase, polar organic mode, and SFC applications without any performance degradation while interchangeably using one mode or another. The representative bonded macrocyclic glycopeptide phases namely; vancomycin, teicoplanin, and teicoplanin aglycone are evaluated and discussed.

4.3. Experimental

4.3.1 Reagents and materials

Anhydrous pyridine, anhydrous *N,N*-dimethylformamide, anhydrous toluene, sodium hydrosulfite, teicoplanin hydrochloride, vancomycin hydrochloride, 1,3-dinitrobenzene, aminopropyl trimethoxysilane, 1,6-di-isocyanatohexane, 3-(triethoxysilyl)propyl isocyanate, methanol (MeOH), ethanol (EtOH), acetonitrile (ACN), heptane, triethylammonium acetate (TEAA), triethylamine (TEA), trifluoroacetic acid (TFA), and acetic acid (AA) were obtained from Sigma Aldrich (St. Louis, MO, USA). All solvents for chromatographic purposes were HPLC grade or better. Distilled water was further purified with Milli-Q water purification system to 18 M Ω (Millipore, Billerica, MA). SFC-grade CO₂ (Airgas) in cylinders supplied with full length eductor tube was used for

supercritical fluid chromatography. Fully porous silica particles with a nominal size of 1.7 μm were purchased from Daisogel (Tokyo, Japan). The particles have a surface area of 346 $\text{m}^2 \text{g}^{-1}$ and pore size of 120 \AA . Commercial chiral columns packed with 5 μm fully porous silica (Chirobiotic V, Chirobiotic T and Chirobiotic TAG) and fully porous silica gel with narrow size distribution (Titan, 1.9 μm , 115 \AA , BET surface area of 294 $\text{m}^2 \text{g}^{-1}$) were provided by Supelco Analytical (Bellefonte, PA). Herein, particle size distribution (PSD) values of the different silica particles were obtained from the manufacturers. PSDs were reported as D_{90}/D_{10} values, which is a ratio of particle sizes, where the D_{90} value is a particle size (diameter) for which 90% of all other particles in the distribution are smaller. Likewise, the D_{10} value is a particle size (diameter) for which 10% of all other particles in the distribution are smaller. Hence, the closer the D_{90}/D_{10} ratio is to unity, the narrower the PSD.

4.3.1. Synthesis of stationary phases

All reactions were carried out in anhydrous solvents. Silica was oven dried and further dried *via* azeotropic distillation in a Dean Stark apparatus. Vancomycin, teicoplanin and teicoplanin aglycone were covalently attached to 1.9 μm NPSD silica (Titan) and 1.7 μm PD (Daisogel) silica using the same procedures as reported previously and.^{9,41} The particles were washed thoroughly with organic solvents and, water and fines were removed by discarding the supernatant liquid in sedimentation process. The stationary phases were packed into 50 \times 4.6 mm i.d. columns (IDEX Health and Science, Oak Harbor, WA) under a constant pressure of 10,000–12,000 psi using a pneumatically driven pump (Haskel, Inc. Burbank, CA, Model DSTV-122). Each stationary phase required optimization of the slurry solvent mixtures and push solvents. The useful slurry optimization tests *via* microscopy have been detailed elsewhere.¹²⁹ All the columns were

tested for efficiency with an achiral probe (1,3-dinitrobenzene) using 70% heptane-30% ethanol at 1.0 mL min⁻¹. All reported efficiencies on the UHPLC were calculated using the peak width at half height.

4.3.2. UHPLC and SFC instrumentation

All separations were performed at room temperature in reversed phase, polar organic mode and normal phase modes on the UHPLC. An Agilent 1290 Infinity Series UHPLC system (Agilent Technologies, Palo Alto, CA) equipped with a quaternary pump, an autosampler, and a diode array detector was used for all liquid chromatography separations. Extra-column effects were minimized by using 0.075 mm i.d. connection tubings (Agilent Technologies, USA) and an ultralow dispersion kit from Agilent (P/N 5067-5189). The kit consists of an ultralow dispersion needle and a needle seat. The data collection rate was set at 160 Hz with a response time of 0.016s to minimize instrumental artifacts and peak broadening. The instrument was controlled by OpenLAB CDS ChemStation software (Rev. C.01.06 [61], Agilent Technologies 2001–2014) in Microsoft Windows 8.1. The mobile phases were degassed using sonication under vacuum. The reported percentages of mobile phases are listed as volume/volume. All separations were performed at ambient temperatures. For SFC separations, a Jasco SFC 2000 system (SFC-2000-7) was used. The system was equipped with a carbon dioxide pump (PU-2086), a modifier pump (PU-2086), a backpressure regulator (BP-2080), an autosampler (AS-2059-SFC), a column oven (CO-2060), a variable wavelength detector (UV-2075) and a makeup pump (PU-2080) supplying additional methanol to the backpressure regulator. The CO₂ pump was chilled to -10 °C using a Julabo chiller. The column was kept at room temperature. The instrument's backpressure regulator was maintained at 10 MP (100 Bar).

4.3.3 Measurement of axial temperature gradient

The temperature changes in the column due to frictional heating of the mobile phases in the 1.9 μm NPSD and 1.7 μm PD packed columns were studied by wrapping the column in an insulating sheet (at room temperature) and inserting a Mastech thermocouple MS8222H (Pittsburgh, PA) inside the column outlet with the help of a screw cap. The flow rate was varied and the resulting temperature was monitored at the column outlet after equilibration of the flow rate.¹¹³

4.4 Results and discussion

Two different types of sub 2- μm fully porous silica were examined namely a narrow particle size distribution (NPSD) silica (1.9 μm diameter) and a polydisperse (PD) silica with a nominal size of (1.7 μm). As per the manufacturer, the 1.9 μm NPSD silica had a D_{90}/D_{10} ratio of 1.30, whereas the 1.7 μm PD silica had a $D_{90}/D_{10} = 1.47$ (see Experimental). The glycopeptide columns based on 5 μm FPPs are commercially available and their characteristics are provided in Table 4.1.

Table 4.1. Physical and chemical characteristics of the silica particles used in this work

Properties	1.9 μm Titan V	1.9 μm Titan T	1.9 μm Titan TAG	1.7 μm Daisogel V	1.7 μm Daisogel T	5 μm Chirobiotic V	5 μm Chirobiotic T	5 μm Chirobioti c TAG
Pore size ^a (Å)	115	115	115	120	120	-	-	-
Surface area ^a (m^2/g)	294	294	294	346	346	-	-	-
Carbon ^b (% wt/wt)	8.3	7.7	11.2	7.8	6.9	-	-	-
N/m (1,3-DNB) ^c	21000	203000	130000	170000	130000	80000	60000	53000
ΔP (bar) ^c	121	123	130	231	220	77	75	83
Reduced plate height	2.5	2.4	3.8	3.5	4.6	2.5	3.5	3.8

^a Starting material information provided by the manufacturer

^b Elemental analysis of the stationary phase

^c 70-30 Heptane-ethanol at 1.0 mL/min.

Table 4.1, summarizes the characteristics of the chiral packing material used in this work. Both sources of sub-2 μm silica particles have similar high surface areas and similar average pore sizes of 115–120 \AA . A previous report has shown that the more narrow disperse 1.9 μm diameter particles have provided exceptionally small intrinsic reduced plate heights of 1.7–1.9 in the reverse phase mode (i.e. with C18).⁶⁵ In Table 4.1, the pore sizes of the different silica sources are also compared. The 1.9 μm NPSD particles are available in 80 \AA and 120 \AA pore sizes. Recently, Gritti et al. showed that 120 \AA , 1.9 μm NPSD particles are more advantageous at higher flow rates than 80 \AA particles. The 80 \AA particles show a van Deemter minimum at low flow rates. Therefore, 120 \AA pore size particles was chosen for this work. The exact reason for this unusually high efficiency in the RPLC mode is still a subject of debate but it provided an incentive to explore the high efficiency of these particles in chiral chromatography using liquid as well as supercritical/subcritical fluids as mobile phases.

4.4.1 Synthesis and loading

The unique bonding procedure for attaching the macrocyclic glycopeptides to the silica imparts exceptionally high hydrolytic stability of these stationary phases.^{9 41} The stability of this stationary phase chemistry originates from the steric bulk of chiral selector and its multi-point attachment to the silica surface, which in turn allows for the use of normal, reverse phase and polar organic modes of chromatography without any loss in retention and selectivity.

The carbon loading of the vancomycin and teicoplanin based chiral stationary phases (CSPs) are compared in Table 4.1. This value can be used to estimate the surface

coverage of the chiral selector. For the 1.9 μm teicoplanin and vancomycin bonded silica, the elemental analysis corresponds to a surface coverage of 0.32 and 0.23 $\mu\text{mol m}^{-2}$ respectively. For the 1.7 μm particles, the surface coverage of teicoplanin and vancomycin is 0.26 and 0.18 $\mu\text{mol m}^{-2}$. The previously reported⁶⁵ potential unique porous structure does not negatively affect the surface coverage of the 1.9 μm particles by the macrocyclic glycopeptide chiral selectors. In fact, the surface coverage was slightly better for the 1.9 μm particles.

4.4.2 Observations on slurry packing sub 2- μm particles

To obtain fast high-resolution chiral separations, two factors are critical (1) sufficiently large selectivity values and (2) high column efficiencies. Only the latter is affected by the quality of the packed bed. Particle size distribution, nature of the slurry, nature of silica, its compressibility and surface features all control the final arrangement of the particles in the column.¹³⁰ To achieve fast separations, short columns and high flow rates are necessary. In such columns it can be practically difficult to achieve axially and radially homogenous beds.¹³¹ Herein, we make several observations on what type of slurries give excellent results for sub-2 μm particle CSPs. When slurry systems were observed under an optical microscope, it was found that solvents which dispersed the particles very well gave column with high efficiencies whereas solvents, which flocculated the particles (e.g. by eliminating electrostatic repulsion with salts), produced columns that performed poorly. This observation is consistent with the packing behavior of SPPs with the same chemistry.¹¹³ Although, there is a general trend to pack sub-2 μm particles at extremely high pressures such as 15,000–20,000 psi, we did not observe any significant advantage of using very high pressures for 1.9 μm particles in 4.6 mm i.d. column formats. In Table 4.1, the practical advantage of packing uniform size particles is evident. In each

case, the vancomycin and teicoplanin bonded 1.9 μm NPSD particles could be packed with higher efficiencies. The teicoplanin aglycone (TAG) column has a unique surface chemistry, which produces higher selectivity but slightly lower efficiency than the related teicoplanin columns. The columns based on 1.7 μm PD particles had lower efficiencies in each case regardless of the optimization procedures in the packing process (several packing approaches were attempted).

Another interesting feature in Table 4.1, is the back-pressure of polydisperse and narrow dispersed packed columns. There is a statistically significant pressure difference in the two different silica particle sizes (ca. 80–90%). In order to rule out any external artifacts such as synthesis, crushing/rupturing of particles, we packed bare silica columns of 1.7 μm PD and 1.9 μm NPSD into 5×0.46 cm columns in the same slurry at 10,000 psi for the same time. The pressure difference between the two columns was again significantly different (180 bar for 1.7 μm PD and 105 bar for 1.9 μm NPSD) under identical conditions. The higher permeability of 1.9 μm NPSD packed columns is from two sources, namely, slightly larger average particle size (~ 2.0 μm) than 1.7 μm , and higher external porosity. Gritti et al. estimated a 40% contribution from larger particle size and a 20% contribution from the larger external porosity than typical 1.7 μm packed columns.⁷ In this case, the pressure difference (180 vs. 105 bar) of bare silica columns corresponds to $\sim 70\%$ difference. Additionally, SEM of the column outlet was done and no breakage of particles was seen. We wish to point out that the D_{90}/D_{10} values do not say anything about the shape of the distribution of particle size. Additionally, the existence of fines also contributes to the column back-pressure. It has been recently proposed that not only particle size distribution but the skewness of the particle size distribution significantly affects the packing density.¹³²

4.4.3. Performance comparison of different particle type CSPs

Fig. 4.1 compares the performance of the same dimension column containing either 5 μm commercially available teicoplanin, vancomycin, and teicoplanin aglycone bonded phases or 1.9 μm NPSD particle based columns which used same bonding chemistry. The same mobile phase and flow rates were used for comparing the respective chromatograms for three different types of chiral molecules. Several patterns are clear in Fig. 4.1. In each case the retention time of the commercially available column and the column containing 1.9 μm particles are similar for teicoplanin and vancomycin, which implies that the absolute chiral selector loading is similar on these columns. The peak shapes, in each case, are better for the 1.9 μm bonded phases. Fig. 4.1(A) shows the enantiomeric separation of the β -blocker propranolol on the teicoplanin-bonded phase; the 1.9 μm particle column showed a 4-fold increase in efficiency and a resolution enhancement from 1.4 to 3.9 compared to the 5 μm based column. In Fig. 4.1(B), thalidomide enantiomers were separated on the vancomycin phase, where a 2.4 \times increase in plate count and a resolution increase from 3.5 to 6.6 was observed compared to a commercial column of the same length containing 5 μm particles. Similarly, on the teicoplanin aglycone phase, there was a 3-fold increase in efficiency when the 1.9 μm particle based column was used. The enhanced resolution on all three column chemistries largely arises from the high efficiency of the 1.9 μm particles rather than the selectivity of the macrocyclic glycopeptide. This is to be expected given the smaller particle diameter. However, what was not expected was the enhanced selectivity (α) observed with the 1.9 μm vancomycin CSP (i.e., $\alpha = 2.77$ for the 5 μm column vs. 2.92 for the 1.9 μm column, see Fig. 4.1).

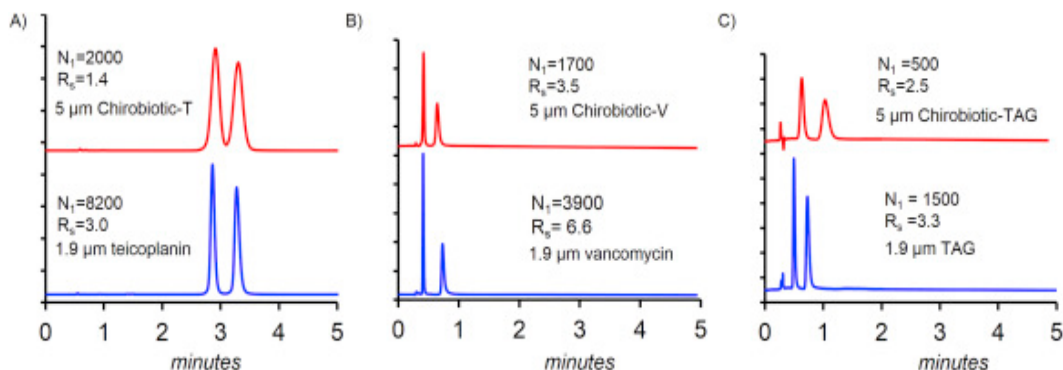


Fig. 4.1.

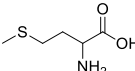
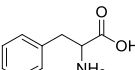
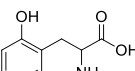
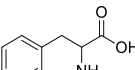
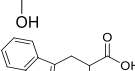
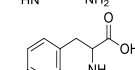
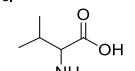
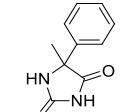
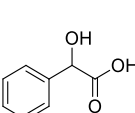
Enantiomeric separation of propranolol, thalidomide and 5, 5-diphenyl-4 methyl-2-oxazolidone using constant mobile phase conditions on teicoplanin, vancomycin and teicoplanin aglycone bonded phases. All columns were 50 mm × 4.6 mm ID in dimension. (A) Propranolol separation at 1.0 mL min⁻¹, MP: 60:40:0.3:0.2 ACN:MeOH:AA:TEA. (B) Thalidomide separation at 2.0 mL min⁻¹. MP: MeOH (C) 5, 5-diphenyl-4 methyl-2-oxazolidone separation at 2.0 mL min⁻¹, MP: 100:0.3:0.2 MeOH:AA:TEA.

4.4.4 Applications of macrocyclic glycopeptide bonded 1.9 µm NPSD particle based CSPs for rapid chiral separations in liquid chromatography

Recently, the advantage of using core-shell chiral bonded phases for enantiomeric separations under 40 s on a variety of chiral stationary phase chemistries was demonstrated.¹¹³ As shown in Section 4.3, rapid, high-resolution enantiomeric separations are possible with 1.9 µm NPSD particles packed in short 5 cm columns due to their high efficiency while maintaining the same or higher selectivity as compared to commercial, state of the art chiral columns. In Table 4.2, the potential of using 1.9 µm NPSD particles for ultrafast chiral chromatography is shown. Twenty three representative analytes are listed for different classes of compounds, which include different types of

amino acids, β -blockers and pharmaceutically important heterocyclic compounds such as oxazolidinones. All three chromatographic modes, namely, reversed phase, polar organic and normal phase mode separations are shown with baseline resolutions ranging from 1.5 to 5.7. The majority of the separations are achieved under a minute with flow rates ranging from 1.4 to 4.5 mL min⁻¹. Such rapid separations are very promising for high-throughput screening of chiral drugs. The fastest separation in Table 4.2, is that of 5-methyl-5-phenylhydantoin where the enantiomers separated under 11 s at a flow rate of 4.5 mL min⁻¹.

Table 4.2 Fast chiral separations on NPSD columns

#	Analyte	Structure	CSP	Mobile phase	Flow rate (mL/min)	t _{R1} (s)	t _{R2} (s)	R _s
1	DL-Methionine		T	40:60 Water:MeOH	2.0	26	35	3.0
			TAG	40:60 Water:MeOH	2.0	26	51	3.7
2	DL-Phenylalanine		T	20:80 Water:MeOH	2.0	37	48	2.8
			TAG	20:80 Water:MeOH	2.0	33	49	2.4
3	o-Tyrosine		T	20:80 Water:MeOH	2.0	37	46	2.2
			TAG	20:80 Water:MeOH	1.5	51	71	2.2
4	m-Tyrosine		T	70:30 Water:MeOH	2.0	28	41	3.1
5	DL-Tryptophan		T	20:80 Water:MeOH	2.0	40	51	2.8
			TAG	30:70 Water:MeOH	1.6	47	68	2.3
6	4-Chlorophenylalanine		T	20:80 Water:MeOH	2.0	36	46	2.3
			TAG	40:60 Water:MeOH	1.4	53	76	2.4
7	DL-Valine		TAG	90:10 Water:MeOH	1.5	26	33	2.3
8	5-Methyl-5-phenylhydantoin		T	MeOH	4.5	8	11	2.8
			TAG	MeOH	4.5	9	14	3.3
			V	MeOH	1.5	26	33	2.2
9	Mandelic Acid		T	80:20 Heptane:EtO	1.0	80	87	1.8
			TAG	70:30 Heptane:EtO	1.0	64	72	1.9

10	Bromacil		T	70:30 Water:MeOH	1.6	56	66	1.7
11	Metoprolol		T	55:45:0.3:0.2 ACN/MeOH:AA/TE A,	3.5	46	51	1.9
12	Pindolol		T	60:40:0.3:0.2 ACN/MeOH:AA/TE A	3.5	49	54	1.7
13	Propranolol		T	60:40:0.3:0.2 ACN/MeOH:AA/TE A	3.5	52	59	2.0
14	Sotalol		T	60:40:0.3:0.2 ACN/MeOH:AA/TE A	3.5	68	77	1.7
15	Coumachlor		V	75:25 1% TEAA pH 4.1:ACN	2.5	63	77	2.2
16	Proglumide		V	80:20 1% TEAA pH 4.1:ACN	2.0	53	61	1.7
17	Thalidomide		V	MeOH	3.0	16	27	5.7
18	Warfarin		V	80:20 1% TEAA pH 4.1:ACN	2.2	58	69	2.1
19	Minaserin		V	100:0.3:0.1 MeOH:AA:TEA	2.5	44	54	2.0
20	4-Methyl-5-phenyl-2-oxazolidinone		TAG	MeOH	1.5	32	51	5.6
21	5,5-diphenyl-4-methyl-2-oxazolidinone		TAG	MeOH	2.0	31	48	3.8

Fig. 4.2, shows representative baseline ultrafast separations on CSPs made with the 1.9 μm particles. The efficiencies in Fig. 4.2 range from 2200 to 4500 plates on the 5 cm columns. For instance, metoprolol, when separated under a minute had a plate count of 90,000 plates m^{-1} which can be considered very high for an enantiomeric separation being performed at 3.5 mL/min. There are certain nuances associated with fast separations, without which the true potential of short high efficiency columns cannot be utilized. As smaller columns are employed, extra-column tubing connections become very important. In this work, narrow diameter connection tubing ($\sim 75 \mu\text{m}$ – $140 \mu\text{m}$) was employed. Additionally, the highest possible sampling frequency 160 Hz and shortest possible response time of 0.016 s was used. The effect of sampling frequency and response time on rapid separations was demonstrated in previous work.^{113,133}

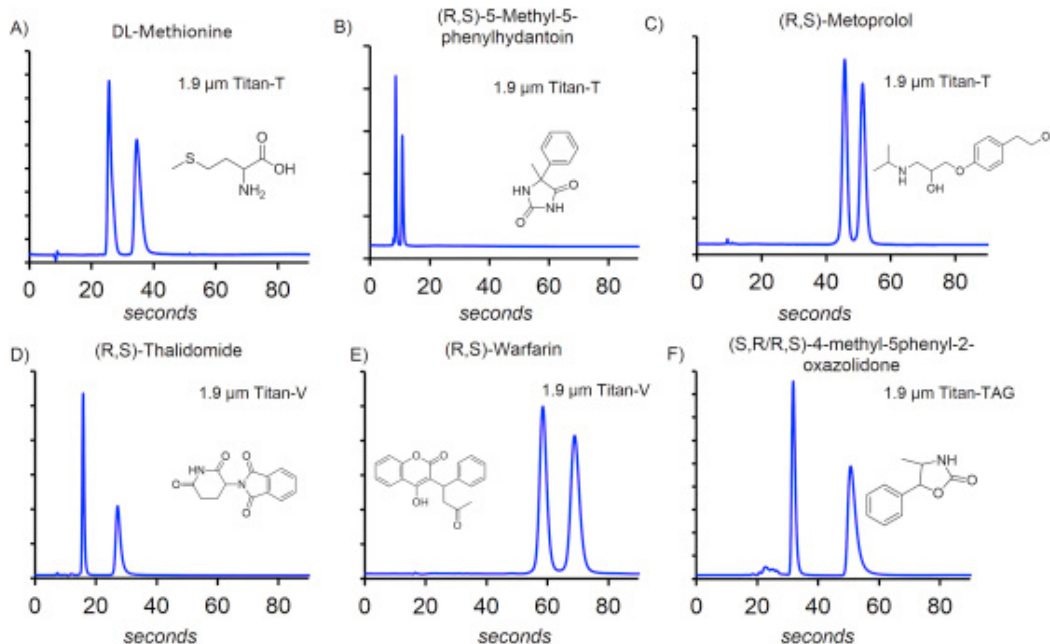


Fig. 4.2 Examples of ultrafast chiral separations on UHPLC (50 mm × 4.6 mm ID columns) with teicoplanin, vancomycin and teicoplanin aglycone bonded phases. A) MP: 30:70 Water: MeOH flow rate: 2.0 mL min⁻¹. B) MP: MeOH, flow rate: 4.5 mL min⁻¹ C) MP: 60:40:0.3:0.2 ACN:MeOH:AA:TEA, flow rate: 3.5 mL min⁻¹D) MP: MeOH, flow rate: 3.0 mL min⁻¹ E) MP: 80:20 1% TEAA pH 4.1:ACN, flow rate: 2.2 mL min⁻¹ F) MP: MeOH, Flow rate: 1.5 mL min⁻¹.

The four representative chromatograms shown in Fig. 4.3 compare the effect of flow rate on efficiency and resolution on CSPs made with the 1.9 μm and 1.7 μm particles. At 1.0 mL min⁻¹, the 1.9 μm NPSD particle based column show approximately 2 times higher efficiency than the 1.7 μm PD particle based column, whereas at 3.0 mL min⁻¹, the efficiencies of both columns are similar but the resolution was still higher with the teicoplanin bonded 1.9 μm NPSD particles i.e. 1.6 vs. 2.2 (see Fig. 4.3), due to slightly better enantiomeric selectivity. The increased efficiency at high flow rate for the 1.7 μm based column will be discussed below.

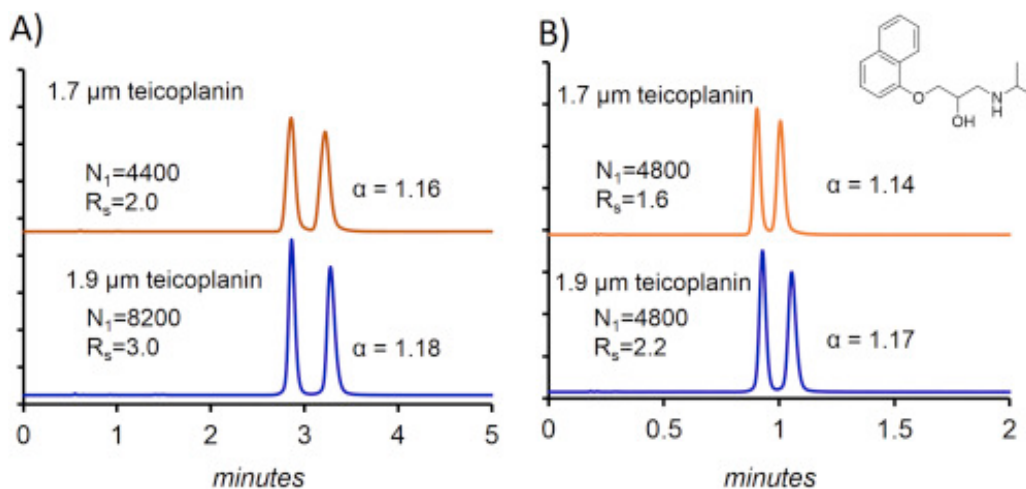


Fig. 4.3 Enantiomeric separation of propranolol using teicoplanin bonded phase (50 mm × 4.6 mm ID columns). A) MP: 60:40:0.3:0.2 ACN:MeOH:AA:TEA, flow rate: 1.0 mL min⁻¹ B) MP: 60:40:0.3:0.2 ACN:MeOH:AA:TEA, flow rate: 3.0 mL min⁻¹.

4.5. van Deemter analysis of sub 2- μm CSPs

For high-speed separations, it is critical to explore plate height as a function of flow rate. Consequently, the van Deemter curves are plotted as plate height (H) vs. volumetric flow rate (mL/min). In this analysis, the UHPLC was optimized to reduce any extra-column effects (see Experimental Section) and no correction was applied to determine the intrinsic column efficiency, as done by Gritti et al. for C18 Titan particles,⁷ because from a practical perspective, typical analysts do not demand intrinsic efficiencies, but rather observed efficiencies. Low viscosity mobile phases containing acetonitrile and methanol allow very high flow rates without significant backpressures as per Darcy's law that relates mobile phase viscosity, linear velocity and back-pressures. Low viscosity mobile phases are typical in the “polar organic mode”.

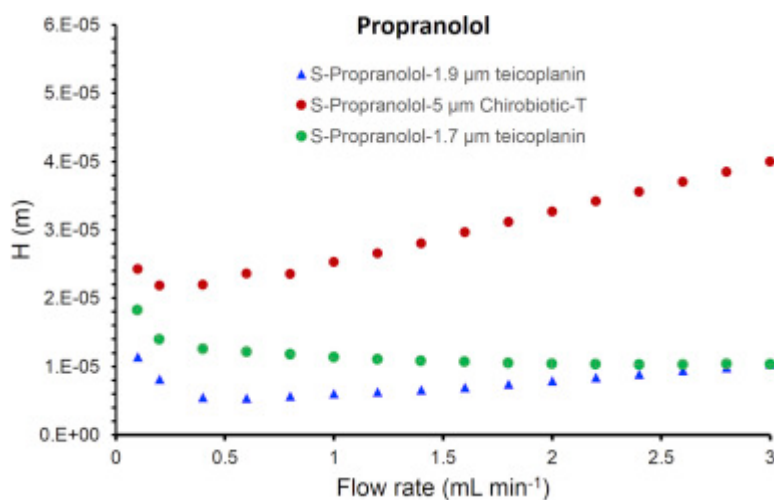


Fig. 4.4 UHPLC van Deemter curves of 50 mm \times 4.6 mm ID teicoplanin bonded columns packed with particles of different sizes. MP: 60:40:0.3:0.2 ACN:MeOH:AA:TEA.

As an example of high-speed polar organic mode chiral separation, we tested the same mobile phase with teicoplanin bonded silica particles of 5 (Chirobiotic), 1.9 (Titan) and 1.7 μm (Daisogel) diameter using racemic propranolol as a probe (Fig. 4.4). As expected, commercial teicoplanin bonded silica had the largest plate heights. The minimum of the 5 μm particle based column was found at 0.4 mL min^{-1} corresponding to an efficiency of 46,000 plates m^{-1} and a reduced plate of 4.3. On the other hand, the minimum for the 1.9 μm NPSD particle based column was at 0.6 mL min^{-1} , where the efficiency of propranolol (first eluted enantiomer) was 190,000 plates m^{-1} . This plate count corresponds to reduced plate height of 2.8. Note that not only are the absolute efficiencies higher, but the reduced plate heights are also 1.5 times smaller. This reinforces the observations in Section 4.2, where it was indicated that the 1.9 μm NPSD particles produced the most uniform packed bed. The case of the 1.7 μm PD particles is interesting, where a clear-cut minimum was not discernable. At 0.6 mL min^{-1} , the efficiency of propranolol was 82,000 plates m^{-1} , corresponding to a reduced plate height of 7.2, while at flow rate of 3 mL min^{-1} the efficiency increased to 96,000 plates m^{-1} (See Fig. 4.3 for representative chromatograms). Additionally, the van Deemter curve (at high flow rates, where the C-term dominates) is not just flatter for the 1.7 μm based column but has a slightly negative slope compared to the 1.9 μm or 5 μm particle based columns. It is known from the literature, that columns made with C18 Titan particles have a larger C-term,⁸ but in this case it is apparent that there is a more likely explanation for the flat/decreasing van Deemter curve for the column containing the 1.7 μm PD material. It has been reported that longitudinal frictional heating can increase the efficiency of some chiral separations when small particles/high flow rates are used.¹¹³ As noted earlier, (Table 4.1 and Section 4.2), the 1.7 μm PD particle based column resulted in 80% higher backpressures. This lower permeability leads to an increased

build-up of longitudinal heat, which can ultimately improve efficiency for the column packed with 1.7 μm PD material at high flow rates. In fact, the column outlet temperature was 6 $^{\circ}\text{C}$ higher for the 1.7 μm PD particle based column compared to the 1.9 μm NPSD based column at 3.0 mL min^{-1} (see Table 4.3).

Table 4.3 Longitudinal temperature gradient as a function of flow rate. Temperature measured at the column outlet. Inlet temperature ($\sim 24^{\circ}\text{C}$) was the same as ambient temperature in each case.

Flow rate (mL min^{-1})	1.9 μm NPSD Teicoplanin		1.7 μm PD Teicoplanin	
	Pressure (bar)	Outlet temperature ($^{\circ}\text{C}$)	Pressure (bar)	Outlet temperature ($^{\circ}\text{C}$)
1.00	71	25	130	26
2.00	155	27	250	29
3.00	250	30	464	36

MP: 60:40:0.3:0.2 ACN:MeOH:AA:TEA. Column dimensions: 5 cm \times 0.46 cm i.d.

In Fig. 4.5(A), the van Deemter curve for mianserin which is a tetracyclic anti-depressant is shown. The enantiomers are separated on a 5 cm \times 0.46 cm column containing vancomycin bonded 1.9 μm NPSD particles in the polar organic mode. The minimum H for mianserin was found at 0.4 mL min^{-1} corresponding to an efficiency of 110,000 plates m^{-1} , for the first eluted enantiomer. A van Deemter minimum at a relatively low flow rate is also seen in reversed phase achiral separations on 1.9 μm NPSD particles.⁷ What is interesting to note in Fig. 4.5(A), is that both enantiomers give identical kinetic plot shapes with the second enantiomer curve shifted slightly upwards. The fact that both curves have similar slopes and minima indicates that both enantiomers have similar absorption/desorption kinetics. This is not the case for the two enantiomers

in Fig. 4.5(B). Here the shape of the van Deemter curves is unusual in several ways. The plate height of D-m-tyrosine is significantly larger than L-m-tyrosine. The thermodynamic interaction of amino acids has been well documented by adsorption isotherms/chromatographic behavior on stationary phases bonded with teicoplanin.^{113,134,135} These studies indicated that teicoplanin selectively adsorbs or binds the D-amino acids as compared to L-amino acids. This behavior is reflected by relatively larger plate heights of the D-m-tyrosine in Fig. 4.5(B). However, as noted in a recent publication the mass transfer of strongly retained D-amino acids are subject to effects of frictional heating at higher flow rates.¹¹³ Table 4.3 shows that as flow rate is increased, this is accompanied by an increase in temperature in the axial direction. The increased temperature, improves the mass transfer kinetics, resulting in flatter C-branch of the van Deemter curve for the D-m-tyrosine.

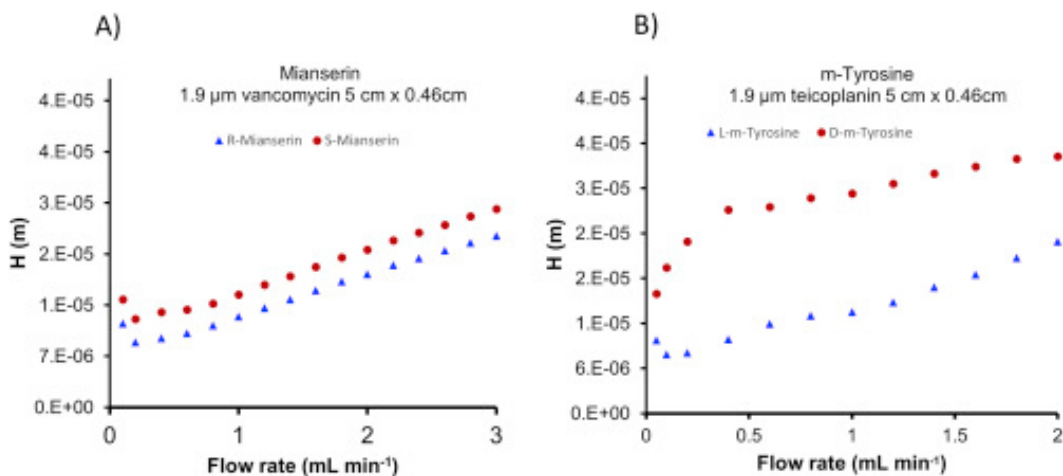


Fig. 4.5 van Deemter plots for chiral analytes in polar organic and reversed phase mode on 1.9 µm- NPSD V and 1.9 µm NPSD T (50 mm × 4.6 mm ID) columns. (A) MP: 100:0.3:0.1 MeOH:AA:TEA. (B) MP: 70:30 Water:MeOH.

Clearly, Fig. 4.5 shows that the combination of unique interactions and high efficiency chiral chromatography can manifest themselves in different ways for different chiral systems.

4.6. Supercritical fluid chromatography applications

One of the major advantages of bonded macrocyclic glycopeptides is their compatibility with mobile phases used in normal phase, reversed phase, polar organic mode, and super/subcritical fluid chromatography (SFC). The latter provides an additional advantage of short separation times and being a “green” separation process.^{10,127,136-139} The speed arises from the fact that the super/subcritical fluid has a low viscosity, as much as two orders of magnitude less than corresponding liquids.^{1,140} The SFC can be considered green because of low organic solvent consumption and the ease of solvent removal. Although the advantage of using smaller particles in SFC was demonstrated three decades ago,¹³⁶ so far, there are very few studies on sub-2 μm particles for achiral compounds, let alone chiral compounds. Recently, Welch et al. showed the promising performance of a CSP that utilized 3 μm particles packed in 15 cm columns.¹²⁷ In this work, we utilized 5 cm packed teicoplanin and teicoplanin aglycone columns with commercially available 5 μm , 1.9 μm , and 1.7 μm particles. Mobile phase conditions were chosen to achieve rapid separations rather than small plate heights H on a standard SFC system. It is well known that introduction of rigidity in the molecule (e.g. heterocycles) near the stereogenic centers, enhances enantiomeric resolution in SFC as well as liquid chromatography.¹⁴¹ In Fig. 4.6, fast SFC separations using teicoplanin and teicoplanin aglycone bonded 1.9 μm diameter particles are shown for heterocyclic compounds such as oxazolidones and hydantoins. In each case, high resolution separations ($R_s = 1.7\text{--}4.0$) were achieved. Comparing the separations of the 5-methyl- 5-phenylhydantoin on

teicoplanin and teicoplanin aglycone CSPs, the higher resolution capability of the latter phase becomes evident. It may be recalled that in Table 4.1, the same molecules can also be separated in the polar organic mode in 11 s. In general, polar organic mode separations can also be performed in the SFC mode, but often not as fast because the weak elutropic strength of SFC mobile phases compared to polar organic mobile phases.

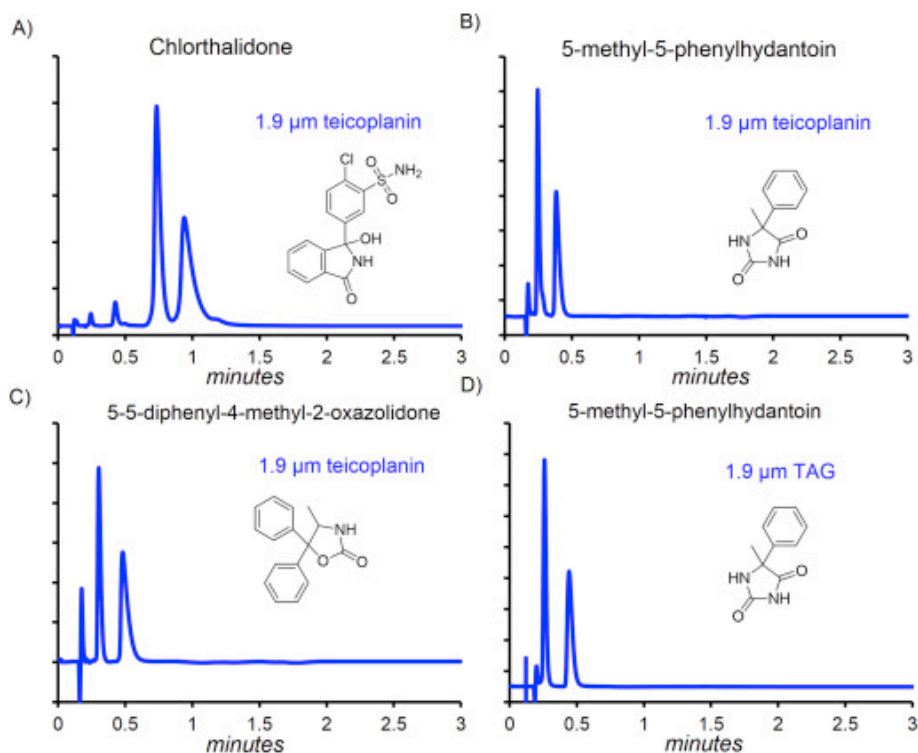


Fig. 4.6. Examples of ultrafast chiral separations on SFC teicoplanin and teicoplanin aglycone bonded phases. Columns (50 mm × 4.6 mm ID) were kept at room temperature. Backpressure regulator was maintained at 80 bar (A) MP: 71:29:0.1:0.1 CO₂:MeOH:TFA:TEA, Flow rate: 7.0 mL min⁻¹. (B) MP: 60:40:0.1:0.1 CO₂:MeOH:TFA:TEA, Flow rate 7.0 mL min⁻¹. (C) MP: 60:40 CO₂:MeOH, Flow rate: 7.0 mL min⁻¹. (D) MP: 60:40 CO₂:MeOH, Flow rate: 7.0 mL min⁻¹.

The advantage of using small particles in SFC mode become evident from Fig. 4.7, which shows the H vs. flow rate curves for columns containing the 5 μm , 1.9 μm and 1.7 μm particles using 91:9 CO_2 :MeOH mobile phase. The interesting feature of the van Deemter curves can be seen in Fig. 4.7; where flat curves at high flow rates for all particles sizes were observed. The reason for the flat curves is ascribed to favorable diffusion coefficients in the SFC mode as compared to liquid chromatography.¹³⁶ Because of this, the 1.9 μm NPSD particle based column maintained its efficiency advantage over the 1.7 μm PD material throughout the entire kinetic plot.

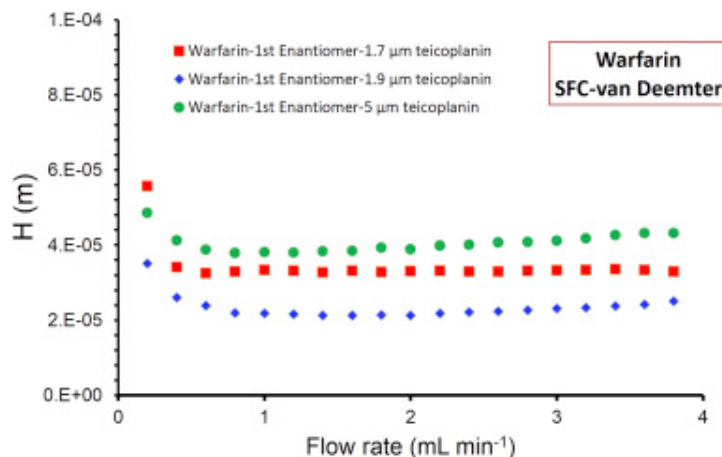


Fig. 4.7 SFC van Deemter curves for the 50 mm \times 4.6 mm ID teicoplanin bonded columns packed with particles of different sizes. Columns were kept at room temperature and back pressure regulator was at 10 MP (100 bar). MP: 91:9 CO_2 :MeOH.

4.5. Conclusions

The results herein establish that small particles with narrow particle size distributions (NPSD) are highly advantageous for fast chiral chromatography. These macrocyclic chiral selectors show excellent selectivity towards large classes of chiral compounds,

such as amino acids, chiral heterocycles, β -blockers and pharmaceutically important drugs. The NPSD particles were easier to pack in 5 cm columns with superior reduced plate heights compared to other polydisperse sub-2 μm particles. Fast chiral separations in short columns are possible with highly optimized instruments where extra-column volumes have been minimized. Fast supercritical fluid chromatography separations were demonstrated on short columns and flat van Deemter curves at higher flow rate were observed in SFC. Finally, the increased permeability of the 1.9 μm NPSD based chiral columns allowed for a decrease in frictional heating and an improved ability to perform fast separations with high flow rates.

Chapter 5

Instrumental Idiosyncrasies Affecting the Performance of Ultrafast Chiral and Achiral Sub/Supercritical Fluid Chromatography

5. 1 Abstract

It is widely accepted that column technology is ahead of existing chromatographic instruments. The chromatographic output may not reflect the true picture of the peak profile inside the column. The instrumental optimization parameters become far more important when peaks elute in a few seconds. In this work, the low viscosity advantage of the supercritical/subcritical CO₂ is coupled with the high efficiency of narrow particle size distribution silica. Using short efficient columns and high flow rates (up to 19 mL/min), separations on the order of a few seconds are demonstrated. In the domain of ultrafast supercritical fluid chromatography (SFC), unexpected results are seen which are absent in ultrafast liquid chromatography. These effects arise due to the compressible nature of the mobile phase and detector idiosyncrasies to eliminate back-pressure regulator noise. We demonstrate unusual connection tubing effects with 50, 75, 127, 254, and 500 μm tubings and show the complex relation of dead time, retention time, efficiency, and optimum velocity with the tubing diameter (via column outlet pressure). Fourier analysis at different back-pressure regulator (BPR) settings shows that some instruments have very specific noise frequencies originating from the BPR, and those specific frequencies vanish under certain conditions. The performance of embedded digital filters, namely, moving average, numerically simulated low pass RC, and Gaussian kernels, is compared. This work also demonstrates, using a simple derivative test, that some instruments employ interpolation techniques while sampling at “true” low frequencies to avoid picking up high frequency noise. Researchers engaged in ultrafast chromatography

need to be aware of the instrumental nuances and optimization procedures for achieving ultrafast chiral or achiral separations in SFC mode.

5.2 Introduction

An ideal chromatographic output should reflect the exact processes taking place inside the column. In reality, peak shape is convoluted by many external factors, more so for fast eluting peaks. The connection tubings,^{142,143} choice of data sampling frequency, and impulse response of embedded “anonymous” digital filters in the detectors¹³³ all affect the apparent symmetry, efficiency, retention time, selectivity, and hence observed resolution. By current standards,^{113,115,133} subminute separation can be termed as ultrafast chromatography, though its meaning may continue to change with technological advances in chromatography. As early as 2010, it was shown that steroids, profens, xanthines, nucleic acids, and sulfonamides could be baseline separated under a minute on a 10 cm column packed with 1.8 μm bare silica particles with reasonable column head pressures (<40 MPa) using supercritical fluids.¹⁴⁴ Since 2015, ultrafast chiral supercritical fluid chromatography (SFC) has gained momentum.^{115,124,125} Recently, Regalado and Welch¹²⁴ separated Tröger’s base in 5 s on a 1 cm column in SFC mode. Chiral separations as fast as 4 s on core–shell or 1.9 μm silica bonded with macrocyclic glycopeptides were reported in ultrahigh pressure liquid chromatography (UHPLC).^{113,115} Although ultrafast SFC/UHPLC separations exist in the current literature,^{15,52,113,115,121,124,125,145} very few papers have focused on the instrumental challenges associated with ultrafast and high efficiency chromatography.¹³³

A survey of the SFC manufacturers enables us to look at the differences and similarities in commercial SFCs, data sampling frequency, and the nature of digital filters. All

instruments have different flow paths and volumes as expected; hence, peak convolution from extra-column variance varies from instrument to instrument. Moreover, SFC is unique from other modes of chromatography in that an additional back-pressure regulator (BPR) is also required after detection to keep the CO₂ in a compressed state. This is an additional source of noise because of the changes in the refractive index of CO₂ as a function of minor changes in the pressure.¹⁴⁶ Several designs using proprietary needle seats or diaphragm-based systems are available. In order to eliminate noise originating from pump heads and BPR, a careful choice of sampling frequency and digital filter is essential at high flow rates. Different SFC manufacturers have different sampling frequency ranges, digital filters ranging from numerical analogues of RC-type filters, simple moving averages, and Gaussian/Hamming windows.

The goal of this work was to demonstrate the challenges, identify the critical parameters, and propose instrument modifications for very fast eluting peaks in SFC columns containing sub-2 μm particles. Although the advantage of using sub-2 μm particles has been widely debated in SFC¹⁴⁷ due to large pressure drops, it was demonstrated that the small particle advantage (seen in UHPLC) also exists for SFC.¹⁴⁸ We show the effects of the connection tubings in fast SFC are very different and unexpected from what is known in the state of the art UHPLC. This work also examines the effects of sampling frequency, the nature of embedded digital filters, and their corresponding response times on fast eluting peaks. Simple mathematical tests (derivative tests and Fourier transform) will be introduced for analyzing unexpected SFC peak profiles. The aim of this work is to show the promise chiral/achiral SFC holds for rapid separations, highlight the critical instrumental parameters, and propose solutions which affect the profiles of rapidly eluting peak

5.3 Experimental Section

5.3.1 Materials

All solvents for SFC were purchased from Sigma-Aldrich (St. Louis, MO). Carbon dioxide was purchased from Airgas (UN1013, Radnor, PA) in cylinders equipped with a full-length educator tube. The mobile phase composition is referenced as volume/volume (mixed by the SFC pumps). The 1.9 μm narrow particle size distribution (NPSD) fully porous silica particles (FPPs) and physical data were provided by Supelco (Titan silica lot no. 68696 Bellefonte, PA) with a D_{90}/D_{10} of 1.21 (a value closer to unity indicates monodisperse particles). The chiral selectors (teicoplanin and teicoplanin aglycone) were bonded by a proprietary procedure.¹¹⁵ Empty column blanks were purchased from IDEX Health and Science, Oak Harbor, WA.

5.3.2 Instrumentation

A Jasco Semi-Prep SFC was used for all ultrafast separations unless otherwise stated. The instrument is controlled by ChromNAV (1.17.01, Build 8) via LC-NET II/ADC. In the Jasco SFC, chilled CO_2 ($-10\text{ }^\circ\text{C}$) is fed to the pump (PU-2086) and the mobile phase modifier is mixed with CO_2 via another identical pump and a mixing chamber. The pumps can deliver up to 20 mL/min at 50 MPa. The safety valve limiting the pressure to 34 MPa was bypassed. The autosampler (AS-2059-SFC) was modified by installing a 2 μL injection loop to reduce extra-column volume. The column oven was bypassed by avoiding connection tubings to prevent band dispersion on very short columns employed herein. Several types of polyether ether ketone (PEEK) and silica lined PEEK tubings with internal diameters of 50, 75, 127, 254, and 508 μm were purchased from SGE Analytical (Austin, TX) and Supelco (Bellefonte, PA). The tubings were cut to have 11.5

cm from the injector to the column and 20 cm from the column to the detector. Two different detectors (UV 2075, X-LC-3070UV) were evaluated for ultrafast SFC. Both detectors have a sampling frequency of 100 Hz. The back-pressure regulator (BP-2080) was maintained at 60 °C at >8 MPa. The makeup pump was set to deliver additional MeOH at 0.1 mL/min to the back-pressure regulator. For comparison purposes, an Agilent Model 4301A SFC, controlled by OpenLabs ChemStation (Model C0.01.03), was used with 5 and 2 × 0.46 or 0.30 cm i.d. columns with the same chemistry. The system consists of a SFC conversion module, a degasser, a binary pump, autosampler, thermostated column oven, and a 80 Hz UV–vis detector.¹⁴⁹

5.3.3 Preparation of Short 2, 3, or 5 × 0.46 cm Columns

Packing a short column with 1.9 μm charged particles (ionizable selector) posed challenges.^{115,129} For short 2–5 cm columns pressures, ~80 MPa (12 000 psi) were sufficient to slurry pack in viscous and dispersing suspensions which ensured layer by layer formation of the bed. Additionally, section packing has been suggested by Guiochon and co-workers,¹³¹ however, no difference in the efficiency of section packed 2 and 3 cm columns vs singly packed columns was found. In fact, the section wise packing of three 2 × 0.46 cm i.d. columns took more than 6 h, and the top two columns packed in series settled within a few hours of usage. In the pharmaceutical industry, retention time reproducibility of <2% relative standard deviation (RSD) is often required. Using a 50 × 3 mm i.d., two ultrafast chiral separations (5-methyl-5phenylhydantoin and *N*-carbobenzoxy-dl-norvaline) were repeated (*n* = 6) at high linear velocities of 60 cm/min. In each case, the RSD was 0.4%. Such fast separations with acceptable reproducibility are very attractive for screening thousands of compounds and columns on a daily basis.

5.4 Results and discussion

Recent studies have indicated that sub-2 μm C-18 silica particles with very narrow particle size distribution ($D_{90}/D_{10} = 1.21$) can provide exceptionally low reduced plate heights (h) in 2.1 mm i.d. columns under optimum conditions (~ 1.7).⁷ However, for ultrafast SFC, 1.9 μm FPP packed columns cannot be operated at the van Deemter minimum. Significantly higher flow rates are required to elute the peak within a few seconds; hence, the ultrafast SFC regime can be dominated by the mass transfer C-term of the van Deemter relationship. As a result, columns with intrinsically high plate numbers are required to achieve a few thousand plates for subminute separations. In chiral SFC, teicoplanin and teicoplanin aglycone are highly promising selectors for enantiomeric and other separations of wide classes of biologically important molecules with $h \sim 2\text{--}3$ under optimum LC conditions.^{10,115,150} The low viscosity advantage of typical binary fluids in SFC (e.g., CO_2/MeOH) coupled with NPSD silica (1.9 μm) packed into 2 to 5 cm columns allows ultrafast chiral and achiral separations. There are numerous nuances in ultrafast SFC, which are *absent* in ultrafast chiral or achiral UHPLC, and these are explored herein.^{113,115,133,151}

5.4.1 Representative Ultrafast Enantiomeric Separations and Instrument Comparison

Figure 5.1 illustrates 5–30 s baseline enantiomeric separations on SFC in 2 or 5 cm columns in 3 or 4.6 mm i.d. formats. These are among the fastest chiral SFC separations reported in the literature.¹²⁴ This speed exceeds the cycling time of most autosamplers (~ 1 min). Even with such short columns and very high flow rates (4–19 mL/min), the efficiencies range from 11 000 to 30 000 plates/m. The working pressures ranged from 15 to 41 MPa. The viscosity of supercritical CO_2 is 9-fold lower than methanol (at 11 MPa)

and 18 times lower than ethanol.¹⁵² As a result, the pressure drops can be as low as 1/15 the pressure drop in LC regardless of the particle size.¹⁴⁴ Table 5.1 gives additional ultrafast separation data for 11 analytes chosen from several classes such as heterocyclic, antimicrobial, chiral acids, and N-blocked amino acids. High flow rates in ultrafast LC waste significant amounts of organic solvents, whereas in SFC, the CO₂ simply escapes into the air. Nevertheless, the results in Figure 5.1 and Table 5.1 cannot be obtained routinely on any commercial SFC unit. As was previously shown in UHPLC,^{113,115,133} the SFC hardware (including detection) and software are not designed to handle very fast and very high efficiency separations.

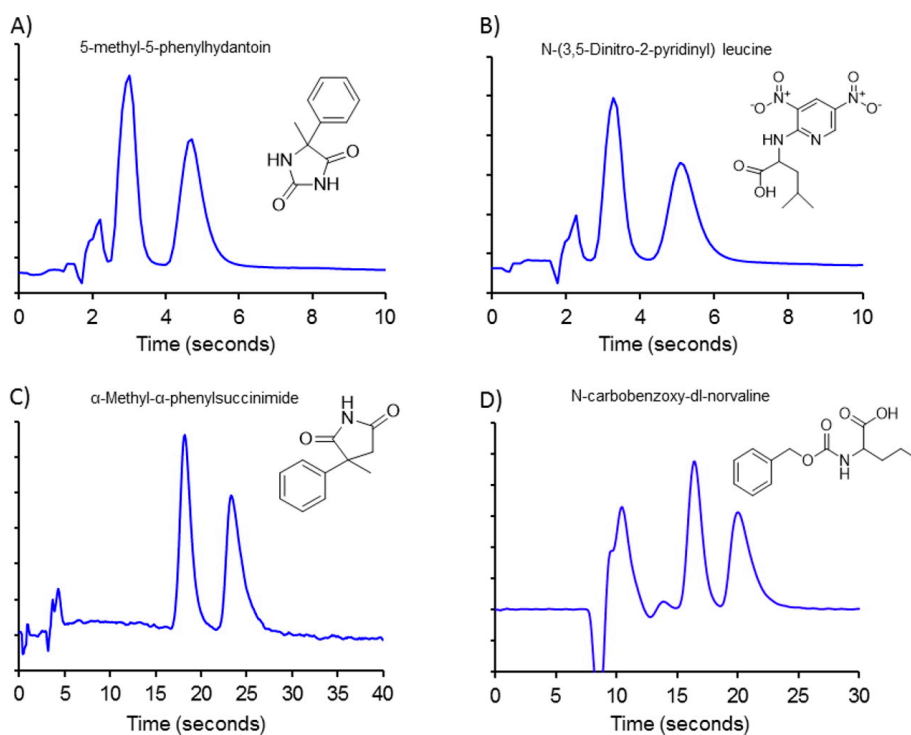


Figure 5.1 Representative ultrafast chiral separations on SFC. Column: Teicoplanin bonded 1.9 μm NPSD silica. Back pressure regulator was maintained at 8 MPa. Column temperature: ambient; (A) 55:45 CO₂/MeOH; column dimensions: 2 \times 0.46 cm; flow rate:

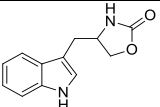
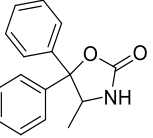
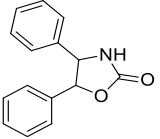
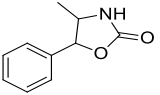
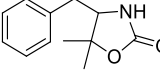
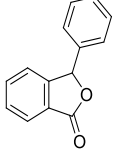
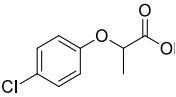
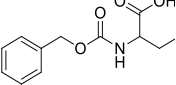
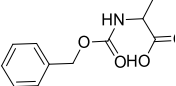
19 mL/min; (B) 60:40:0.1 CO₂/MeOH/TEA; column dimensions: 2 × 0.46 cm; flow rate:

19 mL/min; (C) 96:04 CO₂/MeOH; column dimensions: 2 × 0.46 cm; flow rate: 10

mL/min; (D) 80:20:0.1 CO₂/MeOH/TEA; column dimensions: 5 × 0.30 cm; flow rate: 4.3

mL/min.

Table 5.1 Ultrafast chiral separations on 1.9 μm NPSD based columns

#	Analyte	Structure	CSP	Mobile phase	Flow rate (mL min ⁻¹)	t _{R1} (s)	t _{R2} (s)	R _s
1	4-(1H-indol-3-yl methyl)-2-oxazolidinone		TAG ^b	60:40 CO ₂ :MeOH ^b	19.0 ^b	12.5 ^b	23.5 ^b	1.7 ^b
2	5,5-Diphenyl-4-methyl-2-oxazolidinone		T	60:40 CO ₂ :MeOH ^a	19.0 ^a	5.1 ^a	9.4 ^a	2.0 ^a
3	cis-4,5-diphenyl-2-oxazolidinone		T ^{a,b}	60:40 CO ₂ :MeOH ^a 60:40 CO ₂ :MeOH ^b	6.0 ^a 19.0 ^b	18.7 ^a 3.7 ^b	25.4 ^a 5.0 ^b	2.6 ^a 1.2 ^b
4	4-Methyl-5-phenyl-2-oxazolidinone		T ^b TAG ^b	60:40 CO ₂ :MeOH ^b 60:40 CO ₂ :MeOH ^b	19.0 ^b 19.0 ^b	13.1 ^b 4.4 ^b	7.4 ^b 7.6 ^b	2.6 ^b 2.1 ^b
5	4-benzyl-5,5-dimethyl-2-oxazolidinone		T ^a TAG ^{a,b}	55:45 CO ₂ :MeOH ^a 60:40 CO ₂ :MeOH ^{a,b}	10.0 ^a 19.0 ^b	12.8 ^a 3.4 ^b	18.2 ^a 4.8 ^b	2.0 ^a 1.2 ^b
6	3-Phenylphthalide		T ^{a,b}	90:10 CO ₂ :MeOH ^a 95:05 CO ₂ :MeOH ^b	5.0 ^a 19.0 ^b	24.6 ^a 8.5 ^b	29.7 ^a 11.8 ^b	3.0 ^a 1.7 ^b
7	2-(4-chlorophenoxy) propionic acid		TAG ^a	75:25:0.1 CO ₂ :MeOH:TEA ^a	7.5 ^a	25.3 ^a	33.2 ^a	1.4 ^a
8	N-Carbobenzoxy-dl-norleucine		T ^a	75:25:0.1 CO ₂ :MeOH:TEA ^a	10.0 ^a	14.1 ^a	18.1 ^a	2.0 ^a
9	N-Carbobenzoxy-dl-alanine		T ^a	75:25:0.1 CO ₂ :MeOH:TEA ^a	10.0 ^a	19.5 ^a	27.5 ^a	2.5 ^a

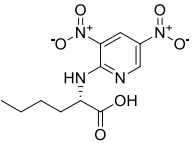
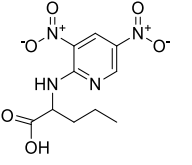
10	N-(3,5-Dinitro-2-pyridinyl) norlucine		T ^{a,b}	60:40:0.1 CO ₂ :MeOH:TEA ^{a,b}	10.0 ^a 19.0 ^b	11.8 ^a 3.4 ^b	22.8 ^a 5.9 ^b	4.7 ^a 1.9 ^b
11	N-(3,5-Dinitro-2-pyridinyl)norvaline		T ^{a,b}	60:40:0.1 CO ₂ :MeOH:TEA ^{a,b}	10.0 ^a 19.0 ^b	12.3 ^a 3.7 ^b	27.1 ^a 5.1 ^b	5.0 ^a 2.3 ^b

Table ^a5.0 × 0.46 cm.
Table ^b2.0 × 0.46 cm.
Table ^cTAG,
teicoplanin aglycone;
T, teicoplanin.

Two different SFCs were utilized (see the Experimental Section). Both instruments were optimized for extra-column volumes by modifying the standard plumbing. In the Jasco SFC, the total tubing length was 31.5 cm (254 μm i.d. PEEK) from the autosampler to the UV detector. This is the minimum length of tubing that one could employ on the SFC using 2 and 5 cm columns and after bypassing the column oven. The Agilent SFC was optimized by using a low dispersion tubing configuration on the standard hardware.¹⁴⁸ This system consisted of 120 μm tubings with a flow cell volume of 2 μL. There is 25 cm of this tubing from the injector to column and 51 cm of the same tubing after the column to the detector. The procedures for optimizing this SFC are detailed in a recent publication.¹⁴⁸ Figure 5.2 highlights the differences in the highly optimized analytical Agilent SFC with a Jasco SFC, which is an analytical/semiprep SFC capable of maintaining flow up to 40 ml/min, but is not optimized for short, small particle containing columns as per their analytical unit. The plate counts of a 5 cm column are higher by 500 plates (on Agilent) for a peak which eluted within 18 s. On the other hand, a 2 cm column showed the same separation of oxazolidone, but the retention time reduced to 7.8 s (Figure 5.2). In that case, similar plates are observed on both instruments. The most

convenient instrument modification is to install low dispersion (narrow) tubings in LC systems to achieve higher efficiency; however, the situation with SFC is not as straightforward.

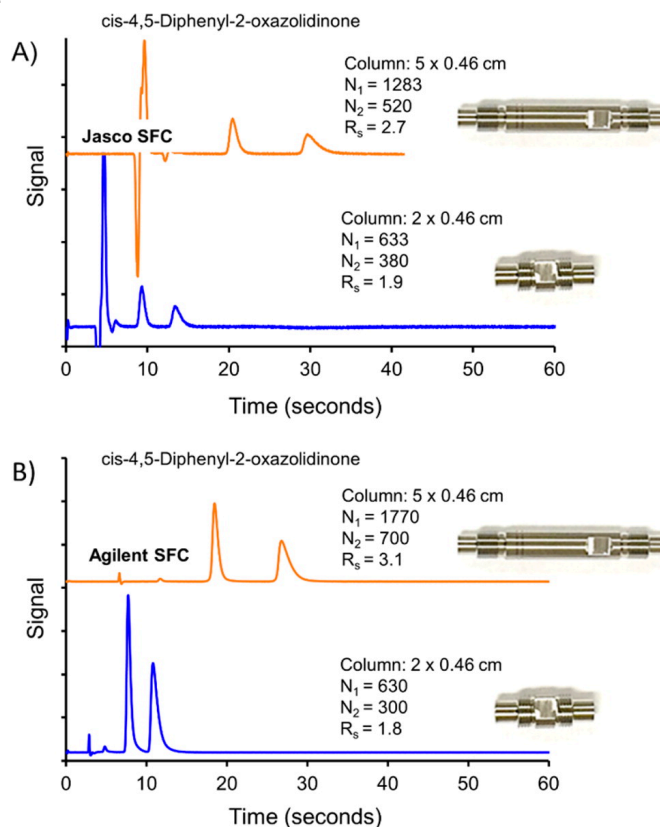


Figure 5.2. Enantiomeric separation of cis-4,5 diphenyl-2-oxazolidinone on optimized Jasco and Agilent SFC systems. Column: Teicoplanin bonded 1.9 μm NPSD silica. Back pressure regulator was maintained at 10 MPa. MP: 55:45 CO₂/MeOH at 5 mL/min.

5.4.2 Ramifications of the Choice of Connection Tubings Ultrafast SFC

Normally, the first step to optimize any chromatographic setup is to minimize the tubing dispersion. The *maximum* dispersion from the tubings,¹⁵³ without the column, can be modeled as a perfect mixer which is simply the extra-column volume squared (from injector loop to detector cell). When 50–500 μm i.d. tubings are employed, one expects the maximum dispersion of 20 to 3845 μL^2 , respectively. As a result, the 50 μm is

expected to perform the best. Figure 5.3A shows a plot of the connection tubing i.d. vs efficiency for racemic (3-phenylphthalide) and achiral (1,3- dinitrobenzene) probes on a 5 × 0.46 cm teicoplanin column. Conditions were chosen to elute these analytes in under 40 s. It is clear that the plate count is a nonlinear function of tubing diameter for both chiral and achiral molecules in SFC. As expected, using a large 500 μm diameter connection tubing, the plate count is lowest because there is significant extra-column dispersion. However, the trends in Figure 5.3A show some counterintuitive behavior with narrow i.d. tubings (50, 75, and 127 μm) under the ultrafast regime. Interestingly, the smallest 50 μm i.d. tubing gives among the poorest plate counts with both chiral and achiral probes, and the 254 μm diameter tubing produces maximum efficiency. Also, it is important to note that the plate counts, dead times, and absolute retention times all change with the diameter of connection tubings (Figure 5.3B).¹⁵⁴ The retention factors (k_s) increase up until ~254 μm i.d. for both achiral and chiral molecules and then remain approximately constant. Interestingly, the retention factor of the second enantiomer appears to be even more strongly affected by the tubing diameters. The retention factors change since each tubing generates a different back-pressure in the SFC system, which in turn affects the density of the mobile phase according to eqn1 and 2:¹⁵⁵

$$\rho = \rho_0 \left(1 - \lambda_\rho \frac{d\rho}{dP} \Delta P \right) \quad (1)$$

$$\ln k = k_0 \left(1 - \lambda_k \frac{d\rho}{dP} \Delta P \right) \quad (2)$$

where ρ is the density of the mobile phase and the subscript indicates the column inlet, λ_ρ is an experimental coefficient, P is the system pressure, and k is retention factor.

Peaden and Lee¹⁵⁵ showed that it is the density of the mobile phase and not its pressure which controls retention in a nonlinear fashion. Thus, the trends in Figure 5.3B are due to the compressible nature of the CO₂/MeOH system, which results in changes of the fluid density, something which is rarely seen in ultrafast UHPLC.¹⁵⁶

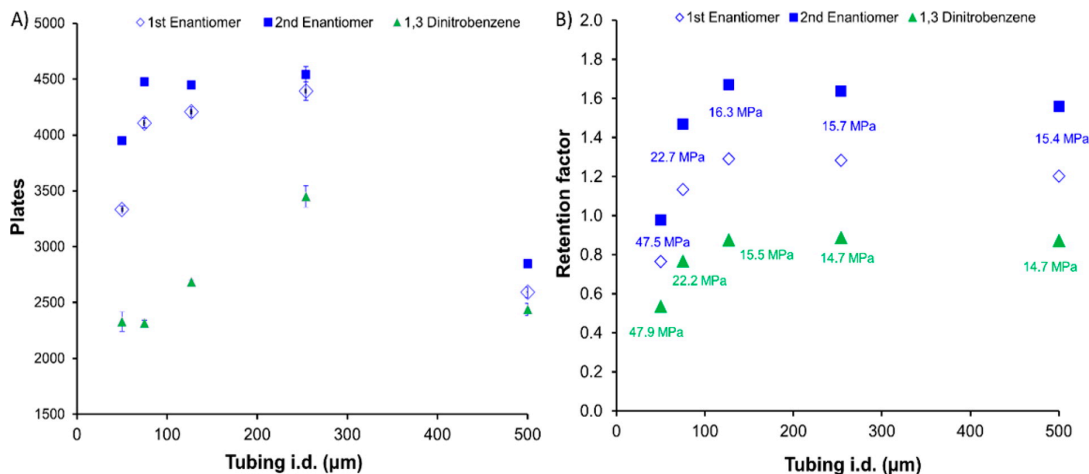


Figure 5.3. (A) Comparison of efficiencies for achiral (1,3 dinitrobenzene) and chiral probes (3-phenylphthalide) as a function of the tubing internal diameters. Column: 5 × 0.46 cm i.d.; teicoplanin bonded 1.9 µm NPSD silica. For chiral analyte, MP: 80:20 CO₂/MeOH at 2.7 mL/min. For 1,3 DNB, 90:10 CO₂/MeOH at 2.8 mL/min. Back pressure regulator was maintained at 10 MPa. Column temperature: ambient. (B) Retention factors of the achiral and chiral probes as a function of tubing internal diameters.

The question of changing efficiency in Figure 5.3A is more challenging to address since the choice of the tubings also affects retention times. Efficiency $N = 5.54 \left(\frac{t^2}{w_{0.5}^2} \right)$ can increase if t increases and $w_{0.5}$ remained constant in Figure 5.3A. It was found that the peak width is dependent on the connecting tubing i.d. and that it reached a minimum width of 254 µm (see the Supporting Information). Therefore, it is not the retention time increase but rather another fundamental phenomenon causing this effect as mentioned above. Using a low viscosity eluent and high flow rates, turbulence is prevalent in narrow i.d. tubings. A Reynolds number (Re) greater than 2000 indicates the onset of turbulence where u is the superficial linear velocity, d is tubing diameter, and ν is the kinematic viscosity (in CGS units) (see the Supporting Information). Reynolds numbers estimated for the narrow bore tubings (50, 75, 127 µm) enter the turbulent regime with flow rates as

low as 2.4 mL/min. Turbulence should play no role in band dispersion from the injector to the column head, since there is no turbulence in wide bore columns (3 or 4.6 mm i.d.). However, one might expect some role of turbulence from the postcolumn tubing and in the detector.^{142,143} Giddings indicated that turbulence should “flatten” the laminar flow profile leading to a reduction in band dispersion.¹⁵⁴ It seems that this is not the case for ultrafast SFC, since the absolute peak widths are actually larger for narrow bore tubings than the 254 μm i.d. tubings. In a previous report, the tubing diameter effect was also investigated with two different SFC detectors with 0.6 and 1.7 μL cell volumes. Interestingly, no effect of postcolumn tubings (65, 120, 250 μm) was found on efficiency using the 1.7 μL flow cell.¹⁴³ However, when the 0.6 μL detector was used, a tubing diameter of 120 μm produced the highest efficiencies. As indicated in Figure 3, the optimum tubing diameter is quite different when using the Jasco instrument with a 4 μL detector volume. Clearly, any recommendations as to extra-column modifications must take into account the exact nature (dimensions) of the instrument and its flow path.

Complex phenomena take place in SFC mobile phases due to the changes in local density and diffusion coefficients along the length of the column.¹⁴⁴ The van Deemter curves (plate height H vs mobile phase linear velocity u) were constructed for SFC separations that differed only in the internal tubing diameter. As expected for a 500 μm tubing, H is significantly larger at all linear velocities. As the tubing diameter is decreased to 254 μm , the lowest plate height is produced, and clearly, it is the optimum tubing diameter in this particular setup. It is interesting to note that the column head pressure was similar for the two tubings. Subsequent reductions in the diameter of the connection tubings hurt the efficiency. Furthermore, with 50 μm tubing, the van Deemter curve assumes a very different form from the rest of the curves, i.e., a U-shape rather than a classical van Deemter shape. Using nonlinear regression, these curves were fitted with

the classical van Deemter equation $H = A + \frac{B}{u} + Cu$, where A, B, and C terms represent the eddy dispersion, longitudinal diffusion, and mass transfer resistance. The optimum linear velocity shifts to larger values in going from 50 μm (1.6 mm/s) to 75 μm (1.9 mm/s), 127 μm (2.2 mm/s), and 254 μm (2.9 mm/s). The “apparent” optimum velocity for 500 μm tubing was around 1.5 mm/s. The inset for Figure 4 shows the values of A, B, and C. The analysis of residuals confirmed the goodness of fit (see the Supporting Information), and the errors in the coefficients (<2%) are shown in the Supporting Information. It is interesting to note that the A and B terms of the 127 and 254 μm are similar, yet the C term of the 127 μm i.d. is almost twice that of 254 μm i.d. The odd shape of the van Deemter curve obtained with a narrow 50 μm tube is possibly due to the diffusion coefficients changing significantly with pressure. Hence, the classic van Deemter does not fit very well in the case of 50 μm tubing.¹⁵⁷ Such a pronounced effect due to the compressibility of the mobile phase is not seen in ultrafast UHPLC, where operating pressures can reach 80 MPa. Thus, Figures 3 and 4 show the counterintuitive effects of ultrafast SFC indicating that the narrow i.d. tubings may not be the best choices for generating a low dispersion system.

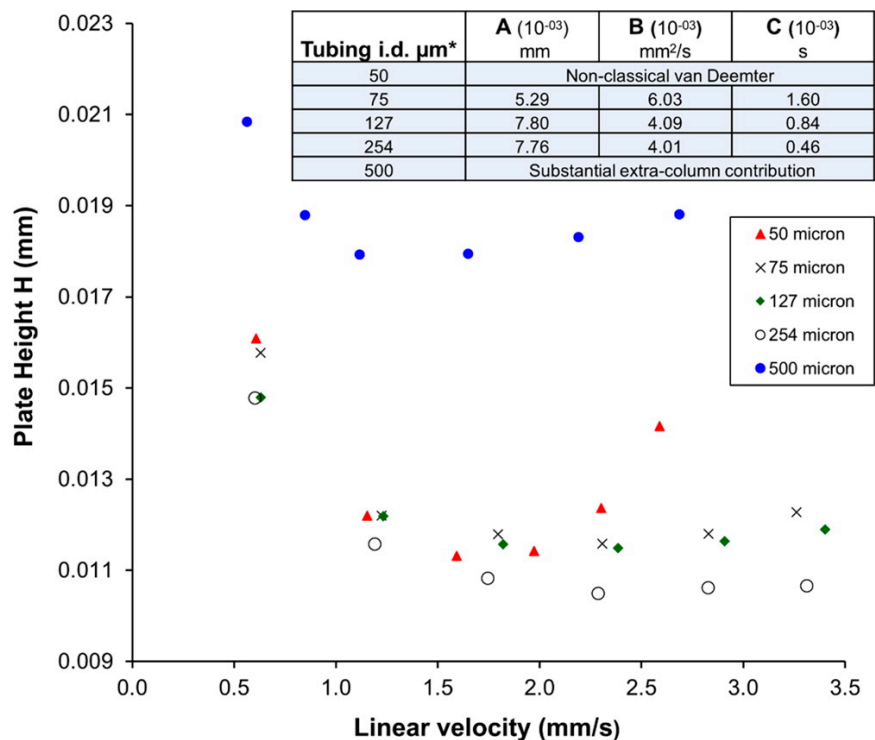


Figure 5.4 van Deemter curves of the first eluting enantiomer of 3-phenylphthalide.

Column: 5×0.46 cm i.d.; teicoplanin bonded $1.9 \mu\text{m}$ NPSD silica. MP: 80:20

CO_2/MeOH . Back pressure regulator was maintained at 10 MPa. Column temperature:

ambient. The inset shows the values of the van Deemter coefficients, $H = A + \frac{B}{u} + Cu$,

using Excel Solver Add in. The average linear velocity was calculated as L/t_0 , where L is

the column length and t_0 is the dead time. (*The coefficients with error analysis are

shown in the Supporting Information).

5.4.3 Impact of Back Pressure Regulator Settings on Ultrafast SFC Chromatograms

Ultrafast SFC requires the use of high flow rates; however, high flow rates have been reported to generate high baseline noise which is usually attributed to turbulence in postcolumn hardware.^{142,143,158} Under atmospheric and ambient temperature, CO_2 has a

poor solvation ability.¹⁴⁹ Additionally, at the column outlet, a back-pressure regulator (usually set above 8 MPa) is required to keep CO₂ in a compressed state.¹⁴⁷ The back-pressure regulator setting must be optimized for fast SFC separations as well. Toluene was chosen as a fast eluting analyte with pure CO₂ as the mobile phase at a flow rate of 5.0 mL/min (Figure 5.5). This flow rate is usually the highest flow rate available in many of the commercial SFCs. In this experiment, the optimum tubing diameter of 254 μm was used and the BPR was changed from 10 to 25 MPa(Figure 5.5A)shows the resulting chromatograms and two interesting trends as the outlet pressure is increased. The retention time of toluene *increases* from 13.2 to 14.6 s and so does the dead time. Second, there is a concomitant decrease in baseline noise as a function of outlet pressure. The average density of CO₂ is dependent on the BPR settings.¹⁵⁹ The increase in the dead time (t_0) in SFC is related to the density of CO₂ in the column inlet as well as the average density along the entire length of the column as shown in eq 3^{154,160}

$$t_0 = \frac{\varepsilon SL}{V_{inlet}} \cdot \frac{\rho_{avg}}{\rho_{inlet}}$$

where ε is the bed porosity, L is the column length, S is the cross-sectional area, V_{inlet} is the volumetric flow rate at the column head, and the fraction $\frac{\rho_{avg}}{\rho_{inlet}}$ represents the average density of the mobile phase and at the column inlet, respectively. The density term is indeed a function of the differential pressure in the column (pump and the back-pressure regulator) as shown in eq 1. Commonly, in the literature, it is stated that retention time would decrease with CO₂ density.^{146,154} Figure 5 makes it clear that the retention time may also increase, but the k will decrease with the higher average density of CO₂. A plot of $\log k$ vs backpressure was found to be linear with R^2 of 0.9849. As can be noted visually, the baseline noise is also changing with the BPR setting. Figure 5B shows the noise analysis of the three chromatograms at different BPR settings by Fourier transform

of the chromatograms. There are two regions of frequency components in the chromatograms. The low frequency region (shaped like a halved Gaussian) originates from the peak in the chromatogram. Fourier transform of a Gaussian function is also a Gaussian function. At low column outlet pressure (10 and 15 MPa) with flow rate of 5.0 mL/min CO₂, a sharp spike at 10 Hz was obtained, which cannot be attributed to pump pulsations. The fixed frequency at 10 Hz must have its origin in the back-pressure regulator; since as the back-pressure is increased to 25 MPa, the spike simply vanishes and there is almost no noise in the chromatogram. Indeed, at a flow rate of 5 mL/min in a 254 μm tubing leading to the detector, pure CO₂ is under turbulent conditions ($Re > 2000$); however, the origin of noise is mainly from the oscillations of the needle in the back-pressure regulator as explicitly demonstrated by the Fourier transform of the chromatogram. It is well-known that the refractive index of CO₂ is highly dependent on the system pressure.^{146,157,161} For example, Shimadzu BPRs shows 10 and 15 Hz spikes; the Jasco shows a 10 Hz spike, and the Agilent BPR design shows no noise spike in the Fourier transform of the chromatographic data. Note that there is a new Jasco BPR not included in this study. To the best of our knowledge, Fourier transforms have never been reported for noise analysis in SFC, and it is an elegant approach for pin-pointing the sources of noise in ultrafast SFC. To illustrate the same concept, a retained chiral analyte (*N*-carboboxy-DL-norvaline) was used. Using 80:20:0.1 CO₂/MeOH/TEA, the peak elutes in 46 s ($k = 3.0$) at 10 MPa BPR; however, at 25 MPa BPR, the peak elutes in 36 s ($k = 1.1$). The noise pattern remains the same.

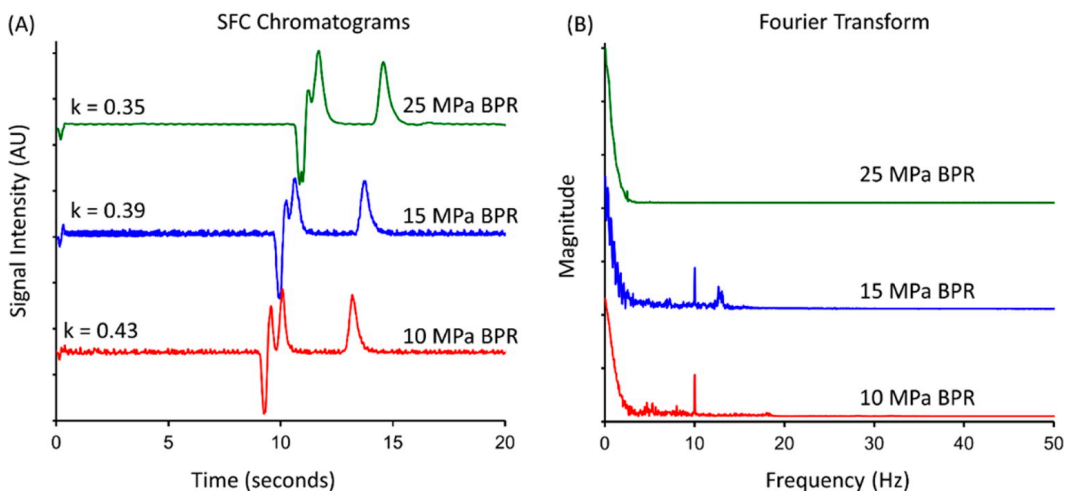


Figure 5.5. (A) Effect of backpressure regulator setting on the dead time, retention time, and baseline noise in ultrafast SFC. Toluene is used as a model analyte. (B) Fourier transform of the corresponding chromatograms (after injection disturbance). FT was performed on OriginPro 2015 software. Column: 5×0.46 cm i.d.; teicoplanin bonded $1.9 \mu\text{m}$ NPSD silica. Column temperature: ambient. MP: 100% CO_2 at 5 mL/min. Data sampling frequency, 100 Hz on XLC-3070 UV detector; 0.03 s response time. Connection tubings: $254 \mu\text{m}$.

5.4.4 Ultrafast Peak Shapes and the Choice of Digital Filters in SFC

Regardless of the source of noise, there are digital filters embedded in all chromatography softwares to eliminate high frequency components of the chromatographic signals. Noise in SFC becomes a problem when it comes to quantitative analysis since it degrades the signal-to-noise ratio. Most SFC manufacturers keep the digital filter information proprietary, and to the best of our knowledge, no comparison is available in the SFC literature on the performance of the filters under fast elution conditions. With each digital filter, a response time is associated with respect to a unit Heaviside step function (a function which suddenly jumps from 0 to 1).¹³³ The time it takes for the “filtered” signal to rise from 10% to 90% height of this unit step function is termed as the response time.¹³³ The Jasco SFC employs three known filters, namely, as

time accumulation (TA), RC, and “digital filter”. Although these terms were used in the instrument manual, the time accumulation refers to a moving average, RC is a numerical version of the classical resistor \times capacitor low pass filter, and the so-called “digital filter” is a Gaussian kernel (Gaussian weighted moving average). Three response times are allowed (Fast, 0.05 s; Standard, 1 s; Slow, 3 s) with TA and RC.

The obvious choice of response times is to choose the smallest number (Fast setting) for rapidly eluting peaks or with high flow rates. As shown in Figure 5.6, the peak shapes of “time accumulation” and RC filters are different even though their response times are *identical*. Each filter convolutes the peak shape in a different fashion. The SFC peaks were fitted as exponentially modified Gaussian peaks in PeakFit software followed by moment analysis. The plate count of the filtered data by TA shows 2800 plates for the first enantiomer and 1700 plates for the second one under optimum conditions. The RC filter with the same response time shows the respective efficiencies as 1980 and 1100 for the two enantiomers. The standard deviation of the baseline is almost the same in both filters under fast conditions, i.e., ± 38 vs ± 39 signal units for a period of 24 s. With a slower response time of 1 s, both TA and RC filters become useless (plates degrade to 980 for TA and 450 for RC). The Gaussian kernel was found to be using a very large window for weighted averaging and was not investigated further. Note that the apparent retention times also increase for TA and RC filters. Out of several types of moving averages, only the centered moving average does not change the retention time.¹³³ This type of filtering is present in Agilent SFCs, where increasing the response time does not alter the peak retention time at all. Clearly, Jasco appears to be using a simple moving average, where retention times are expected to increase as higher response times are chosen. One major drawback of the RC filters is that they introduce an exponential decay type tail which distorts the symmetry of the peak.¹³³ It seems that RC type filters may not be suitable for very fast SFC, especially when they are designed to do heavy filtering since tailing is introduced and the retention shifts to longer times (see Figure 5.6).

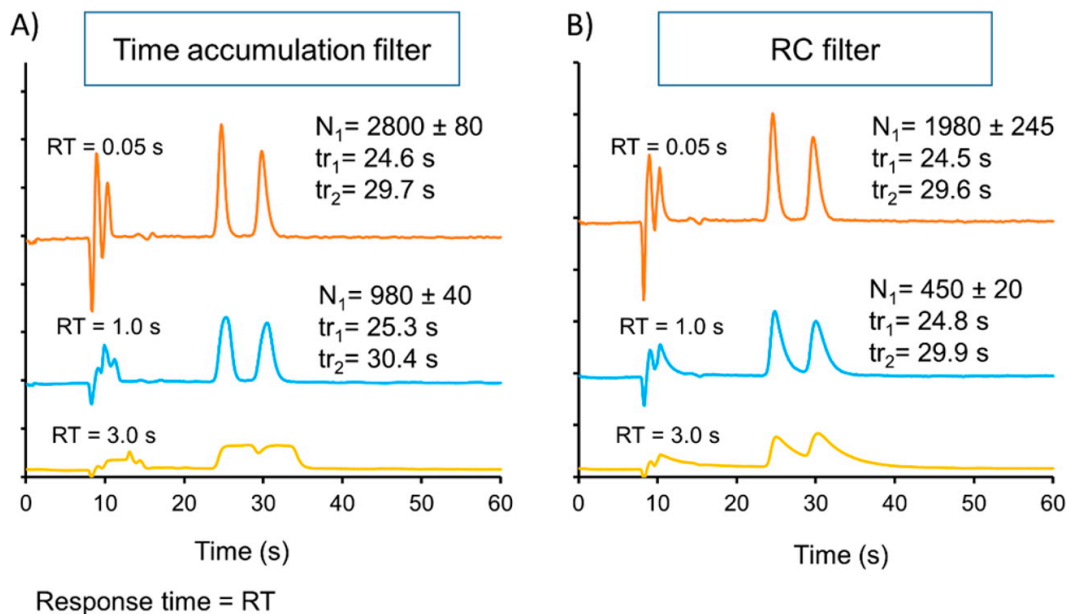


Figure 5.6. Comparison of digital filters in Jasco SFC for a chiral probe (3-phenylphthalide). The efficiencies represent the moment analysis of exponentially modified Gaussians using PeakFit program. Column: 5×0.46 cm i.d.; teicoplanin bonded $1.9 \mu\text{m}$ NPSD silica. Column temperature: ambient. MP: 90:10 CO_2/MeOH at 5 mL/min. Data sampling frequency: 100 Hz (on UV 2075). Connection tubings: $254 \mu\text{m}$.

5.4.5 Not All “Identical” Sampling Frequencies Are Created Equal

Shannon’s theorem imposes a lower theoretical limit on sampling frequency as $2\times$ highest frequency components of the signal, but there is no upper bound on sampling frequency.¹⁶² The higher the sampling frequency, higher is the noise level.^{113,133,163} The sampling frequency should be chosen in such a way that the signal-to-noise ratio is not severely degraded for the smallest peak in the chromatogram.¹³³ Two different UV SFC detectors (UV-2075 and X-LC-3070 UV) with “100 Hz” frequency were examined (see the Experimental Section). The obvious choice was to use the X-LC-3070 UV for performing fast eluting peaks since it has the fastest available response time (0.03 s) as compared to 0.05 s for UV-2075. 1,3 Dinitrobenzene (1,3 DNB) was chosen as a model analyte, which eluted on a teicoplanin column in 8 to 9 s. Figure 5 A shows the

chromatogram of 1,3 DNB along with its time derivative to magnify the signal changes. Even at 10 mL/min, 2750 plates were obtained on the 5 cm column. As the figure shows, the baseline is noisy (± 281 signal units) and the peak has some superimposed ripples. Fourier transform of the chromatogram showed a spike at 10 Hz (c.f. Figure 5). This observation supports the conclusion that the 10 Hz spike, seen in the FT, is not flow rate dependent, but rather, it is a function of the BPR setting and its design. Hence, the noisy baseline is certainly due to the BPR rather than turbulence in the detector or postcolumn tubings, as commonly perceived.^{142,143} For comparison, a pure Gaussian peak was simulated at 100 Hz ($\sigma = 0.153$ s). A “noiseless” Gaussian peak should produce a smooth derivative of the same shape as shown in Figure 5.7 B.

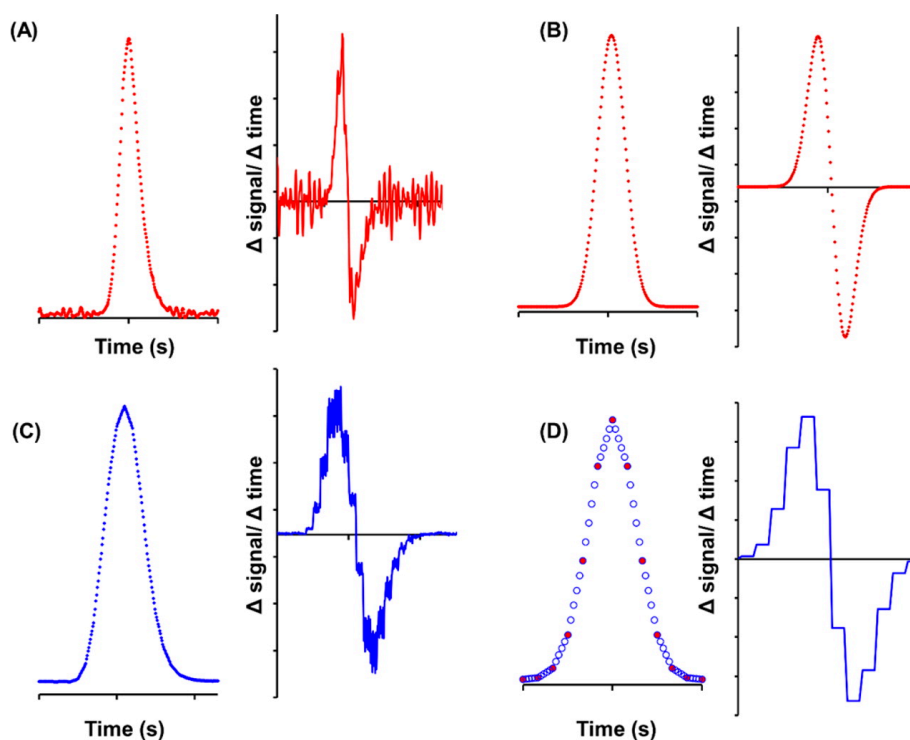


Figure 5.7 Assessment of peak shapes on two detectors used in SFC (UV 2075 and XLC 3070 UV). Column: 5 × 0.46 cm i.d.; teicoplanin bonded 1.9 μm NPSD silica. Column temperature: ambient. MP: 90:10 CO₂/MeOH at 10 mL/min. Back pressure regulator was maintained at 10 MPa. 1,3 Dinitrobenzene elutes in 8 to 9 s. (A) Close-up of 1,3

dinitrobenzene peak and the corresponding time derivative on a real sampling frequency of 100 Hz on XLC 3070 UV (0.03 s response time). (B) Simulated Gaussian peak at 100 Hz with its corresponding time derivative. (C) Close-up of 1,3 dinitrobenzene on upsampled data at 100 Hz with its corresponding time derivative on UV 2075 detector (0.05 s response time). (D) Simulated Gaussian peak upsampled from 20 Hz (red circles) to 100 Hz (blue circles) by linear interpolation (MATLAB 2010Ra) with its corresponding time derivative. Both detectors have the same cell volume (4 μ L). Connection tubings: 254 μ m.

For comparison, the UV-2075 was operated under the same conditions as the previous detector (100 Hz sampling rate, Figure 7C). There was a remarkable decrease in the baseline noise despite the fact that the response times are not significantly different (0.03 s vs 0.05 s). The standard deviation of the baseline noise is ± 47 (83% reduction in noise). The plate count of 1,3 DNB was 1280, which is ~ 1500 plates less than the aforementioned detector. Examination of the peak profile showed a very interesting feature on the peak apex as well as the peak base. The peak appeared to be segmented at many points. Similarly, the derivative of the peak is different from X-LC-3070 UV (and two other UHPLC instruments tested). The time derivative of the peak showed horizontal steps which indicated that the slope was constant in some regions of the peak. This segmentation indicated a linear interpolation of the sampled data, in which two widely spaced data points are interpolated to artificially increase the experimental sampling frequency to any desired sampling frequency. This process is known as upsampling and is well-known in the field of digital signal processing of audio signals.¹⁶⁴(36) To the best of our knowledge, this is the first discussion of the effect of upsampling in the chromatographic literature. In order to confirm our hypothesis, a narrow peak ($\sigma = 0.08$ s) was simulated which eluted in 8 s (Figure 7D). The actual data at 20 Hz is shown in red

points whereas the blue circles indicate the profile of the upsampled peak. The peak profile is similar to the peak shown in Figure 7C. The derivative of this “noiseless” linearly interpolated result shows the same pattern of steps (Figure 7D) as that seen in Figure 7C. What could be the plausible reason for upsampling in SFC? The Fourier transform of this chromatogram showed no spikes at 10 Hz. This clearly implies that the actual peak was not sampled at a true 100 Hz; because if it were, it would have picked up the noise from the back-pressure regulator. It appears that interpolation was used to eliminate noise in SFC. Some instruments such as the Agilent systems do downsampling; i.e., the actual data is collected at a much higher rate and later averaged to appear at lower frequencies. Downsampling also decreases the noise. In this specific case of the Jasco SFC, upsampling had the beneficial effect of eliminating the 10 Hz noise from the BPR which resulted in unwanted ripples on the peak. While these parameters may not matter in routine work, they must be kept in mind when doing ultrafast separations, since segmentation was seen in ultrafast peaks only. The data acquisition rate of having 20 points per peak is a popular number in chromatographic literature without a solid theoretical justification.¹³³(3) Since the peaks in both detectors are more than 1 s wide, there are more than 100 points per peak on both detectors. However, the retention time, peak shape, and plate counts are different. The sampling frequencies on the two detectors appeared the same in software; clearly, all identical sampling frequencies are not created equal. Researchers engaged in ultrafast chromatography need to be aware of these data acquisition artifacts.

5.5 Conclusions

The results herein clearly demonstrate the small particle advantage in ultrafast chiral and achiral supercritical/subcritical fluid chromatography. The enhanced fluidity of mobile phases containing carbon dioxide do not impose pressure limitations encountered in

UHPLC on short columns. A careful choice of connection tubing is needed to achieve the highest efficiency and to maximize resolution. The connection tubings, unlike in UHPLC, change retention time, as well as peak shapes. Each tubing showed a different optimum linear velocity. With low viscosity eluents, turbulence exists in the connection tubings, but the major contributor to noise in SFC comes from back-pressure regulators. Fourier transform proved to be an extremely powerful way to analyze the sources of noise in the SFC BPRs. Different instruments show the presence of either single or multiple frequencies. Similarly, researchers engaged in SFC need to be aware of the nature of digital filters embedded in the software, and the symmetric moving average (along with Gaussian or Hamming weights) is one of the best filters. It is shown for the first time that some instruments may not have the “real” sampling frequency but rather the data consists of (linearly) interpolated or upsampled data points. The derivative test proposed here is a simple yet powerful approach to detect linear interpolation in the signal processing of chromatography instruments.

Chapter 6

Salient Sub-Second Separations

6.1 Abstract

Sub-second liquid chromatography in very short packed beds is demonstrated as a broad proof of concept for chiral, achiral, and HILIC separations of biologically important molecules. Superficially porous particles (SPP, 2.7 μm) of different surface chemistries, namely, teicoplanin, cyclofructan, silica, and quinine, were packed in 0.5-cm-long columns for separating different classes of compounds. Several issues must be addressed to obtain the maximum performance of 0.5 cm columns with reduced plate heights of 2.6 to 3.0. Modified UHPLC hardware can be used to obtain sub-second separations provided extra-column dispersion is minimized and sufficient data acquisition rates are used. Further, hardware improvements will be needed to take full advantage of faster separations. The utility of power transform, which is already employed in certain chromatography detectors, is shown to be advantageous for sub-second chromatography. This approach could prove to be beneficial in fast screening and two-dimensional liquid chromatography.

6.2 Introduction

One of the basic tenets of separation science is to achieve adequate resolution in the shortest possible time. Not surprisingly, the relative meaning of “shortest possible time” has evolved over five decades, where early separation of biological molecules in 30–60 min was once considered fast liquid chromatography.^{153,165} By current standards, ultrafast liquid chromatography is usually considered as sub-minute separations—although the lower limit will continue to decrease with developments in smaller particle synthesis, improved packing technologies, design of the column hardware, and peak detection

methods.^{113,133} Recently, researchers have shown unprecedented separation speeds of 4–5 s in packed beds by using high efficiency particles for both achiral and chiral separations in liquid chromatography as well as supercritical fluid chromatography.^{15,115,124,163,166} It is not uncommon to obtain plate heights $H < 2d_p$ (d_p = particle diameter) with superficially porous particles (SPP) or fully porous sub-2- μm particles with exceptionally narrow size distribution.¹⁶⁷ The excellent performance of the former arises from lower contributions to eddy dispersion in the band broadening processes.⁸⁷ These efficiencies are providing an impetus to separation scientists to push the boundaries of analysis speed by utilizing very short columns. Ultrafast liquid chromatography is a very promising approach for high throughput screening methods¹⁶⁸ or in two-dimensional chromatography of complex samples where it is necessary to have high speed separations in the second dimension.^{23,169,170}

To date, ultrahigh speed separations of a few seconds or as low as milliseconds have been achieved in special electrophoretic microchip plates or in capillary zone electrophoresis.¹⁷¹⁻¹⁷⁴ Other approaches such as shear driven chromatography and wide bore hydrodynamic separations have also shown some promise in this regard.^{175,176} Special detection technologies were employed such as on-column detection followed by image processing to extract the peak profile.^{172,177} Handling of rapidly eluting peaks in the domain of conventional liquid chromatography is currently hindered by extra-column dispersion and even the data sampling rates on many commercial UHPLCs. The ideal chromatographic output from extremely high efficiency columns and fast eluting peaks is convoluted by several factors. The shape of the injector pulse, the cup-flow distribution pattern of the inlet and outlet frits, diffusion and mixing in plumbing unions, flow profiles in the tubings, data sampling rate, and embedded noise suppressing algorithms in any chromatographic setup all affect the true peak shape in deleterious

ways.^{133,178} Second, in the majority of UHPLCs, the maximum flow rate is limited to 2–5 mL/min, which is another factor limiting separation speed.

The aim of this work is to analyze the conceptual and practical aspects of sub-second separations on state of the art ultrahigh performance instruments using 0.5 cm packed columns with 2.7 μm SPP particles. We discuss and propose simple instrumental modifications and simple mathematical approaches allowing chromatographers to circumvent the challenges in ultrafast LC (*vide supra*) and obtain sub-second separations. The shortest possible analytical column dimensions available commercially (0.5 \times 0.46 cm i.d.) are used with four different chemistries (silica, cyclofructan-6, teicoplanin, and quinine bonded phases). These column chemistries are compatible with normal, reversed phase, HILIC, and polar organic/ionic modes and are used for a broad proof of concept. The polar organic mode uses ACN as a major component of the mobile phase, while MeOH is used to adjust the retention time with small amounts of acid/base additives to modify the selectivity.

6.3 Experimental Section

6.3.1 Materials

All HPLC solvents, buffers, and analytes were obtained from Sigma-Aldrich (St. Louis, MO). The 2.7 μm superficially porous particles with 1.7 μm core diameter and 0.5 μm shell thickness were provided by Agilent Technologies (Wilmington, DE). Surface area of the particles is 120 m^2/g , and pore diameter is 120 Å. Mobile phase compositions are given as volume/volume (v/v). The pH and mobile phase additive concentrations are given for the aqueous portion of the mobile phase before mixing with an organic modifier, and all experiments were conducted at room temperature.

6.3.2 Stationary Phases

The stationary phase materials were synthesized by AZYP LLC (Arlington, TX). Teicoplanin, cyclofructan-6, and quinine-based stationary phases were prepared according to the reported methods.^{9,12,179} The stationary phase material was either packed into 0.5 cm × 4.6 mm i.d. empty guard columns by Agilent Technologies, (Wilmington, DE) or packed in our laboratory using dispersed slurry techniques and pneumatic pumps. Superficially porous silica (2.7 μm) guard columns were purchased from Agilent Technologies. As reported earlier,¹¹³ it was found that dispersed suspensions of core-shell particles produced optimum results with pressures of 10 000 psi. These pressures were necessary to stabilize the bed against high flow rates (5 mL/min max on the UHPLC) for sub-second chromatography. For further characterization of the column volume (and to estimate the dead times), pycnometry was performed using the density difference method with water and methanol ($n = 3$).¹⁸⁰ The dead volumes of the column were found to be 75, 69, and 75 μL for SPP silica, SPP teicoplanin, and SPP quinine, respectively. Therefore, at 5 mL/min, the average dead time of the SPP guard column (in Agilent's hardware) would be 0.83 to 0.89 s. These dead times are consistent with the elution time of acetone under HILIC mode conditions.

6.3.3 Instrumentation

The Agilent 1290 UHPLC is equipped with a degasser, quaternary pump, autosampler, temperature controlled column compartment, and diode array detector. The instrument was controlled by OpenLabs CDS ChemStation software (Rev. C.01.06 [61], Agilent Technologies 20012014) under Microsoft Windows 8.1. In order to operate the instrument at the highest flow rate possible (5.0 mL/min, without pressure restriction), the in-line filter was removed. The pump outlet was directly connected to a presaturator column (5 × 0.46 cm i.d.) filled with silica (M.S. Gel, D-50-120A, AGC SciTech Co., Ltd.). This column has two roles (a) to act as a filter and (b) to saturate the incoming mobile phase with

dissolved silica before it hits the analytical column. This process ensures the long life of a column without any back-pressure. The autosampler and the column oven were bypassed. The presaturator column outlet was then connected to a Rheodyne 7520 manual injector (Rheodyne LLC, Rohnert Park, CA) with an internal loop size of 1 μ L. Full loop injections were made. The Rheodyne was connected to the column via 7 cm \times 75 μ m Nanoviper tubing and the column outlet was directly inserted into the UHPLC detector flow cell. The column consists of a 0.5-cm-long barrel with a permanently sealed frit at one end followed by a 3 cm \times 120 μ m stainless steel extension. The detector has a dispersion volume $V(\sigma)$ of 1 μ L (G4212–60008). Although smaller flow cells are available (0.6 μ L dispersion), there is potential of bursting the flow cell with compressible mobile phases at high flow rates. The retention times were determined with respect to the pressure pulse generated by manual injection.

Data Processing

Peak deconvolution and fitting of the peaks as exponentially modified Gaussians (EMG) and moment analysis were performed on PeakFit software v4.12.

6.4. Results and Discussion

6.4.1 Preparation and Characterization of Short 0.5 cm \times 0.46 cm i.d. Columns

In order to achieve sub-second liquid chromatography, short 0.5 cm columns were chosen. There is a question of which column diameter is best. Potentially, the narrow i.d. columns (0.21 or 0.30 cm i.d.) would provide very high superficial linear velocities at the maximum flow rates in the UHPLC; e.g., at 5 mL/min the superficial linear velocities in 0.46, 0.30, and 0.21 cm i.d. columns would be 0.501, 1.17, and 2.40 cm/s, respectively. It might appear that the 0.21 cm i.d. format would be the most suitable diameter for ultrafast separations. Unfortunately, the practical difficulties encountered in packing a 0.21 cm i.d.

column and minimizing the extra-column effects override the benefits of narrow bore columns currently. Even in the long column format for superficially porous particles, the 0.21 cm i.d. columns achieve about 60% of the plates of the 0.46 cm i.d. format. For further work, 0.5 cm × 0.46 cm i.d. columns were chosen for slurry packing, since the wall effects are virtually negligible in 0.46 cm i.d. columns.

6.4.2 Is the Sampling Frequency Available for Sub-Second Chromatography?

For sub-second chromatography, it was necessary to simulate the separation and assess the required sampling frequency based on the efficiencies observed in the 0.5 cm columns. Shannon's theorem dictates that in order to accurately capture the analytical signal, the minimum sampling frequency must be equal to twice the maximum frequency components in the signal being acquired.¹⁶² In Figure 6.1 A, we simulate two sub-second Gaussian peaks in the presence of root-mean-square noise of ± 0.06 units. This is the typical noise expected in a modern UV UHPLC detector. The plate counts of 0.5 cm column (150–200 per second) were set on the basis of realistic numbers obtained under very high flow rates (~ 5 mL/min). In order to extract the frequency components of such signals, Fourier transform (FT) of this simulated chromatogram was done. As the FT shows, >95% of the useful chromatographic information is under 15 Hz. Shannon's theorem guides us to sample the data at a minimum of 2×15 Hz; therefore, 40 and 1000 Hz should be sufficient as shown in Figure 6 C and D. Note the number of points is less than 20 points per peak in the 40 Hz chromatogram. Two modern UHPLCs can sample the data up to 160 to 250 Hz, respectively. In the near future, ever higher efficiencies are likely in very short columns, and then even these sampling frequencies and response times may be insufficient in sub-second chromatography. The Agilent's UHPLC employed here couples the sampling frequency with a rather sophisticated undisclosed digital filter which behaves very closely to a centered moving average with Gaussian weights.¹³³

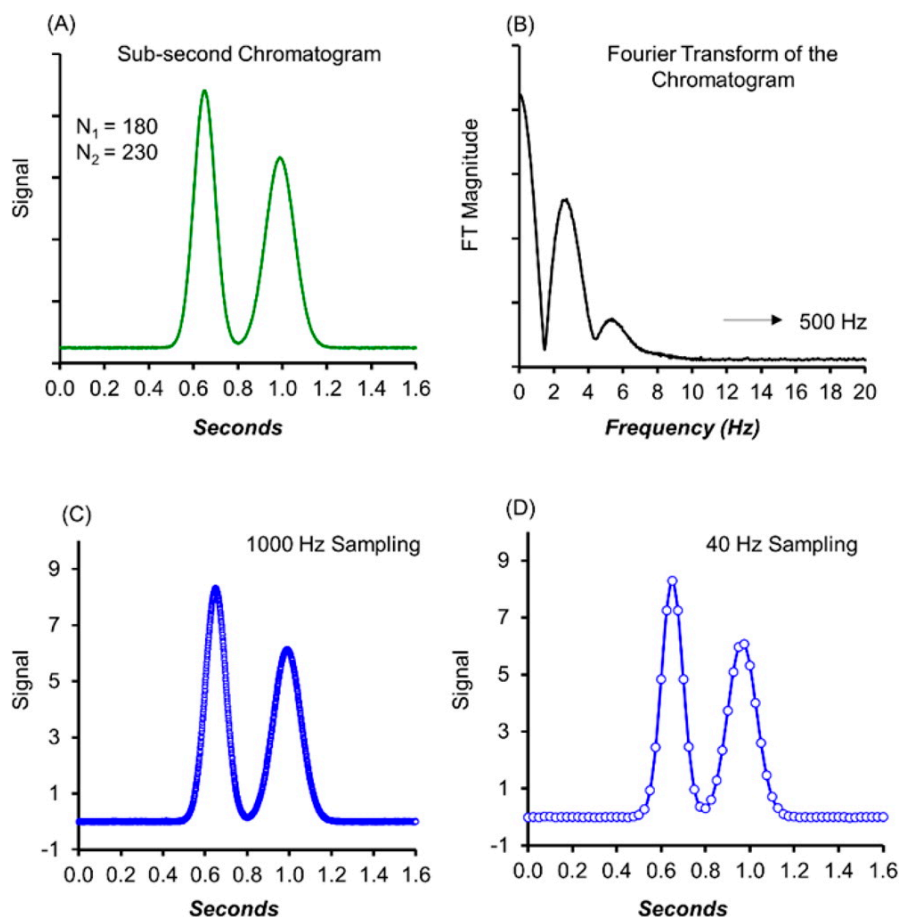


Figure 6.1. Computer simulation of a sub-second separation with RMS noise of ± 0.06 under a second in (A) time domain, (B) frequency domain via Fourier analysis, (C) time domain signal at 1000 Hz of sampling frequency, and (D) time domain signal at 40 Hz of sampling frequency. Computer simulations are done with OriginPro 2015 (Origin Lab Corporation, MA).

6.4.3 Hardware Considerations in Sub-Second Chromatography

To achieve ultrafast separations in packed 0.5×0.46 cm i.d. columns, packing approaches and extra-column dispersion of UHPLC needed extensive optimization. The most convenient approach to making very short columns is to pack the superficially porous particles in available (empty) guard columns using dispersed slurry

techniques.¹²⁹(31) On the basis of the previously optimized hardware¹¹³(4) (low dispersion UHPLC autosampler, 25 cm × 75 μm tubing, and 1 μL detector), 600–700 plates at optimum flow rates (0.8 mL/min) were considered as well-packed columns, as shown in Table S2. This efficiency (N) corresponds to H ~ 2.3dp to 3.0dp without subtracting any source of dispersion. For column lengths of 0.5 cm, the extra-column dispersions on any state of the art UHPLC cannot be ignored.¹⁵³(2) Assuming all the extra-column volumes behaved as a perfect mixer,¹⁵³(2) the extra-column variances were estimated to be 2.2 μL². The second moment analysis also confirmed that the extra-column variance was only ~11% of the chromatographic peak variance at low flow rates. Despite this ultralow dispersion, there is an additional fundamental challenge with very short connection tubings (3 and 7 cm) employed in this work. Indeed, the Aris-Taylor Gaussian dispersion breaks down because of short residence time of the analyte in the tubings.¹⁸¹(32) The eluting peaks (in the absence of column) were observed to produce non-Gaussian tailing profiles, as predicted by Golay along with a “foot” at the tailing end.¹⁸¹(32) The “foot” or the hump is marked with an arrow in Figure 2C. It is interesting that this peak shape fits neither an exponentially modified Gaussian (EMG) nor other empirical versions of peak fitting software (PeakFit v 4.12) such as the “Half Gaussian Modified Gaussian (GMG)” models or their hybrids (EMG-GMG). Obviously, even those relatively poor fit models (R² ~ 0.98) show that the second moment is higher in terms of square microliters than the second moment at low flow rates (0.8 mL/min). Similar peak shapes with a “foot” in the tailing region without columns were reported by Gritti et al.⁸(33) The tailing envelope may be superimposed on the band profile eluting from very short columns. A simple but elegant approach for overcoming such fundamental challenges in sub-second chromatography is outlined in the last section of this article.

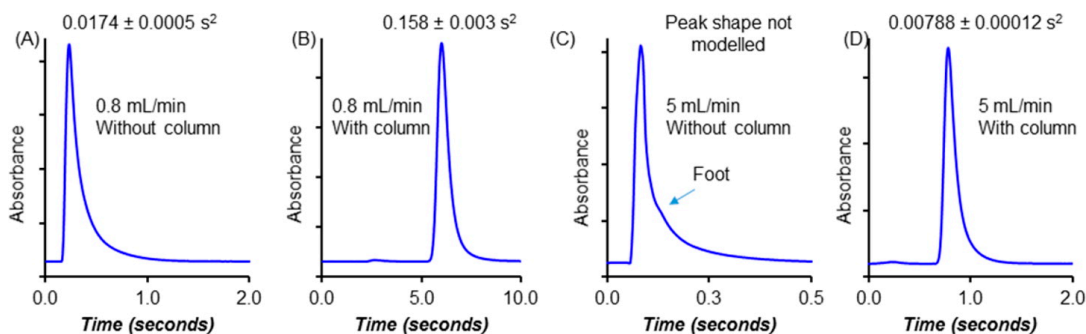


Figure 6.2. Demonstration of effect of extra column effect originating from short connection tubing. Chromatographic conditions: column, 0.5 cm × 4.6 mm i.d. 2.7 μ m core-shell silica guard column (Agilent Technologies); mobile phase, ACN/water (80:20); analyte, thymine; connection tubing, 70 mm × 75 μ m i.d. NanoViper (A) at 0.8 mL/min without the column, (B) at 0.8 mL/min with the column, (C) at 5.0 mL/min without the column, and (D) 5.0 mL/min with the column (second moments are given with the corresponding peak).

6.4.4 Examples of Sub-Second Chromatography

Examples of several different chiral and nonchiral sub-second separations in various chromatographic modes are given in Figure 6.3 and Table 6.1. Baseline sub-second separations are more easily achieved when the first analyte elutes before the dead time, e.g., due Donnan exclusion. The separation window becomes small between the dead time and 1 s. However, this upper 1 s limit is arbitrary in this work, and ultrafast separations can be readily achieved in a few seconds.^{113,166} Using a flow rate of 5 mL/min, the dead time is estimated to be ~0.8 s from pycnometric measurements on the silica column. Figure 6.3A shows the enantiomeric separation of N-(3,5-dinitrobenzoyl)-DL leucine on a SPP quinine phase. In Figure 6.3B, a HILIC mode separation of mellitic acid from benzamide is shown. Note that mellitic acid is repelled from the stationary

phase. Similarly two dipeptides, Glu-Asp and Gly- β Ala, are baseline separated on the teicoplanin bonded SPP column (Figure 6.3C). Examples of four additional pairs of dipeptides are shown in Table 6.1. In Figure 6.3D, we show that it is possible to perform ultrafast screening by resolving three peaks (two sulfonic acids and a derivatized amino acid) under a second using the methods outlined in the next section. A doubly charged sulfonic acid is repelled from the stationary phase like mellitic acid. It is also important to have retention time reproducibility for sub-second separations. Using the HILIC mode, six injections were made and retention times calculated for mellitic acid and 4-aminosalicylic acid. The percent RSD for the retention time of both peaks was found to be <2% (see Supporting Information).

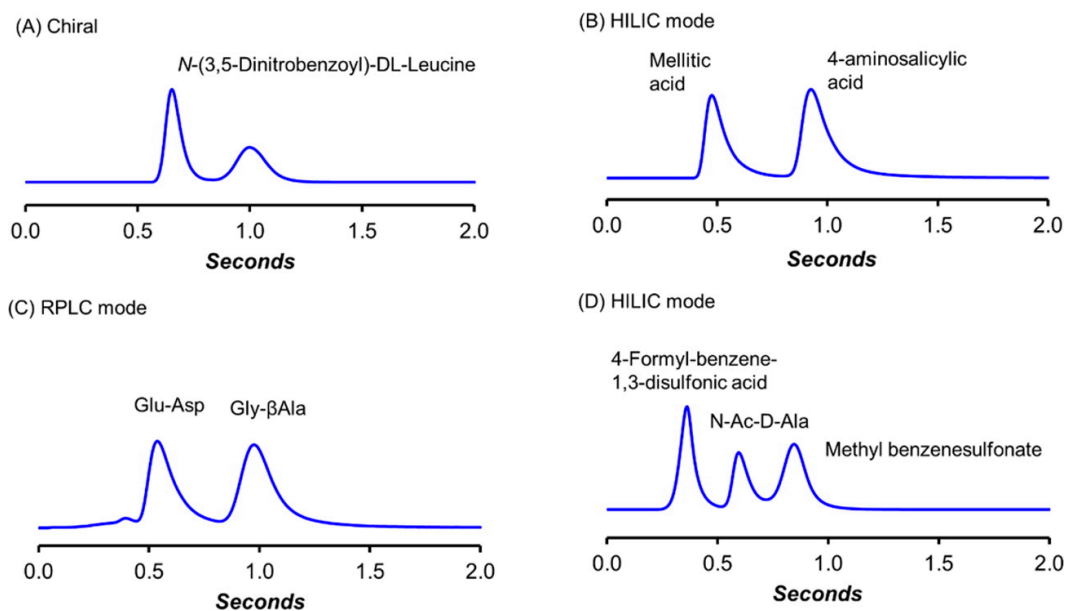


Figure 6.3. Sub-second chromatography on various stationary phases using 0.5×0.46 cm i.d. columns: (A) SPP Quinine, 70:30 (ACN/20 mM $\text{NH}_4\text{CO}_2\text{H}$), 5 mL/min; (B) SPP silica, 94:6 (ACN/15 mM $\text{NH}_4\text{CH}_3\text{CO}_2$), 5 mL/min; (C) SPP Teicoplanin, 42:58 (ACN/20

mM NH₄CO₂H), 5 mL/min; (D) SPP Teicoplanin, 70:30 (ACN/water), 5 mL/min. Data sampling rate 160 Hz. For parts A and D, see next section on power transforms.

Table 6.1 Sub-Second Screening for Achiral, Chiral in Various Chromatographic Modes

Analyte	Chromatographic conditions (stationary phase, mobile phase, and flow rate)	t _{R1} (s)	t _{R2} (s)	Rs*	Rs*
<i>Chiral separations</i>					
1. DNPyr-DL-Leucine	Teicoplanin, 60:40 (MeOH:20 mM NH ₄ CO ₂ H), 5 mL/min	0.56	0.91	1.2	1.6
2. DNPyr-DL-Norvaline	Teicoplanin, 70:30 (MeOH:20 mM NH ₄ CO ₂ H), 5 mL/min	0.66	1.00	1.4	1.9
3. (±)-4-Methyl-5-phenyl-2-oxazolidinone	Teicoplanin, 100% MeOH	0.60	0.98	1.5	2.1
4. N-Acetyl-Alanine	Teicoplanin, 40:20:40 (MeOH: ACN: 5 mM NH ₄ CO ₂ H), 4 mL/min	0.56	0.99	1.5	2.2
5. N-(3,5-Dinitrobenzoyl)-DL-Leucine	Quinine, 70:30 (ACN:20 mM NH ₄ CO ₂ H), 5 mL/min	0.66	0.98	1.3	1.6
<i>Achiral separations - HILIC mode</i>					
6. Mellitic acid + Benzamide	Cyclofructan, 95:5 (ACN:15 mM NH ₄ CH ₃ CO ₂), 5 mL/min	0.49	0.90	2.5	2.5
7. Mellitic acid + Benzamide	Silica, 95:5 (ACN:15 mM NH ₄ CH ₃ CO ₂), 5 mL/min	0.48	0.91	2.4	3.5
8. Mellitic acid + 4-Amino salicylic acid	Silica, 94:6 (ACN:15 mM NH ₄ CH ₃ CO ₂), 5 mL/min	0.48	0.93	1.8	3.9
9. Mellitic acid + 2,3-dihydroxybenzoic acid + 4-Amino salicylic acid	Silica, 94:6 (ACN:15 mM NH ₄ CH ₃ CO ₂), 5 mL/min	0.48	0.66 (t _{R3} = 0.93)	1.2 1.1	2.6 2.8
10. 4-Formyl-benzene-1,3-disulfonic acid + N-Ac-D-Alanine + Methyl benzenesulfonate	Teicoplanin, 70:30 (ACN: Water), 5 mL/min	0.40	0.61 (t _{R3} = 0.87)	1.2 1.1	1.9 1.7
<i>Achiral separations - Reversed phase mode</i>					
11. Acetylsalicylic acid + Salicylamide	Teicoplanin, 35:65 (ACN:20 mM NH ₄ CO ₂ H), 5 mL/min	0.60	0.94	1.8	2.5
12. Salicylic acid + Methylsalicylate	Teicoplanin, 40:60 (ACN:20 mM NH ₄ CO ₂ H), 5 mL/min	0.61	0.93	1.5	2.3
13. 4-Formyl-benzene-1,3-disulfonic acid +	Teicoplanin, 40:60 (ACN:20 mM NH ₄ CO ₂ H), 5	0.55	0.87	1.8	2.8

Methyl benzenesulfonate		mL/min				
14	Dansyl-Asp + Gly	Teicoplanin, 30:70 (ACN:Water), 5 mL/min	0.44	0.81	2.0	3.1
15	Asp-Asp-Asp-Asp + Gly-Gly	Teicoplanin, 33:67 (ACN:20 mM NH ₄ CO ₂ H), 5 mL/min	0.47	0.88	1.9	3.0
16	Asp + β-Ala	Teicoplanin, 35:65 (ACN:Water), 5 mL/min	0.44	0.78	1.8	2.7
17	Gly-Asp + Gly-Val	Teicoplanin, 26:74 (ACN:20 mM NH ₄ CO ₂ H), 5 mL/min	0.59	0.84	1.3	2.0
18	Asp-Asp + Gly-Trp	Teicoplanin, 42:58 (ACN:20 mM NH ₄ CO ₂ H), 5 mL/min	0.56	0.98	1.8	2.9
19	Glu-Glu + Gly-Leu	Teicoplanin, 40:60 (ACN:20 mM NH ₄ CO ₂ H), 5 mL/min	0.52	0.90	1.7	2.8
20	Glu-Asp + Gly-βAla	Teicoplanin, 42:58 (ACN:20 mM NH ₄ CO ₂ H), 5 mL/min	0.54	0.99	1.9	2.9

^aResolutions without power transformation.

^bResolutions with power transformation ($n = 2$).

6.4.5 The Effect of “Power Transform” in Sub-Second Chromatography

It can be noted that under ultrafast separations and short columns, the peaks are non-Gaussian (tailed) due to trans-column velocity biases in the tubings and frits as well as the particulate bed (*vide supra*). Additionally, if the peaks are eluting before the dead time (due to Donnan exclusion), the efficiencies of such peaks can be compromised. In Table 6.1, the efficiency of dansyl aspartic acid and glycine are 90 and 240, respectively. The former analyte elutes at 0.44 s, which is much before the dead time (0.8 s). Under the highest flow rates available on the UHPLC (5 mL/min), the 0.5 cm SPP columns provided about 150 to 200 plates. Using the simplest expression for peak capacity in the isocratic mode, and where there is a possibility of a peak eluting before the dead time, we can write the peak capacity (P) for a sub-second separation in a time span of 0.4 to 1.0 s (see Table 6.1), with a chromatographic resolution of 1 as¹⁸²

$$P = 1 + \int_{0.4}^{1.0} \frac{\sqrt{200}}{4t} dt = 1 + \left(\frac{\sqrt{200}}{4}\right)(\ln 1.0 - \ln 0.4) \approx 4$$

Using the same approach for the peak capacity for analogous higher efficiency separations, it is determined that for $N = 500$, $P = 6$, and for $N = 1200$, $P = 9$. In Table 6.4, we demonstrate the full potential of fitting three peaks under a second in the HILIC mode. The resolution (~ 0.6) is a result of the extra-column tailing effect alluded to above. The chromatographic profile of peaks can be deconvoluted into three exponentially modified Gaussians at 0.48, 0.68, and 0.93 s as shown in Table 6.4B. It is clear from the peak fitting model that tailing is causing this lowered resolution. It is known that raising Gaussian functions to any power ($n > 0$) still maintains them as Gaussian functions with an effect of reducing their standard deviations. Thus, squaring or cubing the output signal yields a peak at the *identical retention time* but with a narrower width (See R_s values in Table 6.1 and Table 6.4). It can be shown mathematically that for Gaussian peaks, the efficiency directly scales as the power n and the resolution scales as \sqrt{n} .¹⁸³ Such an approach is already embedded in some commercial detectors such as the evaporative light scattering detector without the user's control.¹⁸⁴ Recently, Thermo launched a UHPLC that allows the chromatographer to choose the power " n " to transform the chromatograms.

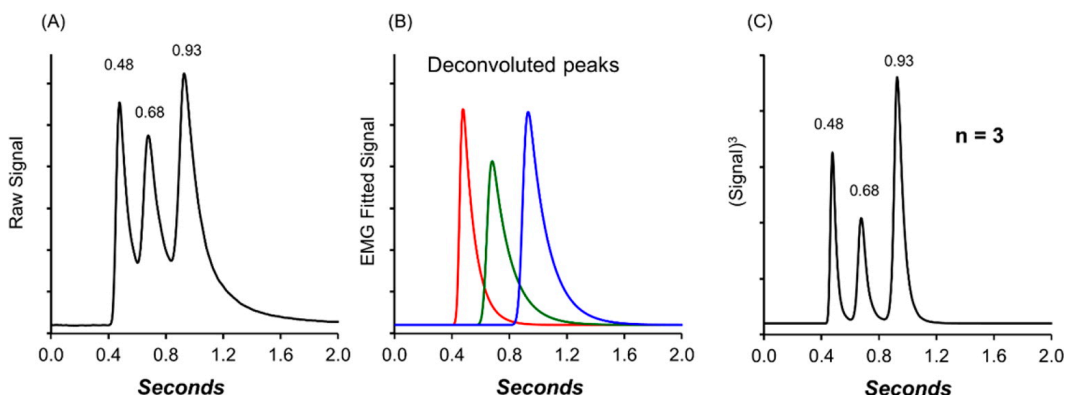


Figure 6.4 Application of power transforms in sub-second chromatography of three components (mellitic acid, 2,3-dihydroxybenzoic acid, and 4-aminosalicylic acid). (A) The original sub-second chromatogram. (B) Deconvoluted chromatogram into three exponentially modified Gaussian peaks. (C) Power transform with cubic of the original data. Column, 0.5 cm × 4.6 mm i.d. 2.7 μm SPP silica; mobile phase, ACN/15 mM ammonium acetate = 94:6 (v/v), 5 mL/min at 220 nm.

Figure 6.4C shows that if the same chromatographic data (y ordinate) is raised to a power of 3, the same separation can now be baseline resolved into three components. This approach is a very powerful method for extracting information for ultrafast screening purposes from a low resolution chromatogram, which is indeed the main purpose of sub-second chromatography. There is a caveat, however, in that the peak areas change in this power transformation as $A_{p,t} = Y_{max}^n (\sigma \sqrt{\frac{\pi}{n}})$, where $A_{p,t}$ is the peak area after applying the power n , Y_{max}^n is the maximum amplitude, and σ is the standard deviation of the peak.¹⁸³(35) Calibration curves constructed can be nonlinear if quantitation is desired.

6.5 Conclusions

The foundations of performing sub-second chromatography in small packed beds using superficially porous particles are outlined. Various modes of chromatography were demonstrated including reversed phase, HILIC, and chiral separations as a proof of concept. Detection and hardware challenges need to be further addressed. Although the sampling frequencies are adequate for the current efficiencies achievable in ultrafast chromatography, they may not be for future improved columns. The bigger challenge so far is the peak shapes due to non-Gaussian dispersion in short tubings, which can be circumvented by on-column injection and on-column detection technologies as is done in electrophoretic methods. Modern UHPLCs are limited to 2–5 mL/min flow rates at higher pressures (>500 bar), and this is less than desirable for these separations. Using power transforms on exponential functions (as those used for modeling peak shapes) is a very simple way to improve peak shapes, reduce variances, and decrease noise in sub-second screening.

Chapter 7

Ultrafast chiral separations for high throughput enantiopurity analysis

7.1 Abstract

Recent developments in fast chromatographic enantioseparations now make high throughput analysis of enantiopurity on the order of a few seconds achievable. Nevertheless, routine chromatographic determinations of enantiopurity to support stereochemical investigations in pharmaceutical research and development, synthetic chemistry and bioanalysis are still typically performed on the 5–20 min timescale, with many practitioners believing that sub-minute enantio- separations are not representative of the molecules encountered in day to day research. In this study we develop ultrafast chromatographic enantioseparations for a variety of pharmaceutically-related drugs and intermediates, showing that sub-minute resolutions are now possible in the vast majority of cases by both supercritical fluid chromatography (SFC) and reversed phase liquid chromatography (RP-LC). Examples are provided illustrating how such methods can be routinely developed and used for ultrafast high throughput analysis to support enantioselective synthesis investigations.

7.2 Introduction

The past few years have seen dramatic improvements in the speed of chromatographic enantioseparations.^{113,122,124,163,166,185} Long a preferred technique for analysis of enantiopurity to support enantioselective synthesis or bioanalytical investigations,^{186,187} chiral chromatography has evolved from typical run times of 20–40 minutes in the 1980s and 1990s to 5–10 minutes in the 2000s, to recent examples of ultrafast sub-minute separations, some taking only a few seconds.¹⁸⁸ A variety of factors have contributed to this speed revolution, including improved chiral stationary phases (CSPs),

instrumentation and chromatographic particle technology.^{52,163,166,188} Equally important has been a growing dissatisfaction with legacy methods that are poorly suited to high throughput experimentation,¹⁸⁹ and an emerging understanding of the theory and practice underlying ultrafast chromatographic separations. At this point in time “world speed records” for chromatographic enantioseparations of particular molecules are broken on a routine basis,^{124,166,185} and the whole movement toward fast chromatographic separations promises to significantly disrupt conventional workflows in enantioselective synthesis and pharmaceutical chemistry.

Ultrafast chiral chromatography offers a tremendous potential for high-throughput enantiopurity assays, with analysis time that is competitive with sensor-based analytical approaches.¹⁹⁰ Nevertheless, most researchers currently utilizing chiral chromatography as an analytical tool are still using analysis times of 5–10 min per sample. While these longer assays may be fine for the analysis of a few samples, they are poorly suited for research investigations involving screening and high throughput experimentation. In this study we investigate the ability to develop fast chromatographic enantioseparations for a variety of pharmaceutical-related drugs and intermediates, showing that sub minute separations are now possible in most cases. We illustrate how such methods can be routinely developed, and how ultrafast chromatographic enantioseparations can be used for high throughput analysis to support enantioselective synthesis investigations.

7.3 Experimental section

7.3.1 Instruments

Chiral SFC screening and optimization experiments were carried out on Waters Acquity UPC2 (Waters Corp., Milford, MA, USA) systems equipped with a fluid delivery module (a

liquid CO₂ pump and a modifier pump), a sampler manager – FL autosampler, two auxiliary column managers allowing six installed columns, a photodiode array detector, and MassLynx® software. Chiral reversed phase high performance liquid chromatography (HPLC) experiments were performed on Agilent 1200. The Agilent 1200 stack comprised of G1379B degasser, G1312B binary pump, G1367C HiP-ALS SL autosampler and G1315C diode-array detector. The system was controlled by Chemstation software. MISER (Multiple Injection in a Single Experimental Run) chiral SFC. Experiments were performed on an Agilent 1200 system with an Aurora SFC Control Module. The system comprised a modified G1322A vacuum degasser, a G1312A binary pump, a G1367B WPALS autosampler, a G1316A column compartment, and a G1315B diode array detector. The system was controlled by Open LAB CDS ChemStation Edition Rev. B.04.03 software. Chemicals and reagents. Methanol (HPLC Grade) was purchased from Fisher Scientific (Fair Lawn, NJ, USA). Compounds 24, 25 and 37 (single diastereomer) and 2-4, 7, 8, 11-13, 17-19, 22-24, 27-30, 32-35 and 38-40 were obtained from the Building Block Collection (Merck & Co., Inc., Kenilworth, NJ, USA). Ammonium formate (NH₄HCO₂), formic acid (HCOOH); perchloric acid (HClO₄), sodium perchlorate monohydrate (NaClO₄·H₂O), 1.0 M triethylammonium acetate buffer (TeAA), isobutylamine (IBA) and all other racemates used in this study were all purchased from Sigma–Aldrich (St. Louis, MO, USA), including compound 50: (2S,5S)-(-)-2-tert-Butyl-3-methyl-5-benzyl-4-imidazolidinone and (2R,5R)-(+)-2-tert-Butyl-3-methyl-5-benzyl-4-imidazolidinone. Ultrapure water was obtained from a Milli-Q Gradient A10 from Millipore (Bedford, MA, USA). Bone dry-grade CO₂ was obtained from Air Gas (New Hampshire, USA). Chiral Stationary phases. Columns packed with Chiralpak (AD, AS, IA, IB, IC, IC, IE, IF) and Chiralcel (OD, OJ, OZ) were purchased from Chiral Technologies (West Chester, PA, USA). Lux (Amylose-2 and Cellulose-4) columns were purchased from

Phenomenex (Torrance, CA, USA). (S,S)- Whelk-O1 column was purchased from Regis Technologies (Morton Grove, IL, USA). Trefoil™ AMY1 and Trefoil™ CEL1 columns were purchased from Waters Co. Teicoplanin (Teico-FPP), teicoplanin aglycone (TAG-FPP), vancomycin (vanco-FPP), isopropyl bonded cyclofructan LARIHC CF6-P (CF6-P-FPP), Hydroxypropyl- β -cyclodextrin (HPRSP-SPP) were obtained from AZYP LLC (Arlington, TX, USA). Chiral SFC screening conditions. Chiral SFC separations were carried out on a diverse set of columns described in table 1; 4.6 and 3.0 mm \times 150 mm length, 3 and 5 μ m columns by gradient elution at a flow rate of 3 mL/min with the backpressure regulator (BPR) set at 200 bar; 3.0 mm \times 100 mm length, Waters Trefoil AMY1 and CEL1 2.5 μ m columns: flow rate 2.5 mL/min, BPR 150 and flow rate 1.3 mL/min, BPR 150, respectively. The SFC eluents were solvent A: CO₂ and solvent B: 25 mM isobutylamine in MeOH. The mobile phases were programmed as follows: linear gradient from 1% to 40% B in 5, hold at 40% B for 1 min. For teicoplanin and teicoplanin aglycone the SFC eluents were solvent A: CO₂ and solvent B: MeOH at 2 mL/min BPR at 120, with similar gradient conditions as above. For LARIHC CF6-P column SFC eluents were solvent A: CO₂ and solvent B: 0.3-0.2 % (v/v) trifluoroacetic acid-triethylamine in MeOH, flow rate 2 mL/min, BPR 120. The column and samples were maintained at a temperature of 40 20 °C, respectively. Chiral RP-LC screening conditions. Chiral RP-LC separations were carried out on a diverse set of columns described in table 1. 4.6 mm \times 50 mm, 3 μ m and 1.9 μ m columns and 4.6 mm \times 30 mm 2.7 μ m column by gradient elution at a flow rate of 3.0 mL/min and 2 mL/min, respectively. 3.0 mm \times 50 mm, 5 μ m Whelk-O1: 0.8 mL/min. The LC eluents were solvent A: 1) 150 mM NaClO₄ in 0.02% HClO₄; 2) 2 mM NH₄HCO₂ solvent B : CH₃CN 3) 1 M TEAA buffer and solvent B: Methanol. The mobile phases were programmed as follows: linear gradient from 20% to 80% B in 10 min, hold at 80% B for 2 min for 3 μ m columns and 5% to 95% B in 10 min,

hold at 80% B for 2 min for 1.9 and 2.7 μm columns. The column and samples were maintained at a temperature of 25 °C and 20 °C, respectively. Calculation of resolution factor and estimation of optimal separation time. The resolution factor (R_s) referred to in this study was determined using the half-height method:

$$R_s = 2 (t_2 - t_1) / 1.7 (w_{0.5,1} + w_{0.5,2})$$

where t_1 and t_2 are the retention times of the two peaks of interest, and $w_{0.5,1}$ and $w_{0.5,2}$ are the peak widths measured at half height. The minimum separation time by column cutting ($t_{\text{min CC}}$) [4] was predicted using the following equation:

$$t_{\text{min CC}} = t_{2,s} \left(\frac{R_{st}}{R_{si}} \right)^2$$

where $t_{2,s}$ is the retention time of second peak and R_{si} is the resolution factor measured from the screening experiments, and R_{st} is the target resolution. Method Optimization. Ultrafast chiral separation methods were obtained by optimization of screening results for each racemic mixture. Calculation of the previously described $t_{\text{min CC}}$ term¹⁹¹ was used for easy selection of the best the best hits from screening conditions, and at the same time, to provide an estimate of the optimal time for ultrafast separations. Ultrafast enantioseparations by both RP-LC and SFC were achieved by optimizing mobile phase composition (by changing the gradient elution used in the screening methods to an isocratic elution), flow rate and column length. All ultrafast RP-LC and SFC chiral separations (figure 4) were performed at highest available sampling frequency and lowest available response time of the instrument. Enzymatic Ketoreductase Screening. Enzymes and cofactors were obtained from Codexis, Inc (Redwood City, CA). The substrate 1-benzyloxycarbonyl-3-pyrrolidinone was obtained from Sigma Aldrich. Enzymes were predosed into a multiwell plate, with 2 mg of enzyme in each well. Solutions of NAD(P) and NAD (1.11 mg/mL) were made by dissolving the appropriate cofactor in 0.1M

phosphate buffer at pH 7.0. A total of 450 μL of the cofactor was added to the enzymes, adding NAD(P) to wells A1-B10, and NAD solution to wells B11-B12. The plate was allowed to sit at room temperature for approximately 15 minutes until the enzyme had dissolved. A solution of the substrate (50 mg/mL) was prepared by dissolving the compound in a 1:1 mixture of DMSO and iPrOH. The substrate solution (50 μL) was then added to each enzyme in the multiwell plate, and the sealed plate was placed on a shaker at 35°C for 22 hours. After the reaction was complete, the enzyme was precipitated out by addition of 200 μL acetonitrile, and the solution was filtered. The solvent was removed from the filtrate by genevac, reconstituted in acetonitrile (200 μL per well), and subsequently analyzed by MISER chromatography. MISER chiral SFC experiment. A method for MISER chiral SFC analysis of reaction mixtures from enzymatic ketoreductase screening was developed by first carrying out chiral RP-LC and SFC screening, and method optimization as described above. MISER chiral SFC data acquisition was carried out using injector programming. Time between injections was 50 sec. Separations were performed on a 4.6 mm \times 100 mm, 3 μm AD-3 column at a flow rate of 3.25 mL/min and an eluent composition of 65% CO₂ and 35% MeOH (25 mM IBA). The column and samples were maintained at a temperature of 40°C and 20°C, respectively.

7.4 Results and Discussion

The chromatographic enantioseparation of a group of 50 different racemates (shown in Figure 7.1) was investigated in order to gauge the generality of sub-minute chromatographic resolutions. Many of the compounds in the group come from a diverse standard set of chiral drugs and synthetic intermediates developed in our labs to assess performance and generality of new CSPs,¹⁹² a sample set that intentionally includes some difficult to resolve analytes such as compounds 11, 18, 24, 30, 38 and 39.

Additional challenging racemates such as ibuprofen (6), 1-tetralol (10) and compounds 3 and 19 were added to increase the range of functional group diversity within the set. In addition, the family of warfarin (41) and related hydroxylated metabolites (42–46) was included. Each of the 50 compounds was then subjected to method development screening using both chiral RP-LC and SFC. Our method development screening involves the use of a standard gradient elution (1 to 40 % organic modifier over 5min for SFC and 5 to 80 % over 10 min for LC) on a series of columns containing different chiral stationary phases (CSPs).

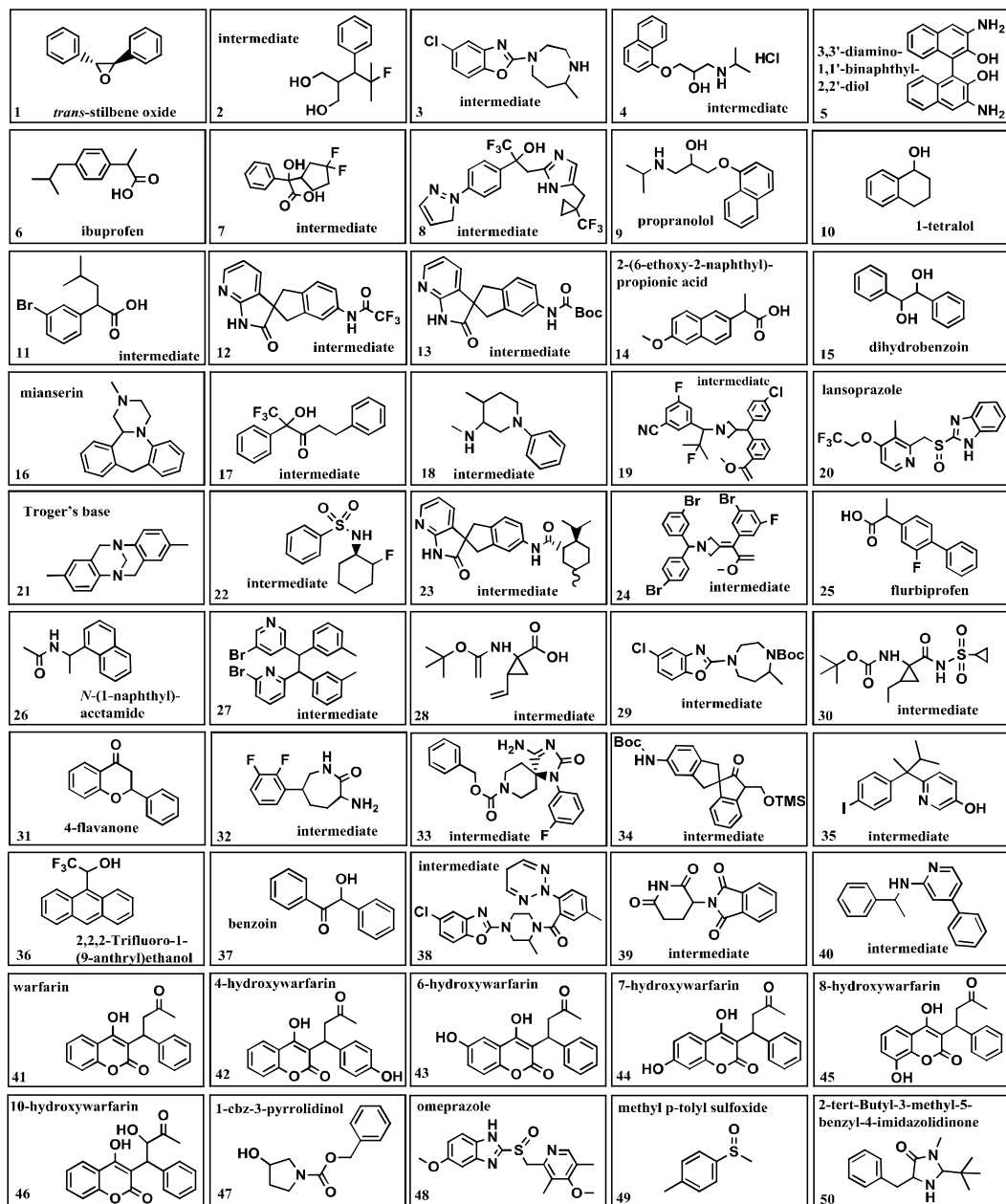


Figure 7.1 Structures of 50 pharmaceuticals and intermediates

The complete list of columns and conditions evaluated in the study is shown in

Table 7.1 total of 13 CSPs in RP-LC and 18 CSPs in SFC from different manufacturers (Waters Co., Chiral Technologies, Regis Technologies, Phenomenex and AZYP LLC) were selected for this evaluation. Most of these columns are conventional 2.5 and 3 mm coated and immobilized polysaccharide-based CSPs. Some other relatively new chiral selectors based on macrocyclic glycopeptide bonded to sub-2 mm fully porous particles (Teico, TAG and Vanco)^{5,16} or 2.7 mm fused-core particles (HPRSP)^{5,17} were included. Some of these CSPs can be used in either the RP-LC or SFC application modes without any performance degradation.

Table 7.1 Chromatographic columns used for chiral screening

Chiral Stationary Phase	Abbreviation	i.d. x length (mm)	Particle Size (µm)	Particle Type	Screening Mode and conditions
Hydroxypropyl-β-cyclodextrin	HPRSP-SPP	4.6 x 3.0	2.7	SPP	RPLC ^{a,b,c}
Vancomycin FPP	Vanco-FPP	4.6 x 5.0	1.9	*NPSD-FPP	RPLC ^{a,b,c}
Teicoplanin FPP	Teico-FPP	4.6 x 5.0	1.9	*NPSD-FPP	RPLC ^{a,b,c} SFC ^{4,5,6,7}
Isopropyl bonded cyclofructan(CF6-P) FPP	CF6-P-FPP	4.6 x 5.0	1.9	*NPSD-FPP	RPLC ^a , SFC ^{1,4}
Teicoplanin aglycone-FPP	TAG-FPP	4.6 x 5.0	1.9	*NPSD-FPP	RPLC ^{a,b,c} SFC ^{4,5,6,7}
Chiralpak AS-3R, AS-3	AS3	4.6 x 150	3	FPP	RPLC ^d , SFC ¹
Chiralpak AD-3R, AD-3	AD3	4.6 x 150	3	FPP	RPLC ^d , SFC ¹
Chiralpak OD-3R, OD-3	OZ3	4.6 x 150	3	FPP	RPLC ^d , SFC ¹
Chiralcel OJ-3R, OJ-3	OD3	4.6 x 150	3	FPP	RPLC ^d , SFC ¹
Chiralcel OZ-3R, OZ-3	OJ3	4.6 x 150	3	FPP	RPLC ^d , SFC ¹
Trefoil TM AMY1	T-AMY1	3.0 x 100	2.5	FPP	SFC ³
Trefoil TM CEL1	T-CEL1	3.0 x 100	2.5	FPP	SFC ²
Chiralpak IA	IA	4.6 x 150	3	FPP	SFC ¹
Chiralpak IB	IB	4.6 x 150	3	FPP	SFC ¹
Chiralpak IC	IC	4.6 x 150	3	FPP	RPLC ^d , SFC ¹
Chiralpak IE	IE	4.6 x 150	3	FPP	SFC ¹
Chiralpak IF	IF	4.6 x 150	3	FPP	SFC ¹
Lux Amylose-2	Lux-2	4.6 x 150	3	FPP	SFC ¹

Lux Cellulose-4 (S,S)-Whelk-O1	Lux-4 Whelk-O	4.6 x 150 3.0 x 150	3 5	FPP FPP	RPLC ^d , SFC ¹ RPLC ^e , SFC ¹
-----------------------------------	------------------	------------------------	--------	------------	--

*NPSD-FPP (Narrow Particle Size Distribution Fully Porous Particles). ^a150 mM NaClO₄ in 0.02 % HClO₄:CH₃CN, 2 mL/min, 10 min. ^b2 mM NH₄CO₂H pH 4.1: CH₃CN, 2 mL/min, 10 min, ^c0.1 % TEAA pH 4.1:MeOH, 2 mL/min, 10 min. ^d150 mM NaClO₄ in 0.02 % HClO₄: CH₃CN, 3 mL/min, 10 min. ^e150 mM NaClO₄ in 0.02% HClO₄: CH₃CN, 0.8 mL/min, 10 min. ¹CO₂:MeOH: 25 mM IBA. 3 mL/min, 6 min. ²CO₂:MeOH: 25 mM IBA, 2.5 mL/min, 6 min. ³CO₂:MeOH: 25 mM IBA, 1.3 mL/min, 6 min. ⁴CO₂:MeOH:0.3 % TFA: 0.2 % TEA, 2 mL/min. ⁵CO₂:MeOH:0.1 % TFA: 0.1 % TEA, 2 mL/min, 6 min. ⁶CO₂:MeOH: 25 mM IBA, 2.0 mL/min, 6 min. ⁷CO₂:MeOH, 2 mL/min, 6 min.

The initial chiral RP-LC and SFC screenings, summarized in Fig. 7.2, help to identify those CSPs and conditions that hold the most promise for developing an ultrafast separation method for each racemate. Some mixtures are easily separated, showing good resolution with a number of different CSPs and conditions, e.g. trans-stilbene oxide (TSO, 1), synthetic intermediates 5, 12, warfarin and hydroxylated warfarin metabolites (41–46). Others are more challenging, showing only partial resolution on a single CSP or just a few hits, e.g. 1-tetralol (10) and compounds 24, 38 and 39. A simple scoring system helps to visualize the best outcome for each mixture across both SFC and RP-LC experiments. We chose to focus on resolution (R_s) and speed, but different scoring systems focusing on other aspects of performance could be imagined.¹⁸ Baseline separations ($R_s \geq 1.5$) are denoted with a bright green color, while separations achieved in less than 3 min with a $R_s \geq 1.5$ or separations above 3 min with $R_s \geq 5.0$ are denoted by a dark green color. The best CSP for separation of each mixture is highlighted with a star.

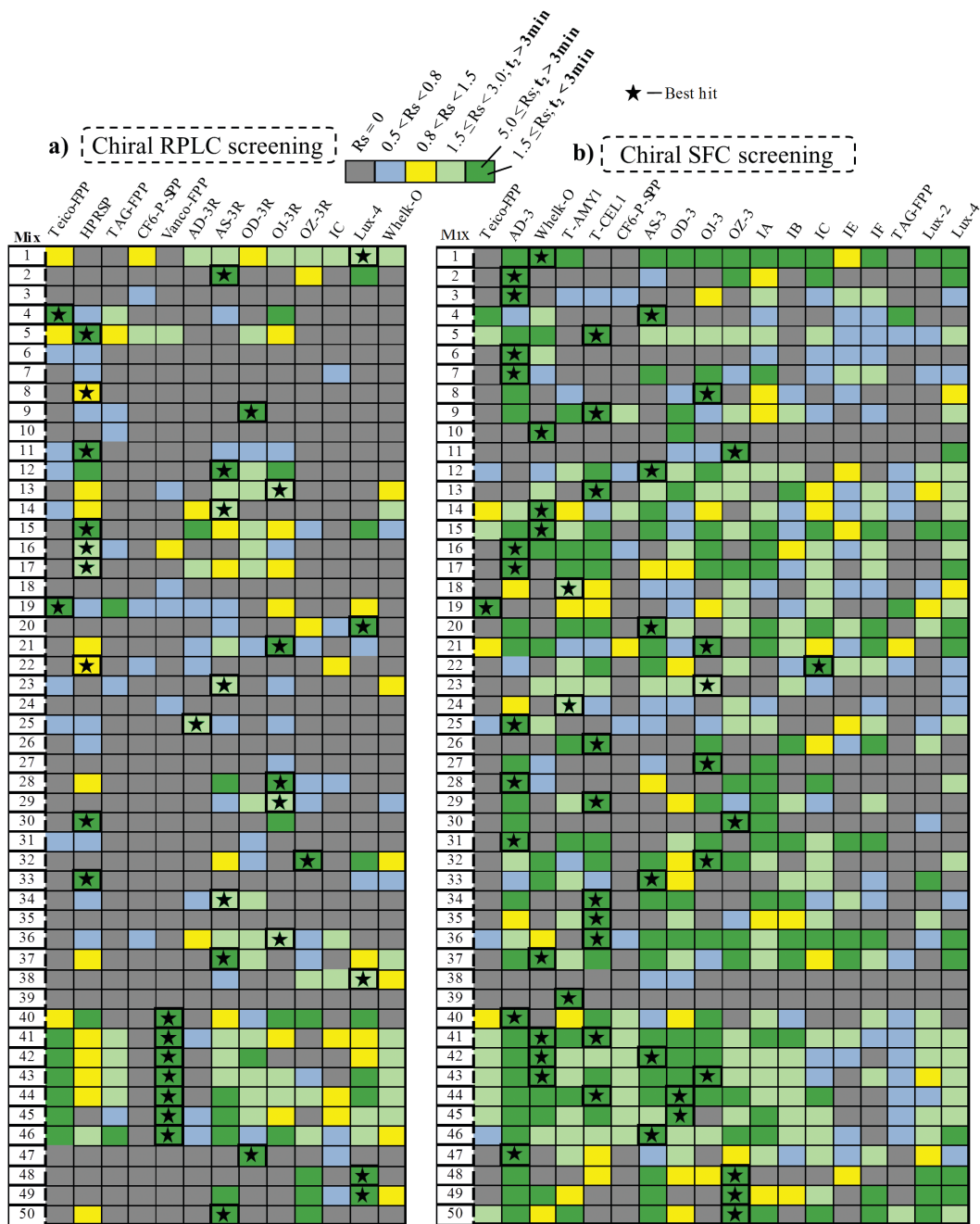


Figure 7.2 Scoring system. (a) Chiral RP-LC screening of 50 enantiomeric mixtures. (b) Chiral SFC screening of 50 enantiomeric mixtures

Table 7.2 Estimation of fast chromatographic separation from selected screening conditions.

RPLC					
Mixture	CSP	$t_{1(\text{min})}$	$t_{2(\text{min})}$	Rs	t_{mincc}
32	OZ-3R	1.09	1.51	3.99	0.38
	LUX-4	1.08	1.42	3.47	0.47
SFC					
Mixture	CSP	$t_{1(\text{min})}$	$t_{2(\text{min})}$	Rs	t_{mincc}
17	AD3	2.2	2.9	3.65	0.87
	T-CEL1	1.4	1.49	1.88	1.69
31	AD-3	3.43	5.34	22.91	0.04
	IA	2.87	4.17	9.02	0.21
	IF	2.95	4.03	11.58	0.12
40	AD-3	3.57	4.03	7.47	0.29
	OJ-3	2.79	3.06	4.50	0.60
41	AD-3	3.66	4.62	7.56	0.32
	Whelk-O	3.37	4.08	8.28	0.24
	T-CEL1	2.70	3.28	7.70	0.22
42	OD-3	3.38	4.25	7.33	0.32
	Whelk-O	3.57	4.59	8.10	0.28
	AS-3	3.45	4.13	8.91	0.21
43	Whelk-O	3.43	4.17	6.71	0.37
	AS-3	3.30	3.91	5.99	0.44
	OJ-3	3.93	4.81	7.21	0.37
44	T-CEL1	3.11	3.96	10.03	0.16
	OD-3	3.51	4.86	13.28	0.11
45	AD-3	4.03	4.94	7.15	0.39
	OD-3	3.44	4.24	8.88	0.22

RP-LC							
Comp.	CSP	column dimension	Flow rate (mL/min)	Mobile Phase	t ₁ (sec)	t ₂ (sec)	α
4	Teico-FPP	4.6 x 50 mm, 1.9 μm	2.0	85:15 2 mM NH ₄ CO ₂ H pH 4.1:ACN	44.0	48.7	1.2
19			2.6	79:29 2 mM NH ₄ CO ₂ H pH 4.1:ACN	53.1	58.6	1.1
5	HPRSP-SPP	3.0 x 50 mm, 2.7 μm	2.0	86:14 2 mM NH ₄ CO ₂ H pH 4.1:ACN	30.9	37.6	1.4
8			1.0	95:05 150 mM NaClO ₄ in 0.02% HClO ₄ :ACN	110.3	125.0	1.2
11			2.0	78:22 2 mM NH ₄ CO ₂ H pH 4.1:ACN	41.1	47.2	1.2
15			2.0	87:13 2 mM NH ₄ CO ₂ H pH 4.1:ACN	20.2	23.3	1.4
16			3.0	88:12 2 mM NH ₄ CO ₂ H pH 4.1:ACN	43.4	50.2	1.2
17			3.0	88:12 2 mM NH ₄ CO ₂ H pH 4.1:ACN	43.3	50.1	1.2
22			1.8	92:08 150 mM NaClO ₄ in 0.02% HClO ₄ :ACN	80.8	90.2	1.1
30			3.0	91:09 2 mM NH ₄ CO ₂ H pH 4.1:ACN	17.5	20.6	1.3
33			3.0	85:15 2 mM NH ₄ CO ₂ H pH 4.1:ACN	21.3	25.4	1.3
40			2.0	85:15 2 mM NH ₄ CO ₂ H pH 4.1:ACN	26.2	31.9	1.9
41			2.6	70:30 150 mM NaClO ₄ in 0.02% HClO ₄ :ACN	26.6	30.7	1.3
42	2.6	75:25 150 mM NaClO ₄ in 0.02% HClO ₄ :ACN	27.5	34.4	1.6		
43	Vanco-FPP	4.6 x 50 mm, 1.9 μm	2.6	75:25 150 mM NaClO ₄ in 0.02% HClO ₄ :ACN	28.0	34.3	1.5
44			2.6	70:30 150 mM NaClO ₄ in 0.02% HClO ₄ :ACN	23.5	28.0	1.5
45			2.6	78:22 150 mM NaClO ₄ in 0.02% HClO ₄ :ACN	31.9	36.4	1.3
46			2.8	73:27 150 mM NaClO ₄ in 0.02% HClO ₄ :ACN	23.3	26.8	1.4
25			AD3-3R	4.6 x 50 mm, 3 μm	4.0	60:40 150 mM NaClO ₄ in 0.02% HClO ₄ :ACN	53.2
2	AS3-3R	4.6 x 50 mm, 3 μm	3.4	78:22 150 mM NaClO ₄ in 0.02% HClO ₄ :ACN	42.2	55.2	1.4
12			3.4	63:37 150 mM NaClO ₄ in 0.02% HClO ₄ :ACN	30.8	41.3	1.5
14			3.6	61:39 150 mM NaClO ₄ in 0.02% HClO ₄ :ACN	46.9	54.4	1.2
23			3.6	53:47 150 mM NaClO ₄ in 0.02% HClO ₄ :ACN	92.3	111.7	1.2
34			3.6	40:60 150 mM NaClO ₄ in 0.02% HClO ₄ :ACN	39.1	49.7	1.4
37			3.8	60:40 150 mM NaClO ₄ in 0.02% HClO ₄ :ACN	40.4	49.1	1.3
50			3.0	75:25 150 mM NaClO ₄ in 0.02% HClO ₄ :ACN	104.7	125.3	1.2
9	OD-3R	4.6 x 50 mm, 3 μm	4.5	70:30 150 mM NaClO ₄ in 0.02% HClO ₄ :ACN	49.1	65.3	1.4
47			3.0	75:25 150 mM NaClO ₄ in 0.02% HClO ₄ :ACN	55.8	65.1	1.2
13	OJ-3R	4.6 x 50 mm, 3 μm	3.8	66:34 150 mM NaClO ₄ in 0.02% HClO ₄ :ACN	83.0	96.0	1.2
21			3.8	30:70 150 mM NaClO ₄ in 0.02% HClO ₄ :ACN	13.2	17.0	2.0
28			3.8	77:23 150 mM NaClO ₄ in 0.02% HClO ₄ :ACN	34.0	40.8	1.3
29			4.3	50:50 150 mM NaClO ₄ in 0.02% HClO ₄ :ACN	50.9	61.7	1.3
36			4.7	40:60 150 mM NaClO ₄ in 0.02% HClO ₄ :ACN	22.9	29.6	1.5
32	OZ-3R	4.6 x 50 mm, 3 μm	3.9	67:33 150 mM NaClO ₄ in 0.02% HClO ₄ :ACN	21.0	27.9	1.7
1	LUX-4	4.6 x 50 mm, 3 μm	5.0	30:70 150 mM NaClO ₄ in 0.02% HClO ₄ :ACN	14.1	17.5	1.5
20			4.2	67:33 150 mM NaClO ₄ in 0.02% HClO ₄ :ACN	32.9	42.8	1.4
38			4.2	27:73 150 mM NaClO ₄ in 0.02% HClO ₄ :ACN	40.3	53.9	1.4
48			3.5	60:40 150 mM NaClO ₄ in 0.02% HClO ₄ :ACN	24.8	32.2	1.6
49			3.5	77:23 150 mM NaClO ₄ in 0.02% HClO ₄ :ACN	49.8	57.2	1.2

Table 7.3 Detailed chromatographic conditions of ultrafast chiral RP-LC methods.

Overall, the SFC screens (Fig. 7.2 b) show greater generality for enantioseparation than the RP-LC screens where the separations were dominated by only a few CSPs (Fig. 7.2 a). These results clearly illustrate why in recent years SFC has become the workhorse technique for separation and purification of enantiomers in the pharmaceutical industry

and the benefits of a broad screening approach.¹⁹³ However, the two techniques are in some ways complimentary, with compounds that are poorly resolved across almost all SFC columns and conditions (e.g. intermediates 11 and 38) sometimes showing improved resolution by RP-HPLC, affording additional options for method development. Interestingly, all warfarin and hydroxylated metabolites can be baseline resolved in less than 2 min using a single screening method on the vancomycin FPP column with 150 mM NaClO₄ in 0.02% HClO₄:CH₃CN mobile phase. It is noteworthy that all compounds in the study showed at least some resolution on at least one of the CSPs, a testimony to both the power of contemporary enantio- selective chromatography and the value of the combined CSP screening approach. In some cases it can be challenging to determine which of the different enantioseparations offers the greatest potential for developing an ultrafast method, for example, when comparing a 2 minute method with baseline resolution ($R_S = 1.5$) and a 4 min method where $R_S = 4$. In such cases, calculation of the previously described $t_{\min cc}$ term¹²⁴ not only allows for easy selection of the best method, but also provides an estimate of the optimal time for ultrafast separation (Table 7.2).

Table 7.4 Detailed chromatographic conditions of ultrafast chiral SFC methods

SFC									
Comp.	CSP	Column dimensions	Temp. (°C)	BPR (bar)	Flow rate (mL/min)	Mobile Phase	t ₁ (sec)	t ₂ (sec)	α
19	Teico-FPP	4.6 x 30 mm, 1.9 μ m	40	200	2.0	60:40 CO ₂ :MeOH	27.0	33.6	1.4
2	AD3	4.6 x 50 mm, 3 μ m	40	200	2.0	95:05 CO ₂ :MeOH 25mM IBA	92.4	107.4	1.4
3		4.6 x 50 mm, 3 μ m	40	200	3.5	75:25 CO ₂ :MeOH 25mM IBA	39.6	53.6	1.6
6		4.6 x 50 mm, 3 μ m	40	200	3.5	80:20 CO ₂ :MeOH 25mM IBA	18.6	24.0	1.9
7		4.6 x 50 mm, 3 μ m	40	200	4.0	60:40 CO ₂ :MeOH 25mM IBA	20.4	26.4	1.6
17		4.6 x 150 mm, 3 μ m	40	200	2.5	80:20 CO ₂ :MeOH 25mM IBA	48.6	54.0	1.6
21		4.6 x 10 mm, 3 μ m	50	200	4.0	60:40 CO ₂ :MeOH 25mM IBA	3.6	5.4	3.0
25		4.6 x 50 mm, 3 μ m	40	200	1.5	75:25 CO ₂ :MeOH 25mM IBA	31.2	40.2	1.7
28		4.6 x 50 mm, 3 μ m	40	200	3.0	90:10 CO ₂ :MeOH 25mM IBA	21.0	25.2	2.4
31		4.6 x 10 mm, 3 μ m	40	200	4.0	40:60 CO ₂ :MeOH 25mM IBA	4.8	6.8	2.0
47		4.6 x 150 mm, 3 μ m	40	200	3.5	65:35 CO ₂ :MeOH 25mM IBA	45.0	49.8	1.4
40		4.6 x 10 mm, 3 μ m	50	200	4.0	60:40 CO ₂ :MeOH 25mM IBA	9.6	18.0	2.3
1		Wheik-O	3.0 x 20 mm, 5 μ m	40	200	3.0	60:40 CO ₂ :MeOH 25mM IBA	5.6	7.6
10	3.0 x 50 mm, 5 μ m		40	200	3.0	60:40 CO ₂ :MeOH 25mM IBA	13.2	17.4	1.6
14	3.0 x 50 mm, 5 μ m		40	200	3.0	60:40 CO ₂ :MeOH 25mM IBA	15.6	25.4	2.3
15	3.0 x 150 mm, 5 μ m		40	200	2.5	60:40 CO ₂ :MeOH 25mM IBA	30.6	34.2	1.4
37	3.0 x 50 mm, 5 μ m		40	200	3.0	60:40 CO ₂ :MeOH 25mM IBA	9.6	12.0	1.8
41	3.0 x 50 mm, 5 μ m		40	200	3.0	60:40 CO ₂ :MeOH 25mM IBA	13.8	20.4	1.9
42	3.0 x 20 mm, 5 μ m		40	200	3.0	60:40 CO ₂ :MeOH 25mM IBA	5.4	9.0	2.2
43	3.0 x 50 mm, 5 μ m		40	200	3.0	60:40 CO ₂ :MeOH 25mM IBA	13.2	21.0	2.2
5	T-CEL-1	3.0 x 50 mm, 2.5 μ m	40	150	3.0	60:40 CO ₂ :MeOH 25mM IBA	20.4	24.0	1.3
9		3.0 x 150 mm, 2.5 μ m	40	150	2.5	60:40 CO ₂ :MeOH 25mM IBA	29.4	36.0	1.7
13		3.0 x 50 mm, 2.5 μ m	40	150	3.5	60:40 CO ₂ :MeOH 25mM IBA	7.8	15.6	4.1
29		3.0 x 50 mm, 2.5 μ m	40	150	1.3	97:03 CO ₂ :MeOH 25mM IBA	66.6	76.2	1.8
34		3.0 x 50 mm, 2.5 μ m	40	150	3.0	80:20 CO ₂ :MeOH 25mM IBA	11.4	36.4	7.0
35		3.0 x 50 mm, 2.5 μ m	40	150	2.0	90:10 CO ₂ :MeOH 25mM IBA	40.8	46.8	1.2
36	3.0 x 50 mm, 2.5 μ m	40	150	3.0	60:40 CO ₂ :MeOH 25mM IBA	18.6	37.8	2.7	
18	T-AMY-1	3.0 x 150 mm, 2.5 μ m	40	150	1.7	85:15 CO ₂ :MeOH 25mM IBA	85.8	99.0	1.3
24		3.0 x 150 mm, 2.5 μ m	40	150	1.7	85:15 CO ₂ :MeOH 25mM IBA	86.4	98.4	1.3
39		3.0 x 50 mm, 2.5 μ m	40	150	4.0	60:40 CO ₂ :MeOH 25mM IBA	27.6	43.8	1.8
4	AS3	4.6 x 150 mm, 3 μ m	40	200	3.5	90:10 CO ₂ :MeOH 25mM IBA	48.6	57.6	1.8
12		4.6 x 50 mm, 3 μ m	40	200	3.0	60:40 CO ₂ :MeOH 25mM IBA	15.6	19.8	2.4
20		4.6 x 150 mm, 3 μ m	40	200	3.5	75:25 CO ₂ :MeOH 25mM IBA	39.6	43.4	1.5
33		4.6 x 50 mm, 3 μ m	40	200	3.0	60:40 CO ₂ :MeOH 25mM IBA	19.8	44.4	4.5
46		4.6 x 10 mm, 3 μ m	40	200	3.0	60:40 CO ₂ :MeOH 25mM IBA	5.4	16.2	4.6
44	OD3	4.6 x 50 mm, 3 μ m	40	200	4.0	60:40 CO ₂ :MeOH 25mM IBA	12.6	19.8	5.0
45		4.6 x 50 mm, 3 μ m	40	200	3.0	60:40 CO ₂ :MeOH 25mM IBA	18.6	23.4	2.1
8	OJ3	4.6 x 150 mm, 3 μ m	40	200	3.0	90:10 CO ₂ :MeOH 25mM IBA	64.2	69.0	1.2
16		4.6 x 50 mm, 3 μ m	40	200	3.0	60:40 CO ₂ :MeOH 25mM IBA	16.2	18.6	1.7
23		4.6 x 50 mm, 3 μ m	40	200	3.0	75:25 CO ₂ :MeOH 25mM IBA	24.0	27.0	1.4
27		4.6 x 50 mm, 3 μ m	40	200	3.0	75:25 CO ₂ :MeOH 25mM IBA	27.0	32.4	1.4
32		4.6 x 50 mm, 3 μ m	40	200	3.0	90:10 CO ₂ :MeOH 25mM IBA	21.6	25.8	1.5
11	OZ3	4.6 x 150 mm, 3 μ m	40	200	4.0	60:40 CO ₂ :MeOH 25mM IBA	66.6	73.2	1.2
30		4.6 x 150 mm, 3 μ m	40	200	3.5	80:20 CO ₂ :MeOH 25mM IBA	47.4	57.6	1.6
48		4.6 x 10 mm, 3 μ m	40	200	4.0	70:30 CO ₂ :MeOH 25mM IBA	7.8	13.8	2.5
50		4.6 x 50 mm, 3 μ m	40	200	3.0	75:25 CO ₂ :MeOH 25mM IBA	22.8	26.4	1.4
49		4.6 x 50 mm, 3 μ m	40	200	4.0	70:30 CO ₂ :MeOH 25mM IBA	18.0	19.8	1.4
22	IC	4.6 x 150 mm, 3 μ m	40	200	3.7	60:40 CO ₂ :MeOH 25mM IBA	52.2	58.8	1.5

With the selection of the best CSP for each of the 50 racemates in hand, we next focused on the development of ultrafast chiral methods for each compound. This generally involves changing the gradient elution used in the screening methods to an isocratic elution profile where the solvent composition remains constant throughout the separation. Using isocratic mode rather than gradient elution for ee analysis offers a significant advantage from a speed and simplicity perspective, as column equilibration is no longer required between sample runs. In addition, shorter columns are often used, typically operating at significantly higher flow rates than those used in the CSP screening methods. The detector sampling frequency and the detector response time settings become critically important for rapidly eluting analytes and highly efficient separations, as highlighted in recent studies.^{133,166} Using a detector setting of 80 Hz sampling frequency and the lowest available response time, combined with the use of high flow isocratic elution on short columns packed with the optimal CSP identified in screening, ultrafast enantioseparations were developed for 38 out of 50 analytes by RP-LC and 49 out of 50 by SFC (Fig. 7.3). Tables 7.3 and 7.4 summarize the chromatographic conditions for the optimized separations, as well as the respective retention time of each enantiomer (t_1 and t_2) and separation factors (α). In general, SFC provides better peak shape and faster analysis, but also much better overall selectivity than RP-LC. Fig. 2a also shows that all 38 of the RP-LC enantioseparations can be performed in less than 2.1 min, with nine of them under 30 s (highlighted in red), 21 separations between 30 and 60 s (highlighted in blue), and nine between 60 and 125 s (highlighted in violet). On the other hand, all 49 baseline SFC enantioseparations illustrated in Fig. 2b were achieved in less than 2.0 min, with 25 of them under 30 s, 18 separations between 30 and 60 s, and six between 60 and 108 s. It is important to point out that all of the 11 racemic mixtures that were not be resolved by RP-LC (3, 6, 7, 10, 18, 24, 26, 27, 31, 35 and 39), were easily separated

using SFC.

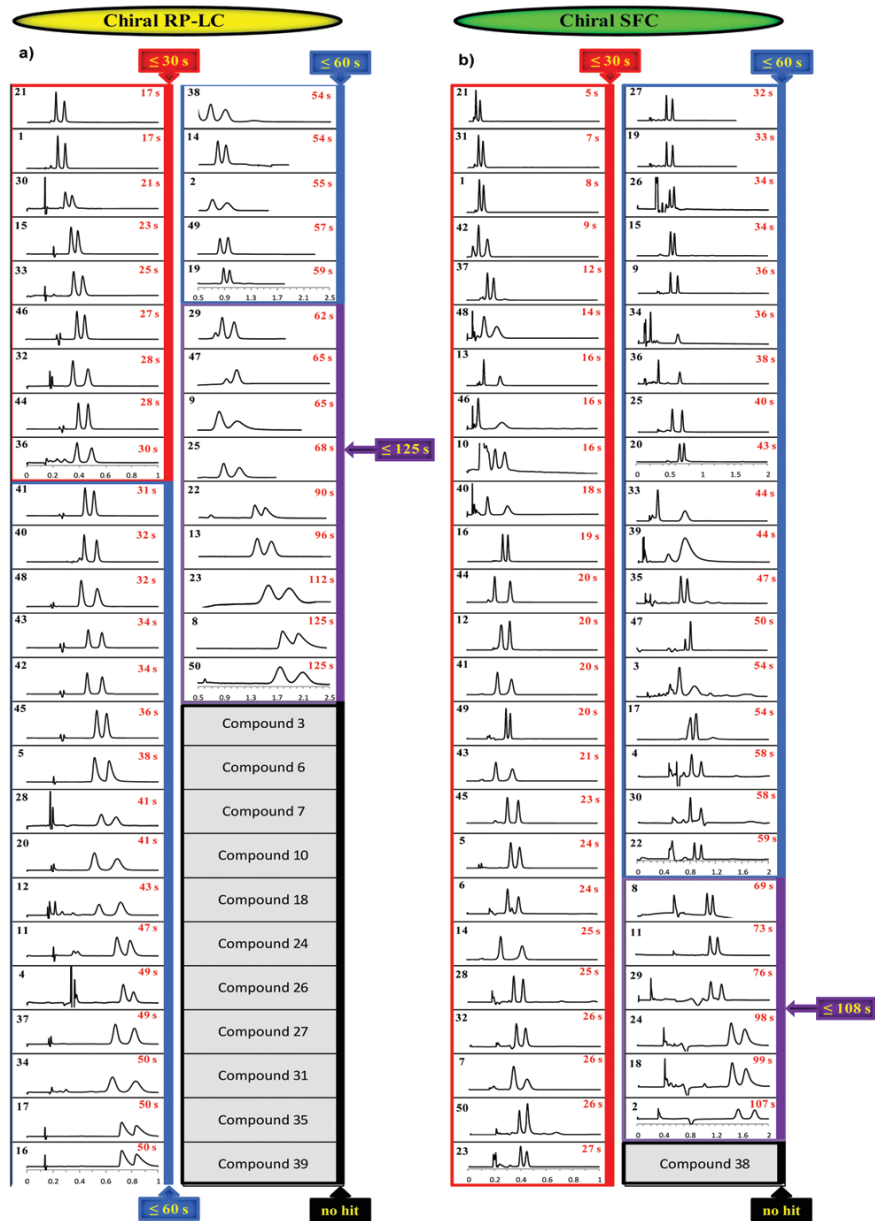


Figure 7.3 Ultrafast chiral separations of all mixtures by RP-LC (a) and SFC (b). Method conditions are detailed in table 7.3 and 7.4. Detection was performed at sampling

frequency of 80 Hz and the lowest available response time.

Only a single racemate (38) was not baseline resolved by SFC, however this compound was nicely resolved by several RPLC methods, highlighting the complementary nature of the two techniques. Separations factors (α) ranged from 1.14 to 2.02 by RP-LC and 1.20 to 5.10 by SFC. These results clearly show that ultrafast chromatographic enantioseparation methods can be developed for many pharmaceutical drugs and synthetic intermediates, with half of all separations in this study being achieved in less than 30 s and 86% in less than 1 min. Even more exciting is the fact that the slowest enantioseparations (violet bracket) ranged from only 1 to 2.1 min (18% by RP-LC and 12% by SFC), which are much faster than the standard enantioseparation methods generally practiced by researchers in enantioselective synthesis. Additional gains in speed can be obtained for some of these separations with the use of shorter 1–2 cm columns (e.g. compound 34 and 36 by SFC). It is expected that continuing development of column, CSP and instrument technologies over the coming years will lead to even further improvements in chiral chromatographic performance, with many, or even most, separations becoming achievable in just a few seconds.

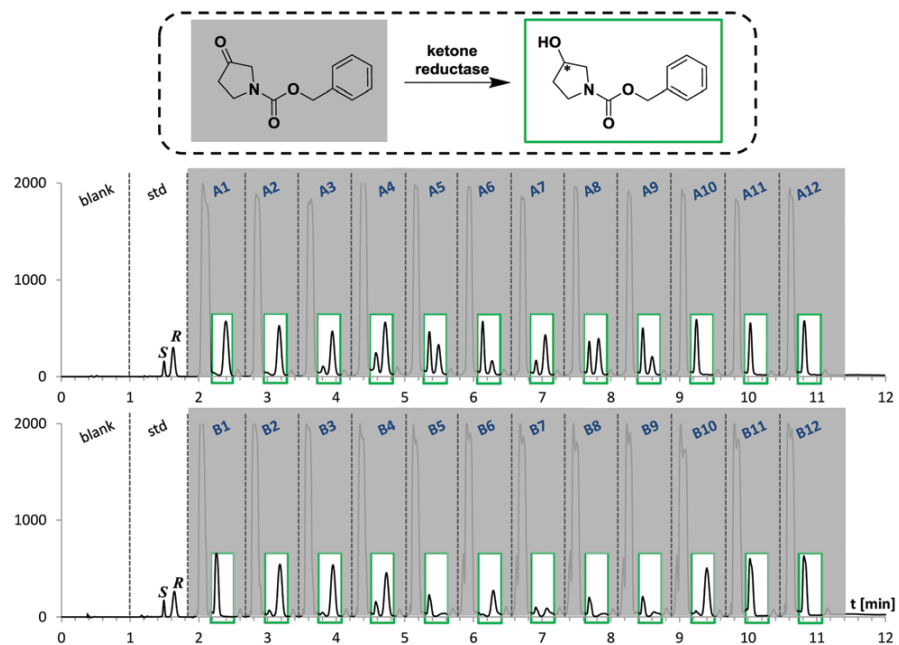


Figure 7.4 MISER chiral SFC for high-throughput enantiopurity analysis of an alcohol obtained from a ketone via enzymatic catalysis. Conditions for reactions and MISER SFC experiments are described in the Experimental section

Table 7.5 Results from enzymatic catalysis screening by MISER chiral SFC

Well	Enzyme	Selectivity	Conv. (%)	ee
A1	P1B02	<i>R</i>	>99.9	> 99
A2	P1B10	<i>R</i>	>99.9	> 99
A3	P1D3	<i>R</i>	>99.9	77
A4	P1D05	<i>R</i>	>99.9	56
A5	P1H09	<i>R</i>	>99.9	-12
A6	P1H10	<i>R</i>	>99.9	-53
A7	P2B11	<i>R</i>	>99.9	64
A8	P2C02	<i>R</i>	>99.9	24
A9	P2D11	<i>R</i>	>99.9	-36
A10	P3C3	<i>S</i>	>99.9	> -99
A11	P3D1	<i>S</i>	>99.9	> -99
A12	P3D11	<i>S</i>	>99.9	> -99
B1	P3H2	<i>S</i>	>99.9	> -99
B2	MIF-20	<i>R</i>	>99.9	88
B3	KRED-208	<i>R</i>	>99.9	91
B4	KRED 101	<i>R</i>	98.6	63
B5	KRED 108	<i>R</i>	31.6	-81
B6	KRED 112	<i>R</i>	44.7	91
B7	KRED 119	<i>R</i>	22.90	-3
B8	KRED 124	<i>R</i>	29.10	-84
B9	KRED 130	<i>R</i>	32.80	-63
B10	KRED 134	<i>R</i>	>99.9	88
B11	KRED NADH 101	<i>S</i>	>99.9	> -99
B12	KRED NADH 102	<i>S</i>	>99.9	> -99

While this study employs relatively state of the art LC and SFC instrumentation, for most laboratories, significant gains in speed do not require a wholesale replacement of existing analytical equipment. However, modification of older instrument to minimize extracolumn volumes by replacing high volume mixers and connecting fittings with low volume alternatives is recommended,¹⁸⁵ as is the aforementioned switch to fast sampling rates and detector response times. It should also be noted that this study focuses on simple two component enantiomer separations, while some real world stereochemical problems require an enantioseparation to be performed in the presence of a variety of additional

peaks and components, thereby increasing the difficulty of developing ultrafast analysis methods. Fig. 7.4 showcases an example of how ultrafast enantiopurity analysis can be swiftly integrated into standard work-flows for catalyst identification and process optimization. In this instance, a high throughput analysis method was required to enable screening of the enzymatic ketoreductase-catalyzed reduction of a prochiral ketone to afford the corresponding alcohol (compound 47) in high enantiopurity. CSP screening (Figure 7.2) followed by method development optimization afforded the 50 s ultrafast chiral SFC assay shown in Figure 7.3, with co-injection of starting ketone showing early elution well away from the desired enantiomer pair (Figure 7.4). While this method would be well suited for the direct study of a few samples, larger scale screening can benefit from MISER analysis (multiple injections within a single experimental run),¹⁹⁴ where injections from a number of different samples within a single chromatogram facilitates visual comparison and the rapid selection of the best performing reaction conditions. Rapid MISER SFC analysis using a sample injection interval of 50 s afforded a convenient high throughput analysis method with a plate time (time for analysis of a 96 well microplate) of only 80 min. Two rows of 12 samples each are shown in Table 7.5, with a number of enzymes identified that afford not only good conversion but also high enantioselectivity for the formation of either the (R) or the (S) enantiomer. Ultrafast chiral chromatographic analysis is well suited to such first round in a high-throughput mode, with conventional chromatographic analysis often being used as a confirmatory assay.

7.5 Conclusion

In conclusion, chromatographic enantioseparations taking less than 1 minute can now be achieved for most racemic mixtures using state of the art stationary phases, columns and chromatographic equipment. Fast enantioseparations are also possible employing older

instrumentation, with the use of relatively inexpensive stationary phases packed into high efficiency short columns. A simple and straightforward approach to method development involves initial screening of a variety of stationary phases to identify a leading candidate, followed by optimization of column length, flow rate and eluent composition. The resulting ultrafast method can be used for routine stereo- chemical analysis, or can form the basis for a MISER method for high throughput enantiopurity analysis. While 5–30 minute methods for the chromatographic analysis of enantiopurity are still used to support research investigations in many synthetic chemistry, bioanalysis and pharmaceutical research laboratories, in many cases these assays can be easily replaced by much faster methods enabling ee analysis of over one thousand samples in an 8 h workday. Consequently, ultrafast chromatographic enantio- separations are expected to greatly enable faster and more efficient research investigations and the broader adoption of high through- put experimentation approaches in stereochemical research.

Chapter 8

Ultrafast Chiral Chromatography as the Second Dimension in Two-Dimensional Liquid Chromatography Experiments

8.1 Abstract

Chromatographic separation and analysis of complex mixtures of closely related species is one of the most challenging tasks in modern pharmaceutical analysis. In recent years, two-dimensional liquid chromatography (2D-LC) has become a valuable tool for improving peak capacity and selectivity. However, the relatively slow speed of chiral separations has limited the use of chiral stationary phases (CSPs) as the second dimension in 2D-LC, especially in the comprehensive mode. Realizing that the recent revolution in the field of ultrafast enantioselective chromatography could now provide significantly faster separations, we herein report an investigation into the use of ultrafast chiral chromatography as a second dimension for 2D chromatographic separations. In this study, excellent selectivity, peak shape, and repeatability were achieved by combining achiral and chiral narrow-bore columns (2.1 mm × 100 mm and 2.1 mm × 150 mm, sub-2 and 3 μm) in the first dimension with 4.6 mm × 30 mm and 4.6 mm × 50 mm columns packed with highly efficient chiral selectors (sub-2 μm fully porous and 2.7 μm fused-core particles) in the second dimension, together with the use of 0.1% phosphoric acid/acetonitrile eluents in both dimensions. Multiple achiral × chiral and chiral × chiral 2D-LC examples (single and multiple heart-cutting, high-resolution sampling, and comprehensive) using ultrafast chiral chromatography in the second dimension are successfully applied to the separation and analysis of complex mixtures of closely related pharmaceuticals and synthetic intermediates, including chiral and achiral drugs and

metabolites, constitutional isomers, stereoisomers, and organohalogenated species.

8.2 Introduction

Chromatographic separation and analysis of complex mixtures of closely related species is one of the most challenging tasks in modern pharmaceutical analysis. In recent years, two-dimensional liquid chromatography (2D-LC) has become a valuable tool for improving peak capacity and selectivity. However, the relatively slow speed of chiral separations has limited the use of chiral stationary phases (CSPs) as the second dimension in 2D-LC, especially in the comprehensive mode. Realizing that the recent revolution in the field of ultrafast enantioselective chromatography could now provide significantly faster separations, we herein report an investigation into the use of ultrafast chiral chromatography as a second dimension for 2D chromatographic separations. In this study, excellent selectivity, peak shape, and repeatability were achieved by combining achiral and chiral narrow-bore columns (2.1 mm × 100 mm and 2.1 mm × 150 mm, sub-2 and 3 μm) in the first dimension with 4.6 mm × 30 mm and 4.6 mm × 50 mm columns packed with highly efficient chiral selectors (sub-2 μm fully porous and 2.7 μm fused-core particles) in the second dimension, together with the use of 0.1% phosphoric acid/acetonitrile eluents in both dimensions. Multiple achiral × chiral and chiral × chiral 2D-LC examples (single and multiple heart-cutting, high-resolution sampling, and comprehensive) using ultrafast chiral chromatography in the second dimension are successfully applied to the separation and analysis of complex mixtures of closely related pharmaceuticals and synthetic intermediates, including chiral and achiral drugs and metabolites, constitutional isomers, stereoisomers, and organohalogenated species.

The chromatographic separation of complex mixtures of closely related species is becoming increasingly important in pharmaceutical and biomedical research, reflecting

the ever-increasing complexity of both fundamental biology and the therapeutics used to treat disease.¹⁹⁵⁻¹⁹⁸ Multidimensional separation techniques have emerged as a preferred tool for dealing with complex samples, with new liquid chromatography–mass spectrometry hybrid techniques laying the foundation for the ongoing omics revolution in biomedicine.¹⁹⁹⁻²⁰⁴ (8-16) Recent years have seen a rapid growth in the use of multidimensional chromatography for the study of complex mixtures, with two-dimensional (2D) chromatography emerging as a valuable tool for pharmaceutical, biomedical research, and other disciplines.^{18-20,22-24} However, this technique continues to evolve rapidly as it moves from the realm of isolated studies by experts using custom equipment to the realm of routine use by nonspecialists using platform technology solutions.

Achiral–chiral two-dimensional chromatographic analysis has been known for decades; for example, enantioselective bioanalysis from the 1980s often employed column switching, where serum proteins or other interfering components are removed by a first-dimension separation, with a heart cut of the desired component of interest passing to a second-dimension separation employing a chiral stationary phase (CSP) column.^{25,205} Modern 2D chromatography experiments have often investigated chiral–achiral or achiral–chiral column configurations,²⁰⁶⁻²¹⁴ but, except for applications where only a single peak is transferred to second dimension, it has become something of an axiom that chiral chromatography is too slow for use as a second dimension in comprehensive 2D chromatography.²¹⁵⁻²¹⁷ Consequently, the use of chiral separations as the second dimension in comprehensive two-dimensional liquid chromatography (2D-LC) experiments is scarce and limited to readily resolved enantiomeric mixtures.²¹⁸⁻²²⁰ While it is possible to address this issue using peak storage in loops for subsequent analysis, such solutions are slow, in addition to being technically complex. Another alternative is

the use of supercritical fluid chromatography (SFC) in the second dimension^{218,221} in order to speed up chiral separations. However, this requires interface customization to couple reversed-phase LC (RPLC) and SFC, in addition to the need of trapping columns²¹⁸ or other approaches^{221,222} to reduce injecting high volumes of water from the RPLC into the SFC back-end. As a result, 2D chromatographic separations employing a chiral–achiral column configuration, with a rapid reversed-phase or other achiral separation methods as the second dimension are currently more attractive from a speed and throughput perspective.^{215,223}

Recent reports from these and other laboratories have shown that the speed of RPLC or SFC chiral chromatographic separations can be significantly increased, often to only a few seconds using a combination of new stationary phases, new particle technologies, new column configurations, and new experimental approaches.^{3,113,122,163,166,191} Realizing that these ultrafast chiral separations could now form the basis for faster comprehensive 2D RPLC × RPLC, we herein report an investigation into the use of ultrafast chiral RPLC as a second dimension for 2D chromatographic separations.

8.3 Experimental Section

8.3.1 Instrumentation

All experiments were performed on an commercially available Agilent 1290 Infinity 2D-LC.⁽⁵⁶⁻⁵⁸⁾ All instrument modules were obtained from Agilent Technologies (Waldbronn, Germany). The first dimension consisted of a 1260 quaternary pump (model G1311B), 1260 autosampler (model G1367E) with 1290 thermostat (model G1330B), 1100 series column compartment (model G1316A), and 1260 Infinity II diode array detector (DAD) (model G4212B) with 1 μ L cell (model G4212-60008). The second dimension consisted

of a 1290 high-speed pump (model G7120A), 1290 column compartment (G1316C), and 1290 DAD (model G7117B) with 1 μ L cell (model G4212-60008). The 1D and 2D were interfaced through a 1290 valve drive (model G1170A), and multiple heart cutting was achieved with two 1290 valve drives (model G1170A), each equipped with six 40 μ L sample loops (model G4242-64000) and a 2D-LC pressure release kit (model G4236-60010).⁽⁵⁹⁾ The instrument was controlled by Agilent OpenLab CDS ChemStation software (rev. C.01.07 SR2 [255]).

8.3.2 Chemicals and Reagents

Phosphoric acid, methanol (MeOH), and acetonitrile (ACN) (HPLC grade) were purchased from Fisher Scientific (Fair Lawn, NJ, U.S.A.). Mixture 1, warfarin (1), 4-hydroxywarfarin (2), 6-hydroxywarfarin (3), 7-hydroxywarfarin (4), 8-hydroxywarfarin (5), and 10-hydroxywarfarin (6), were all purchased from Sigma-Aldrich (St. Louis, MO, U.S.A.). Mixture 2, synthetic intermediates 7–14, mixture 3, synthetic intermediates 15–23, and mixture 4, phenylacetic acid (24), 2-fluorophenylacetic acid (25), 4-fluorophenylacetic acid (26), 3-fluorophenylacetic acid (27), 2,3-difluorophenylacetic acid (28), 2,4-difluorophenylacetic acid (29), 3,5-difluorophenylacetic acid (30), 2,3,6-trifluorophenylacetic acid (31), 2,4,6-trifluorophenylacetic acid (32), 2,4,5-trifluorophenylacetic acid (33), 2,3,4-trifluorophenylacetic acid (34), and pentaphenylacetic acid (35), were all obtained from the Building Block Collection (Merck & Co., Inc., Kenilworth, NJ, U.S.A.). Ultrapure water was obtained from a Milli-Q Gradient A10 from Millipore (Bedford, MA, U.S.A.).

8.3.3 Stationary Phases

8.3.3.1 Achiral

The 2.1 mm i.d. by 100 mm length, 1.8 μm Zorbax RRHD Eclipse Plus C18 was purchased from Agilent Technologies. The 2.1 mm \times 150 mm, 1.6 μm Cortecs C18 column was purchased from Waters Corp. (Milford, MA, U.S.A.).

8.3.3.2 Chiral

Columns packed with Chiralcel (OJ-3R, 2.1 mm \times 150 mm, 3 μm and OD-3R, 4.6 mm \times 50 mm, 3 μm) were purchased from Chiral Technologies (West Chester, PA, U.S.A.). The 4.6 mm \times 20 mm and 4.6 mm \times 50 mm vancomycin bonded to narrow particle distribution size fully porous particles 1.9 μm (Vanco-FPP), 4.6 mm \times 50 mm teicoplanin bonded to narrow particle size distribution fully porous particles 1.9 μm (Teico-FPP), and 4.6 mm \times 30 mm hydroxypropyl- β -cyclodextrin bonded to superficially porous silica 2.7 μm (CDShell-RSP:HPRSP) were all obtained from AZYP LLC (Arlington, TX, U.S.A.). Table S1 (Supporting Information) details all columns used in both first and second dimension.

8.4 Results and Discussion

Separation and purification of enantiomers is now routine within the pharmaceutical industry; however, the direct determination of enantiomeric excess (ee) in complex multicomponent reaction mixtures can be very problematic. This challenge has often been dealt with by combining an achiral method for monitoring the end of the reaction with a chiral method for ee determination. Alternatively is the use of a single optimized chiral method for analysis of both achiral and chiral species.⁽⁶⁰⁾ Although this approach works quite well in some cases, method development can be challenging in the absence of standards or when dealing with more complex mixtures of closely related species. The example shown in Figure 8.1 illustrates the kind of complex isomeric mixtures often encountered in drug metabolism or late-stage functionalization studies within the

pharmaceutical industry. Analysis time using the achiral–chiral 2D configuration required about 200 min due to the need of injecting all the enantiomeric mixtures into a CSP using a much slower protocol.(37)

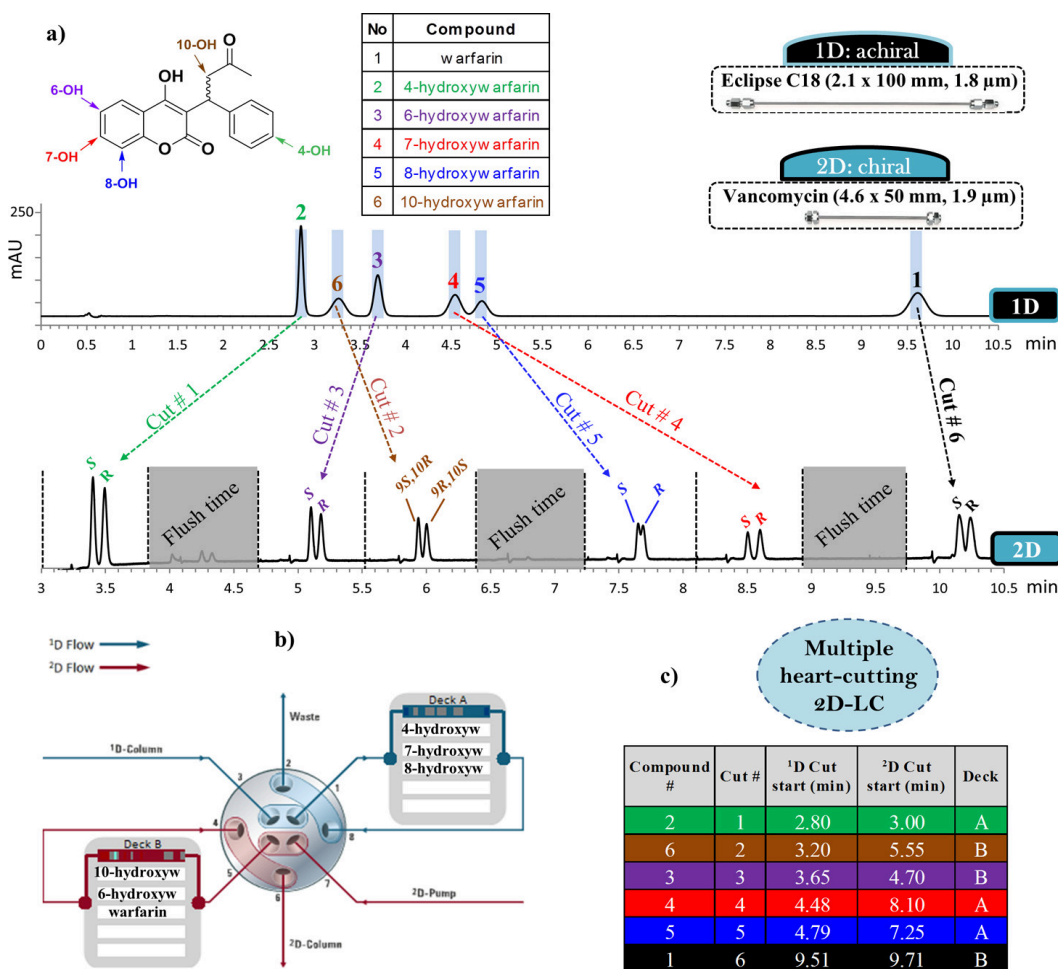


Figure 8.1 Multiple heart-cutting 2D-LC analysis of warfarin and hydroxywarfarin stereoisomers (1–6; sites of hydroxylation are indicated by arrows). Conditions, first dimension (achiral): column, Zorbax RRHD Eclipse Plus C18 (2.1 mm × 100 mm, 1.8 μm); temperature, 36 °C. Detection: UV 220 nm. Flow rate: 0.4 mL/min. Mobile phase:

eluent A, 0.1% H₃PO₄ in H₂O; eluent B, ACN. Step gradient: hold 35% B for 2.5 min; 2.5–10 min, 60% B; 10–11 min, 80% B. Sampling frequency: 80 Hz. Conditions, second dimension (chiral): column, vancomycin (4.6 mm × 50 mm, 1.9 μm); ambient temperature. Detection: UV 280 nm. Flow rate: 2.5 mL/min. Isocratic mobile phase: 0.1% H₃PO₄ in H₂O/ACN (70:30). Sampling frequency: 240 Hz.

Figure 8.1a illustrates a multiple heart-cutting 2D-LC method (achiral LC–chiral LC) on a commercially available 2D-LC system in which all the six warfarin and hydroxywarfarin species (1–6) are baseline-separated using a narrow-bore UHPLC column (Eclipse C18) in the first dimension, with a 4.6 mm × 5 cm column packed with a highly efficient, narrow particle size distribution, 1.9 μm based macrocyclic glycopeptide (vancomycin FPP) being used for subminute resolution of the enantiomers of each of the eluted compounds (a total 12 species) in the second dimension. The second-dimension chromatographic analysis was carried out concurrently with the first-dimension separation, allowing completion of the last enantioseparation in the second dimension only 42 s after the end of the first-dimension separation, affording a total analysis time of ~10.3 min. The absolute configuration of all warfarin and hydroxywarfarin stereoisomers was established by HPLC coupled to circular dichroism (HPLC-CD) and comparison with previous data.²²⁴ The injection order in the second dimension is a unique part of this approach. The software and instrumentation allows for parking of multiple heart cuts while analyzing in the second dimension. The multiple heart-cutting algorithm minimizes the number of valve switches but follows the rule of promptly processing heart cuts that are sampled or parked. The first heart cut is always sampled in loop 1 of deck A and immediately submitted for analysis in the second dimension. As shown in Figure 8.1b when the time difference between consecutive cuts is shorter than the 2D cycle time, the central valve

switches to deck B. Cuts parked within the same deck are injected in reverse order (e.g., injection of cut no. 3 before cut no. 2 or cut no. 5 before cut no. 4 in Figure 8.1). However, the software automatically generates a very convenient sampling table (Figure 8.1c) that simplifies data interpretation. As outlined in Table 8.1 both first- and second-dimension separations show excellent repeatability of retention time, peak area and resolution (R_s) values.

Table 8.1 Repeatability of retention times, peak areas and R_s values for the 2D-LC method shown in figure 8.1 (n = 3)

1D				
Elution order	Compound #	Cut #	R_t (min) \pm RSD	Peak Area (mAU*s) \pm RSD
Peak 1	2	1	2.85 \pm 0.03	718.48 \pm 0.13
Peak 2	6	2	3.26 \pm 0.05	412.79 \pm 0.13
Peak 3	3	3	3.69 \pm 0.06	553.27 \pm 0.14
Peak 4	4	4	4.54 \pm 0.03	448.94 \pm 0.15
Peak 5	5	5	4.83 \pm 0.03	310.83 \pm 0.13
Peak 6	1	6	9.62 \pm 0.07	672.48 \pm 0.14
2D				
Cut #	Enantiomer	R_t (min) \pm RSD	Peak Area (mAu*s) \pm RSD	$R_s \pm$ RSD
Cut # 1	<i>S</i>	3.40 \pm 0.04	26.44 \pm 0.22	1.60 \pm 0.29
	<i>R</i>	3.49 \pm 0.05	26.81 \pm 0.54	
Cut # 2	<i>9S,10R</i>	5.94 \pm 0.01	11.73 \pm 1.86	1.24 \pm 1.91
	<i>9R,10S</i>	6.00 \pm 0.03	11.72 \pm 0.32	
Cut # 3	<i>S</i>	5.10 \pm 0.02	15.17 \pm 1.62	1.42 \pm 0.57
	<i>R</i>	5.18 \pm 0.03	15.30 \pm 2.47	
Cut # 4	<i>S</i>	8.50 \pm 0.01	6.93 \pm 1.59	1.61 \pm 0.77
	<i>R</i>	8.60 \pm 0.01	8.84 \pm 0.00	
Cut # 5	<i>S</i>	7.65 \pm 0.01	8.46 \pm 0.50	0.61 \pm 0.77
	<i>R</i>	7.69 \pm 0.02	9.27 \pm 0.13	
Cut # 6	<i>S</i>	10.16 \pm 0.09	19.08 \pm 1.43	1.00 \pm 2.94
	<i>R</i>	10.25 \pm 0.06	19.84 \pm 2.10	

This multiple heart-cutting 2D-LC method proved to be a very powerful tool for the simultaneous measurement of enantiopurity of multicomponent samples, complementing a suite of powerful 1D chiral methods recently developed in these laboratories.³ Ultrafast chiral chromatography in the order of a few seconds often employs short columns from 0.5 to 5 cm in length. However, using very short columns and high-speed methods in 2D-LC mode can be more complex. Several key parameters have to be taken into consideration in 2D chromatography including sampling rate,²²⁵⁻²²⁷ dilution effect,¹⁷⁰ changes in the first-dimension flow rate,²²⁸ column orthogonality,(1) as well as solvent and pH mismatch.^{229,230} In this study, excellent selectivity and peak shape was achieved by using achiral and chiral narrow-bore columns (2.1 mm × 100 mm and 2.1 mm × 150 mm, 3 and sub-2 μm) in the first dimension and 4.6 mm × 30 mm and 4.6 mm × 50 mm columns packed with highly efficient chiral selectors (sub-2 μm fully porous and fused-core particles) in the second dimension, together with the use of 0.1% phosphoric acid/acetonitrile as eluents in both dimensions.

Table 8.2 Injection, Column Volume Percent Loop Filled in Volume Units

column dimension	sampling time (s)	loop volume (μL)	loop filling (%)	loop filling (μL)
4.6 mm × 20 mm and 4.6 mm × 50 mm	1.2	40	20	8
	1.8		30	12
	2.4		40	16
	3.6		60	24
	4.8		80	32

In addition, mass or volume overload in the injection sample can lead to degradation of peak efficiency and loss of resolution. Figure 8.2 demonstrates that optimization of sampling rate, loop filling, and column length (see volume units in Table 8.2) is key to improving the quality of the separation in the second dimension, especially when applying ultrafast chiral chromatography. In this figure the influence of sample overload (20–80% loop filling) on the resolution of some of these peaks (warfarin, 6- and 8-

hydroxywarfarins) using both 2 and 5 cm columns was investigated. As a result, when using the 20% loop filling, only one-fifth of the sample volume is injected to the second dimension, compared with default heart-cutting settings. It should be noted that the 20% loop filling means that a narrower time slice of the first-dimension chromatogram is taken, rather than a smaller volume sample from the same time slice. Consequently, information contained when using the 100% loop filling could potentially be lost when operating with the 20% setting.

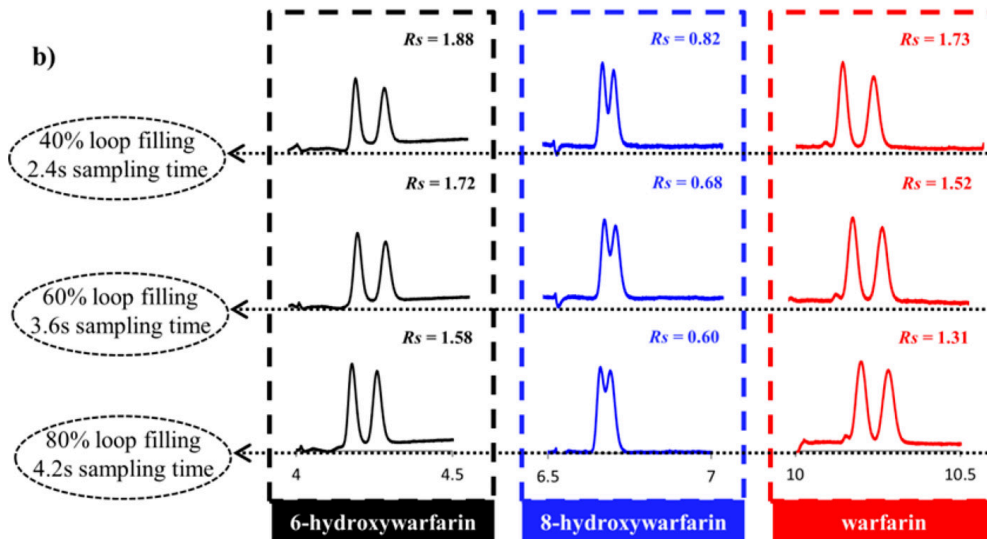
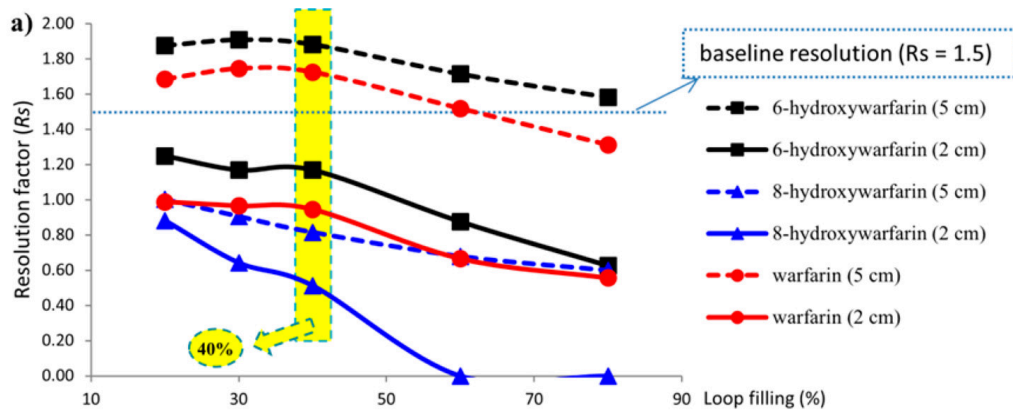


Figure 8.2 Optimization of loop filling (%) and column length in the second dimension for the separation of warfarin and hydroxywarfarin stereoisomers. (a) Discontinuous plots are used for the 5 cm column and continuous plots for the 2 cm column. (b) Chromatographic profiles obtained using the 5 cm column at different sample times and loop filling.

As shown in Figure 8.2a and Table 8.3), the 2 cm chiral column (continuous plots) is incapable of baseline resolution of any of the three racemic mixtures ($R_s \leq 1.5$). The less challenging mixture (6- hydroxywarfarin enantiomers) is baseline-separated on the 5 cm column at any of the sampling times (s) and loop filling (%) settings. A significant improvement trend for the resolution of warfarin enantiomers is observed when varying the loop filling from 80% ($R_s = 1.31$) to 40% ($R_s = 1.73$). It is important to note that reducing loop filling to 20% does not improve the separation of either warfarin or 6-hydroxywarfarin enantiomers. On the other hand, baseline resolution of 8-hydroxywarfarin proved to be very challenging, especially when using the default 2D settings (Figure 8.1 caption). However, the separation can be significantly improved by reducing loop filling from 80% to 20% (sampling time from 4.8 to 1.2 s, respectively). Overall, these results indicate that 40% loop filling (2.4 s sampling time) on a 5 cm column in the second dimension works quite well for separation of critical enantiomer pairs (Figure 8.2a highlighted in yellow and chromatograms in Figure 8.2b). In addition, the impact of loop filling on enantioseparations is more drastic when using even shorter columns, reflecting problems with volume overload as the volume of the sample diverted grows with respect to the dwell volume of the second-dimension separation. As outlined in Table S3, repeatability across all these 2D-LC experiments is quite high, with standard deviations of retention time values below 0.06 min.

Table 8.3 R_s values and repeatability of injections of warfarin, 6 and 8-hydroxywarfarins on 2 and 5 cm chiral columns at different sampling time and loop filling % in the second dimension (n = 3)

Second Dimension			6-hydroxywarfarin		8-hydroxywarfarin		warfarin	
Column Length	Sampling time (s)	Loop filling (%)	R_s	STDev	R_s	STDev	R_s	STDev
2 cm	1.2	20	1.25	0.03	0.88	0.05	0.99	0.06
	1.8	30	1.17	0.05	0.64	0.01	0.97	0.01
	2.4	40	1.17	0.03	0.51	0.01	0.95	0.03
	3.6	60	0.88	0.02	0.00	-	0.67	0.02
	4.8	80	0.63	0.03	0.00	-	0.56	0.02
5 cm	1.2	20	1.88	0.08	1.00	0.08	1.69	0.01
	1.8	30	1.91	0.04	0.91	0.02	1.75	0.03
	2.4	40	1.88	0.01	0.82	0.05	1.73	0.01
	3.6	60	1.72	0.02	0.68	0.03	1.52	0.03
	4.8	80	1.58	0.02	0.60	0.01	1.31	0.01

Recent trends in modern pharmaceutical and synthetic chemistry have shown an increase in drugs and intermediates containing multiple stereocenters. It is important to point out that most of the 2D-LC applications^{18,199,231} are focused on increasing peak capacity, which is essential when dealing with highly complex multicomponent mixtures (sometimes over 50 or 100 components). Chromatographic separation and analysis of complex mixtures of closely related stereoisomers (compounds 7–14) can often be very challenging, especially using 1D chromatography. In the example shown in Figure 8.3, no single chiral stationary phase was able to deliver the selectivity needed to separate all of the stereoisomers of an important intermediate in the synthesis of a recently developed hepatitis C protease inhibitor.²²⁶ Fully comprehensive chiral × chiral 2D- LC analysis of

this mixture using a very slow gradient (130 min) on a narrow-bore column (2.1 mm × 150 mm Chiralcel OJ-3R) in the first dimension combined with an ultrafast chiral separation on a 4.6 mm × 50 mm chiral column (Chiralcel OD- 3R) in the second dimension clearly shows that the second eluted peak is composed of a mixture of stereoisomers 13 and 14 (Figure 8.3a). One of the greatest advantages of comprehensive LC × LC is the ability to obtain a full view of sample composition for a complex mixture. However, the biggest limitation is the fact that slow speed of the second- dimension separation often leads to undersampling and missing information unless the first-dimension separation is drastically slowed, resulting in extremely broad peaks and slow analysis time. A solution to that problem is illustrated in Figure 8.3a. This example illustrates the power of performing ultrafast chiral chromatography as the second dimension, enabling comprehensive enantioselective analysis with good peak shape and analysis time.

Once the comprehensive 2D-LC analysis is completed and interpreted, a practical time-saving alternative is to perform selective comprehensive LC × LC experiments^{18,232,233} where 2D analysis is refocused on areas of significant peak coelution. This approach simplifies optimization of both the first- and second-dimension separations to proceed at higher speeds, providing significantly faster analysis compared with comprehensive 2D methods. The recently introduced “high-resolution sampling” 2D-LC feature allows segmentation of the first- dimension target peak into multiple cuts all of which are parked in the same deck A (Figure 8.3 center right) and subsequently injected in reverse order onto the second-dimension column. In high-resolution sampling 2D-LC, the 1D effluent is diverted to the second separation dimension by switching the valve at the beginning and at the end of each cut. In addition, loop underfill is used to avoid loss of 1D effluent, with up to 10 consecutive cuts being possible. While the use of high-resolution sampling 2D-

LC is not the main focus of this study, it is clear that the technique shows tremendous potential for analyzing broad unresolved peaks and achieving the optimum resolution in both dimensions. High-resolution sampling also delivers precise and reproducible 2D-LC quantitation because the entire sample volume for a peak in the first dimension is transferred to the second dimension. The resulting 30 min chiral × chiral 2D-LC method shown in Figure 8.3 can also be used for monitoring all eight isomeric species, with excellent overall repeatability of retention times, peak areas, and R_s values (Table 8.4).

Table 8.4 Repeatability of retention times, peak areas and R_s values for the 2D-LC method shown in figure 8.3 (n = 3)

<i>1D</i>				
Elution order	Cut #	Compound #	R_t (min) ± RSD	Peak Area (mAU*s) ± RSD
Peak 1	-	7	16.98 ± 0.10	1980.84 ± 0.36
Peak 2	HiRes	13 and 14	17.57 ± 0.10	3519.67 ± 0.78
Peak 3	-	8	20.55 ± 0.15	2026.74 ± 0.43
Peak 4	-	9	23.02 ± 0.13	1739.31 ± 0.41
Peak 5	-	10	25.38 ± 0.13	220.70 ± 8.91
Peak 6	-	11	28.44 ± 0.18	4222.21 ± 0.50
Peak 7	-	12	29.58 ± 0.19	1661.52 ± 0.78
<i>2D</i>				
Cut #	Peak	R_t (min) ± RSD	Peak Area (mAU*s) ± RSD	R_s ± RSD
Cut # 5	1	19.04 ± 0.01	120.37 ± 49.84	2.61 ± 4.88
	2	19.36 ± 0.00	163.9 ± 57.41	
Cut # 4	1	21.09 ± 0.01	120.37 ± 49.84	2.73 ± 1.37
	2	21.41 ± 0.00	163.9 ± 57.41	
Cut # 3	1	23.14 ± 0.00	122.98 ± 45.78	2.66 ± 1.85
	2	23.46 ± 0.01	174.45 ± 45.41	
Cut # 2	1	25.19 ± 0.01	134.05 ± 30.36	2.62 ± 3.07
	2	25.51 ± 0.01	159.76 ± 62.56	
Cut # 1	1	27.25 ± 0.01	114.69 ± 50.29	2.58 ± 2.11
	2	27.56 ± 0.00	169.47 ± 50.89	

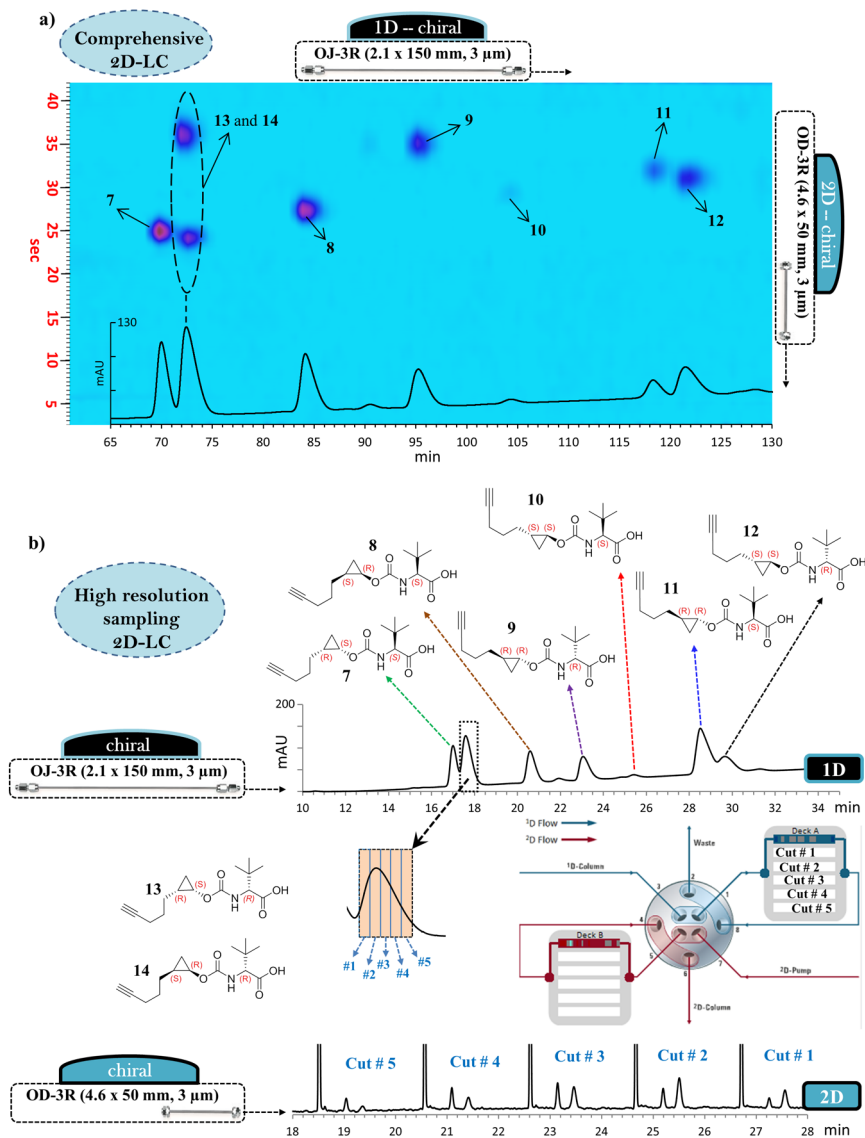


Figure 8.3. (a) Comprehensive chiral \times chiral 2D-LC method for complete resolution of isomers of a synthetic intermediate. Conditions, first dimension (chiral): column, OJ-3R column (2.1 mm \times 150 mm, 3 μ m); temperature, 40 $^{\circ}$ C. Detection: UV 195 nm. Flow rate: 0.05 mL/min. Mobile phase: eluent A, 0.1% H_3PO_4 in H_2O ; eluent B, ACN/MeOH (70:30, v/v %). Step gradient: hold 30% B for 20 min; 20–120 min, 35% B; 120–120.8 min, 30% B; 120.8–160 min, 30% B; 40 μ L loops. Conditions, second dimension (chiral): column,

Chiralcel OD-3R (4.6 mm × 50 mm, 3 μm); ambient temperature. Detection: UV 195 nm. Flow rate: 3.0 mL/min. Isocratic mobile phase: 0.1% H₃PO₄ in H₂O/ACN (60:40). (b) High-resolution sampling 2D-LC method. Conditions, first dimension (chiral): column, OJ-3R column (2.1 mm × 150 mm, 3 μm); temperature, 40 °C. Detection: UV 195 nm. Flow rate: 0.2 mL/min. Mobile phase: eluent A, 0.1% H₃PO₄ in H₂O; eluent B, ACN/MeOH (70:30, v/v %). Step gradient: hold 30% B for 5 min; 5–30 min, 35% B; 30–40 min, 30% B. Sampling frequency 80 Hz. Conditions, second dimension (chiral): column, Chiralcel OD-3R (4.6 mm × 50 mm, 3 μm); ambient temperature. Detection: UV 195 nm. Flow rate: 2.0 mL/min. Isocratic mobile phase: 0.1% H₃PO₄ in H₂O/ACN (60:40). Sampling frequency: 240 Hz.

The proliferation of pharmaceutical candidates containing multiple stereocenters is leading to a growing need for analysis of closely related stereoisomeric impurities. Figure 8.4 illustrates the use of a single heart-cutting achiral–chiral 2D-LC method 2 for separation of a complex mixture of nine closely related 3 stereoisomers related to an anti-HCV therapeutic (compounds 15-23). As outlined in Table S5 (Supporting Information), this method reproducibly combines a narrow-bore UHPLC column (Cortecs C18) for separation of eight peaks in the first dimension with a 4.6 mm × 50 mm column packed with the 1.9 μm teicoplanin CSP in the second dimension for baseline resolution of two isomers that coelute in the first dimension (15 and 16). A very important point to highlight from both Figures 8.3 and 8.4 is the fact that 2D chromatography can be applied to screen different columns in the second dimension for separation of coeluting peaks within complex mixtures. The screening of stationary phases for separation of complex mixtures of closely related species can often be very difficult or, for all practical purposes, impossible. In both examples, several chiral columns were manually screened to identify

the best performing combinations, but one could imagine a set of valves in the second dimension to enable automated screening and streamlined selection of second-dimension columns.

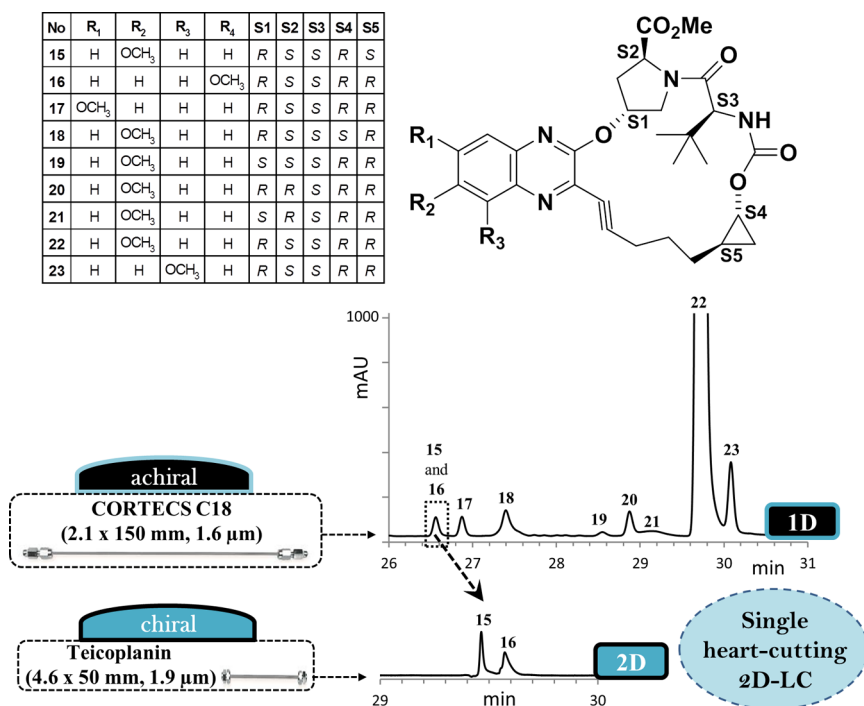


Figure 8.4. Single heart-cutting 2D-LC method for separation of complex mixture of closely related stereoisomers from an anti-HCV therapeutic. Conditions, first dimension (achiral): column, Cortecs (2.1 mm × 150 mm, 1.6 μm); temperature, 40 °C. Detection: UV 215 nm. Flow rate: 0.220 mL/min. Mobile phase: eluent A, 0.1% H₃PO₄ in H₂O; eluent B, ACN/MeOH (80:20, v/v %). Step gradient: 20–45% B in 7 min; 7–20 min, 90% B; 20–32 min, 20% B. Sampling frequency 80 Hz. Conditions, second dimension (chiral): column, teicoplanin (4.6 mm × 50 mm, 1.9 μm); ambient temperature. Detection: UV 215 nm. Flow rate: 1.0 mL/min. Isocratic mobile phase: 5:95 0.1% H₃PO₄ in H₂O/ACN. Sampling frequency: 240 Hz.

Table 8.5 Repeatability of retention times, peak areas and Rs values for the 2D-LC method shown in figure 8.4 (n = 3)

<i>1D</i>				
Elution order	Cut #	Compound #	R _t (min) ± RSD	Peak Area (mAU*s) ± RSD
Peak 1	1	15 and 16	26.56 ± 0.03	412.14 ± 4.04
Peak 2	-	17	26.87 ± 0.03	399.43 ± 2.29
Peak 3	-	18	27.39 ± 0.03	944.58 ± 1.21
Peak 4	-	19	28.54 ± 0.03	130.62 ± 8.36
Peak 5	-	20	28.86 ± 0.03	632.99 ± 4.22
Peak 6	-	21	29.12 ± 0.03	447.71 ± 8.56
Peak 7	-	22	29.69 ± 0.17	23069.33 ± 1.12
Peak 8	-	23	30.07 ± 0.03	1737.13 ± 6.15
<i>2D</i>				
Cut #	Compound	R _t (min) ± RSD	Peak Area (mAU*s) ± RSD	Rs ± RSD
Cut # 1	15	28.41 ± 0.00	94.51 ± 1.45	2.66 ± 1.41
	16	28.52 ± 0.00	148.18 ± 5.66	

Chromatographic resolution is vitally important for the analysis of complex mixtures of dehalogenation impurities and mixtures of halogen isomers in modern pharmaceutical analysis.^{15,98-100} Separation of small starting material-like compounds such as the fluorophenylacetic acids (24–35) shown in Figure 5 can be extremely challenging using only a single LC dimension. The use of chiral chromatography for separation of achiral isomers has become a very useful strategy in the pharmaceutical industry,⁶⁰ especially in cases where achiral columns deliver incomplete resolution or poor chromatographic performance. This example of multiple heart-cutting 2D-LC employs a narrow-bore reversed-phase column (Eclipse C18) in the first dimension and a relatively new cyclodextrin-based chiral selector bounded to superficially porous particle (DextroShell-RSP, 4.6 mm × 30 mm, 2.7 μm) in the second dimension to afford baseline separation of

all 12 fluorinated species. Six of these components (24, 25, 32–35) can be directly separated in the first dimension, while the other six (26–30) are separated in three heart-cut injections into the second-dimension chiral column. Again, excellent repeatability of retention times, peak areas, and R_s values is observed across the entire 2D experiment.

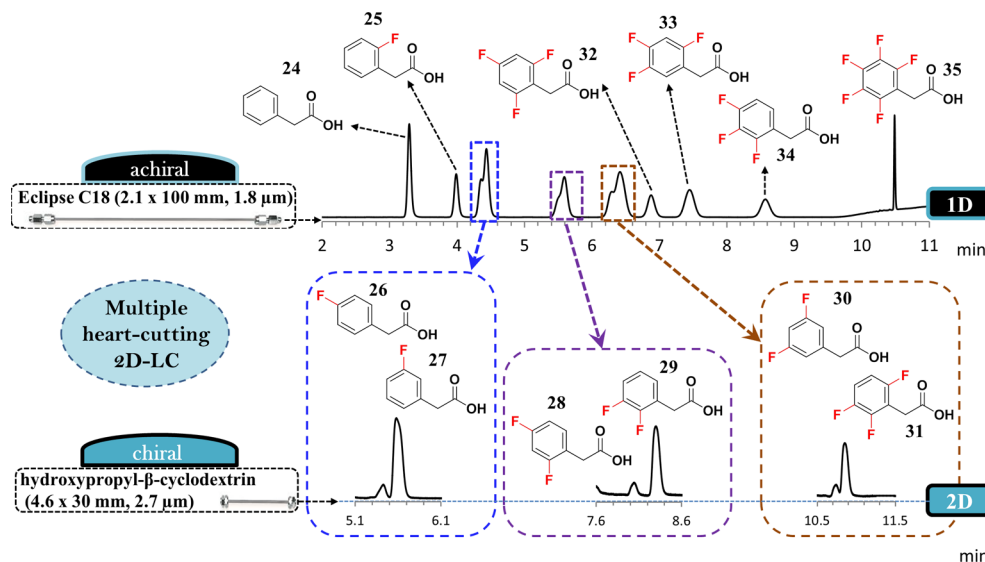


Figure 8.5. Multiple heart-cutting 2D-LC method for separation of complex mixture of fluorophenylacetic acid isomers. Conditions, first dimension (achiral): column, Zorbax RRHD Eclipse Plus C18 (2.1 mm × 100 mm, 1.8 μm); temperature, 40 °C. Detection: UV 210 nm. Flow rate: 0.5 mL/ min. Eluent A, 0.1% H₃PO₄ in H₂O; eluent B, ACN. Step gradient: hold 20% B for 7 min; 7–9 min, 95% B. Conditions, second dimension (chiral): column, HPRSP (4.6 mm × 30 mm, 2.7 μm). Flow rate: 1 mL/min. Isocratic mobile phase: 95:5% H₃PO₄/ACN. Detection: UV 210 nm. Sampling frequency: 240 Hz.

Table 8.6 Repeatability of retention times, peak areas and R_s values for the 2D-LC method shown in figure 8.5 (n = 3)

<i>1D</i>				
Elution order	Cut #	Compound #	R _t (min) ± RSD	Peak Area (mAU*s) ± RSD
Peak 1	-	24	3.26 ± 0.03	384.19 ± 0.01
Peak 2	-	25	3.95 ± 0.06	211.78 ± 0.09
Peak 3	1	26 and 27	4.40 ± 0.08	400.78 ± 0.41
Peak 4	2	28 and 29	5.55 ± 0.12	380.39 ± 0.11
Peak 5	3	30 and 31	6.37 ± 0.13	554.45 ± 13.26
Peak 6	-	32	6.83 ± 0.12	184.69 ± 0.32
Peak 7	-	33	7.40 ± 0.14	301.21 ± 0.10
Peak 8	-	34	8.51 ± 0.16	191.96 ± 0.24
Peak 9	-	35	10.48 ± 0.01	131.13 ± 4.91
<i>2D</i>				
Cut #	Compound #	R _t (min) ± RSD	Peak Area (mAU*s) ± RSD	Rs ± RSD
Cut # 1	26	5.43 ± 0.01	9.14 ± 6.33	0.92 ± 1.64
	27	5.58 ± 0.04	84.48 ± 3.96	
Cut # 2	28	8.05 ± 0.00	5.89 ± 0.00	1.70 ± 0.00
	29	8.30 ± 0.05	37.49 ± 5.56	
Cut # 3	30	10.85 ± 0.02	34.96 ± 3.02	2.96 ± 1.18
	31	11.33 ± 0.03	6.87 ± 9.04	

A number of high-speed enantioseparations in the 26–52 s time scale have been successfully developed and used as the second dimension of 2D-LC experiments for separation of complex multicomponent mixtures. It is important to mention that each first-dimension fraction containing a critical pair can be separated at a certain rate that might be different from another pair (under 30 s or from 30 to 50 s). However, the second-dimension cycle time has to be set at the slowest rate to guarantee full separation of the whole mixture with a single method. One could imagine 2D-LC software improvements that enable multiple cycle time injections within a second- dimension method. Another option is to have multiple column choices in the second dimension, which would allow separation of some 1D fractions under 30 s using a column and some other fractions also under 30 s on a different chiral column. This would improve the overall cycle time of a 2D-LC experiment, especially when injecting a large number of heart cuts onto a second

dimension. Clearly, the use of ultrafast chiral chromatography as the second dimension in 2D-LC offers an impressive ability to speedily address challenging problems of interest to pharmaceutical chemists during analysis of closely related species. While equipment and methods are still in a state of flux and rapid evolution, the fact that commercial instrumentation can be used for relatively rapid problem solving and method development is gratifying, suggesting that more general uptake of this methodology may be imminent.

8.5 Conclusions

In this study we have demonstrated that ultrafast chiral chromatography is effective as a second dimension for 2D chromatographic separations. Excellent chromatographic performance and an ability to achieve complete separation of challenging mixtures of closely related species were achieved by combining achiral and chiral narrow-bore columns (2.1 mm × 100 mm and 2.1 mm × 150 mm, sub-2 and 3 μm) in the first dimension with 4.6 mm × 30 mm and 4.6 mm × 50 mm columns packed with highly efficient chiral selectors (sub-2 μm fully porous and 2.7 μm fused-core particles) in the second dimension. Multiple achiral × chiral and chiral × chiral 2D-LC examples involving single and multiple heart-cutting, high-resolution sampling and comprehensive 2D-LC with ultrafast chiral chromatography in the second dimension have been developed. These methods have been successfully applied to the analysis of complex mixtures of closely related pharmaceutical, synthetic intermediates, drugs, and metabolites.

Chapter 9

General Summary

The dissertation demonstrated that sub-second and sub-minute chromatography is possible using ultrahigh efficiency silica particles in short columns. Chapter 2 addressed the synthesis of core-shell particle based chiral stationary phases and theoretical studies on ultrafast chiral separations. Enantiomeric separations of few seconds were shown. Frictional heating effects were discussed in detail. Chapter 3 focused on the applications of core-shell based chiral columns for ultrafast separations of pharmaceutically important compounds, namely fluoro and desfluoro analogs. Chapter 4 was based on the synthesis and packing studies of high efficiency, narrow particle size distribution chiral columns and their applications. Chapter 5 focused on ultrafast chiral separations studies in SFC. This work showed very unusual effects which were not encountered in liquid chromatography specially the extra-column tubing studies showed counterintuitive results. The choice of digital filter plays a critical role in achieving symmetric peak shapes in ultrafast chromatography. Simple derivative test was proposed to detect linear interpolation in the signal processing of some chromatographic data acquisition systems. Chapter 6 showed extreme speeds in sub-second regime. Practical and theoretical challenges were addressed. Chapter 7 demonstrated real life applications of ultrafast enantioseparations with important pharmaceuticals and synthetic intermediates. These separations can be routinely developed and swiftly integrated into standard workforce and catalytic identification to support enantioselective synthesis. Chapter 8 is based on the analysis of complex mixtures and closely related species by two-dimensional liquid chromatography using ultrafast methods in the second dimension. As demonstrated in all the chapters that superficially porous particles are extremely promising for ultrafast screening, shape

selective separations and two-dimensional applications. The question that remains to be solved is that can fully porous particles of narrow particle size distribution outperform superficially porous particles of the same dimensions. Understandably the packing eventually controls the practically attainable efficiencies. Future studies should explore whether the observed differences are due to difficulties in packing sub-2 μm particles or there are some other inherent particle features which control the performance of these particles. Future work should focus on column injection and on column detection where state of the art UHPLC lag behind in order to achieve ultrahigh efficiencies in 0.5 to 1 cm long columns.

APPENDIX A

NAMES OF CO-CONTRIBUTING AUTHORS

Chapter 2: Patel D.C., Breitbach, Z.S., Wahab, M.F., Barhate, C.L. and Armstrong

Chapter 3: Barhate, C.L., Breitbach, Z.S., Pinto, E.C., Regalado, E.L., Welch, C.J.
and Armstrong, D.W.,

Chapter 4: Barhate, C.L., Wahab, M.F., Breitbach, Z.S., Bell, D.S. and Armstrong,
D.W.

Chapter 5: Barhate, C.L., Wahab, M.F., Tognarelli, D.J., Berger, T.A. and Armstrong,
D.W.

Chapter 6: Wahab, M.F., Wimalasinghe, R.M., Wang, Y., Barhate, C.L., Patel, D.C.
and Armstrong, D.W.

Chapter 7: Barhate, C.L., Joyce, L.A., Makarov, A.A., Zawatzky, K., Bernardoni, F.,
Schafer, W.A., Armstrong, D.W., Welch, C.J. and Regalado, E.L.

Chapter 8: Barhate, C.L., Regalado, E.L., Contrella, N.D., Lee, J., Jo, J., Makarov,
A.A., Armstrong, D.W. and Welch, C.J.

APPENDIX B
RIGHTS AND PERMISSIONS

3/30/2017

Permission Grant - Barhate, Chandan

Permission Grant

John Ochs <J_Ochs@acs.org>

Wed 3/22/2017 3:34 AM

To: Barhate, Chandan <chandan.barhate@mavs.uta.edu>;

Cc: Copyright <Copyright@ACS.org>;

Dr. Barhate,

Thank you for contacting the ACS about permission to use the following publications in your forthcoming thesis:

- *Gone in Seconds: Praxis, Performance, and Peculiarities of Ultrafast Chiral Liquid Chromatography with Superficially Porous Particles*, DOI: 10.1021/acs.analchem.5b00715
- *Salient Sub-Second Separations*, DOI: 10.1021/acs.analchem.6b02260

Your permission requested is granted and there is no fee.

In your planned use, please note to readers that the excerpted material is included with permission from (*include complete reference citation*); Copyright (*year*) American Chemical Society and is available under the terms of the ACS AuthorChoice license.

If your thesis or dissertation to be published is in electronic format, please include a direct link to the published works using the ACS Articles on Request author-directed link (see <http://pubs.acs.org/page/policy/articlesonrequest/index.html>).

If you have any difficulty in finding the link, please contact our Journal Help Desk at support@services.acs.org or call 800-227-9919. The Help Desk is open Monday – Friday 24 hours per day.

We wish you every success with your thesis.

Best regards,

Jack Ochs.

John P. Ochs
VP – Strategic Planning & Analysis
Publications Division
[1155 16th St., NW | Washington | DC 20036](http://1155.16th.St.,NW|Washington|DC.20036)
T 202-872-6321 | F 202-872-6060 | 800-227-5558
www.acs.org

From: Barhate, Chandan [<mailto:chandan.barhate@mavs.uta.edu>]

Sent: Monday, March 20, 2017 4:16 PM

To: Craig Palmer

Subject: Permission to reprint in thesis

Dear Palmer,

I am writing this email request permission to reproduce open access articles I co-authored in ACS Analytical Chemistry journal.

The articles I am requesting reprint are:

1) Patel, D.C., Breitbach, Z.S., Wahab, M.F., **Barhate, C.L.** and Armstrong, D.W., 2015. Gone in seconds: praxis, performance, and peculiarities of ultrafast chiral liquid chromatography with superficially porous particles. *Analytical chemistry*, 87(18), pp.9137-9148.

<http://pubs.acs.org/doi/abs/10.1021/acs.analchem.5b00715>

2) Wahab, M.F., Wimalasinghe, R.M., Wang, Y., **Barhate, C.L.**, Patel, D.C. and Armstrong, D.W., 2016. Salient Sub-Second Separations. *Analytical Chemistry*, 88(17), pp.8821-8826.

<http://pubs.acs.org/doi/full/10.1021/acs.analchem.6b02260>

The dissertation will be about 250 pages long and will be completed by April 2017. The Title of dissertation

FUNDAMENTAL STUDIES ON ULTRAFAST CHIRAL AND ACHIRAL SEPARATIONS IN LIQUID CHROMATOGRAPHY AND SUB/SUPERCRITICAL FLUID CHROMATOGRAPHY

The permission can be emailed to this address. Thank you for your time.

Sincerely
Chandan L. Barhate
Graduate Research Assistant,
Department of Chemistry and Biochemistry,
University of Texas at Arlington,
Arlington, TX-76019
Email: chandan.barhate@mavs.uta.edu
Contact: 813-381-2374

**RightsLink®**[Home](#)[Create Account](#)[Help](#)**ACS Publications**
Most Trusted. Most Cited. Most Read.**Title:** Instrumental Idiosyncrasies Affecting the Performance of Ultrafast Chiral and Achiral Sub/Supercritical Fluid Chromatography**Author:** Chandan L. Barhate, M. Farooq Wahab, D. J. Tognarelli, et al**Publication:** Analytical Chemistry**Publisher:** American Chemical Society**Date:** Sep 1, 2016

Copyright © 2016, American Chemical Society

[LOGIN](#)

If you're a [copyright.com user](#), you can login to RightsLink using your copyright.com credentials. Already a [RightsLink user](#) or want to [learn more?](#)

PERMISSION/LICENSE IS GRANTED FOR YOUR ORDER AT NO CHARGE

This type of permission/license, instead of the standard Terms & Conditions, is sent to you because no fee is being charged for your order. Please note the following:

- Permission is granted for your request in both print and electronic formats, and translations.
- If figures and/or tables were requested, they may be adapted or used in part.
- Please print this page for your records and send a copy of it to your publisher/graduate school.
- Appropriate credit for the requested material should be given as follows: "Reprinted (adapted) with permission from (COMPLETE REFERENCE CITATION). Copyright (YEAR) American Chemical Society." Insert appropriate information in place of the capitalized words.
- One-time permission is granted only for the use specified in your request. No additional uses are granted (such as derivative works or other editions). For any other uses, please submit a new request.

[BACK](#)[CLOSE WINDOW](#)



RightsLink®

[Home](#)[Create Account](#)[Help](#)

Title: Ultrafast Chiral Chromatography as the Second Dimension in Two-Dimensional Liquid Chromatography Experiments

Author: Chandan L. Barhate, Erik L. Regalado, Nathan D. Contrella, et al

Publication: Analytical Chemistry

Publisher: American Chemical Society

Date: Jan 1, 2017

Copyright © 2017, American Chemical Society

[LOGIN](#)

If you're a [copyright.com user](#), you can login to RightsLink using your [copyright.com](#) credentials. Already a [RightsLink user](#) or want to [learn more?](#)

PERMISSION/LICENSE IS GRANTED FOR YOUR ORDER AT NO CHARGE

This type of permission/license, instead of the standard Terms & Conditions, is sent to you because no fee is being charged for your order. Please note the following:

- Permission is granted for your request in both print and electronic formats, and translations.
- If figures and/or tables were requested, they may be adapted or used in part.
- Please print this page for your records and send a copy of it to your publisher/graduate school.
- Appropriate credit for the requested material should be given as follows: "Reprinted (adapted) with permission from (COMPLETE REFERENCE CITATION). Copyright (YEAR) American Chemical Society." Insert appropriate information in place of the capitalized words.
- One-time permission is granted only for the use specified in your request. No additional uses are granted (such as derivative works or other editions). For any other uses, please submit a new request.

[BACK](#)[CLOSE WINDOW](#)

**ELSEVIER LICENSE
TERMS AND CONDITIONS**

Mar 20, 2017

This Agreement between Chandan L. Barhate ("You") and Elsevier ("Elsevier") consists of your license details and the terms and conditions provided by Elsevier and Copyright Clearance Center.

License Number	4073181215738
License date	
Licensed Content Publisher	Elsevier
Licensed Content Publication	Analytica Chimica Acta
Licensed Content Title	High efficiency, narrow particle size distribution, sub-2 μm based macrocyclic glycopeptide chiral stationary phases in HPLC and SFC
Licensed Content Author	Chandan L. Barhate, M. Farooq Wahab, Zachary S. Breitbach, David S. Bell, Daniel W. Armstrong
Licensed Content Date	22 October 2015
Licensed Content Volume	898
Licensed Content Issue	n/a
Licensed Content Pages	10
Start Page	128
End Page	137
Type of Use	reuse in a thesis/dissertation
Portion	full article
Format	both print and electronic
Are you the author of this Elsevier article?	Yes
Will you be translating?	No
Order reference number	
Title of your thesis/dissertation	FUNDAMENTAL STUDIES ON ULTRAFAST CHIRAL AND ACHIRAL SEPARATIONS IN LIQUID CHROMATOGRAPHY AND SUB/SUPERCRITICAL FLUID CHROMATOGRAPHY
Expected completion date	Apr 2017
Estimated size (number of pages)	200
Elsevier VAT number	GB 494 6272 12
Requestor Location	Chandan L. Barhate 1801 westview ter apt C ARLINGTON, TX 76013 United States Attn: Chandan L. Barhate
Publisher Tax ID	98-0397604
Total	0.00 USD
Terms and Conditions	

**ELSEVIER LICENSE
TERMS AND CONDITIONS**

Mar 20, 2017

This Agreement between Chandan L. Barhate ("You") and Elsevier ("Elsevier") consists of your license details and the terms and conditions provided by Elsevier and Copyright Clearance Center.

License Number	4073181473861
License date	
Licensed Content Publisher	Elsevier
Licensed Content Publication	Journal of Chromatography A
Licensed Content Title	Ultrafast separation of fluorinated and desfluorinated pharmaceuticals using highly efficient and selective chiral selectors bonded to superficially porous particles
Licensed Content Author	Chandan L. Barhate,Zachary S. Breitbach,Eduardo Costa Pinto,Erik L. Regalado,Christopher J. Welch,Daniel W. Armstrong
Licensed Content Date	24 December 2015
Licensed Content Volume	1426
Licensed Content Issue	n/a
Licensed Content Pages	7
Start Page	241
End Page	247
Type of Use	reuse in a thesis/dissertation
Intended publisher of new work	other
Portion	full article
Format	both print and electronic
Are you the author of this Elsevier article?	Yes
Will you be translating?	No
Order reference number	
Title of your thesis/dissertation	FUNDAMENTAL STUDIES ON ULTRAFAST CHIRAL AND ACHIRAL SEPARATIONS IN LIQUID CHROMATOGRAPHY AND SUB/SUPERCRITICAL FLUID CHROMATOGRAPHY
Expected completion date	Apr 2017
Estimated size (number of pages)	200
Elsevier VAT number	GB 494 6272 12
Requestor Location	Chandan L. Barhate 1801 westview ter apt C

ARLINGTON, TX 76013
United States
Attn: Chandan L. Barhate

3/30/2017

RE: Permission Request Form: Chandan L. Barhate - Barhate, Chandan

RE: Permission Request Form: Chandan L. Barhate

CONTRACTS-COPYRIGHT (shared) <Contracts-Copyright@rsc.org>

Fri 3/24/2017 7:03 PM

To: Barhate, Chandan <chandan.barhate@mavs.uta.edu>;

Dear Chandan

The Royal Society of Chemistry (RSC) hereby grants permission for the use of your paper(s) specified below in the printed and microfilm version of your thesis. You may also make available the PDF version of your paper(s) that the RSC sent to the corresponding author(s) of your paper(s) upon publication of the paper(s) in the following ways: in your thesis via any website that your university may have for the deposition of theses, via your university's Intranet or via your own personal website. We are however unable to grant you permission to include the PDF version of the paper(s) on its own in your institutional repository. The Royal Society of Chemistry is a signatory to the STM Guidelines on Permissions (available on request).

Please note that if the material specified below or any part of it appears with credit or acknowledgement to a third party then you must also secure permission from that third party before reproducing that material.

Please ensure that the thesis states the following:

Reproduced by permission of The Royal Society of Chemistry

and include a link to the paper on the Royal Society of Chemistry's website.

Please ensure that your co-authors are aware that you are including the paper in your thesis.

Regards

Gill Cockhead
Publishing Contracts & Copyright Executive

Gill Cockhead
Publishing Contracts & Copyright Executive
Royal Society of Chemistry,
Thomas Graham House,
Science Park, Milton Road,
Cambridge, CB4 0WF, UK
Tel +44 (0) 1223 432134

Follow the Royal Society of Chemistry:
www.rsc.org/follow

Winner of The Queen's Award for Enterprise, International Trade 2013

-----Original Message-----

From: chandan.barhate@mavs.uta.edu [<mailto:chandan.barhate@mavs.uta.edu>]

Sent: 22 March 2017 14:35

To: CONTRACTS-COPYRIGHT (shared) <Contracts-Copyright@rsc.org>

Cc: chandan.barhate@mavs.uta.edu

Subject: Permission Request Form: Chandan L. Barhate

3/30/2017

RE: Permission Request Form: Chandan L. Barhate - Barhate, Chandan

Name : Chandan L. Barhate
Address :

Department Of Chemistry and Biochemistry University Of Texas at Arlington

Tel : 8133812374
Fax :
Email : chandan.barhate@mavs.uta.edu

I am preparing the following work for publication:

Article/Chapter Title : FUNDAMENTAL STUDIES ON ULTRAFAST CHIRAL AND ACHIRAL SEPARATIONS IN LIQUID CHROMATOGRAPHY AND SUB/SUPERCRITICAL FLUID CHROMATOGRAPHY

Journal/Book Title :
Editor/Author(s) : Chandan L. Barhate
Publisher : University of Texas at Arlington

I would very much appreciate your permission to use the following material:

Journal/Book Title : Ultrafast chiral separations for high throughput enantiopurity analysis
Editor/Author(s) : C. L. Barhate, L. A. Joyce, A. A. Makarov, K. Zawatzky, F. Bernardoni, W. A. Schafer, D. W. Armstrong, C. J. Welch and E. L. Regalado
Volume Number : 53
Year of Publication : 2017
Description of Material : article
Page(s) : 509-512

Any Additional Comments :

I would like to request permission to reproduce open access articles I co-authored in Chemical Communications

The articles I am requesting reprint is:

Barhate, C.L., Joyce, L.A., Makarov, A.A., Zawatzky, K., Bernardoni, F., Schafer, W.A., Armstrong, D.W., Welch, C.J. and Regalado, E.L., 2017. Ultrafast chiral separations for high throughput enantiopurity analysis. Chemical Communications, 53(3), pp.509-512.

The dissertation will be about 200 pages long and will be completed by April 2017.

The Title of dissertation

FUNDAMENTAL STUDIES ON ULTRAFAST CHIRAL AND ACHIRAL SEPARATIONS IN LIQUID CHROMATOGRAPHY AND SUB/SUPERCRITICAL FLUID CHROMATOGRAPHY

Thank you for your time.

Sincerely
Chandan L. Barhate
Graduate Research Assistant,
Department of Chemistry and Biochemistry, University of Texas at Arlington, Arlington, TX-76019
Email: chandan.barhate@mavs.uta.edu
Contact: 813-381-2374

This communication is from The Royal Society of Chemistry, a company incorporated in England by Royal Charter (registered

3/30/2017

RE: Permission Request Form: Chandan L. Barhate - Barhate, Chandan

number RC000524) and a charity registered in England and Wales (charity number 207890). Registered office: Burlington House, Piccadilly, London W1J 0BA. Telephone: 0207 4378 6556, Facsimile: 0207 4490 3393 (Head Office). This communication (including any attachments) may contain confidential, privileged or copyright material. It may not be relied upon or disclosed to any person other than the intended recipient(s) without the consent of The Royal Society of Chemistry. If you are not the intended recipient(s), please (1) notify us immediately by replying to this email and delete all copies from your system and (2) note that disclosure, distribution, copying or use of this communication is strictly prohibited. Any advice given by The Royal Society of Chemistry has been carefully formulated but is necessarily based on the information available, and The Royal Society of Chemistry cannot be held responsible for accuracy or completeness. In this respect, any views or opinions presented in this email are solely those of the author and may not represent those of The Royal Society of Chemistry.

The Royal Society of Chemistry owes no duty of care and shall not be liable for any resulting damage or loss as a result of the use of this email and/or attachments. The Royal Society of Chemistry acknowledges that a disclaimer cannot restrict liability at law for personal injury or death arising through a finding of negligence. The Royal Society of Chemistry does not warrant that its emails or attachments are Virus-free: Please rely on your own screening.

References:

- (1) *J. Org. Chem.* **1962**, *27*, 700-706.
- (2) Kirkland, J. *Journal of chromatographic science* **2000**, *38*, 535-544.
- (3) Barhate, C. L.; Joyce, L. A.; Makarov, A. A.; Zawatzky, K.; Bernardoni, F.; Schafer, W. A.; Armstrong, D. W.; Welch, C. J.; Regalado, E. L. *Chemical Communications* **2017**, *53*, 509-512.
- (4) Foley, J. P. *Analyst* **1991**, *116*, 1275-1279.
- (5) Halasz, I.; Naefe, M. *Analytical Chemistry* **1972**, *44*, 76-84.
- (6) Cabooter, D.; Fanigliulo, A.; Bellazzi, G.; Allieri, B.; Rottigni, A.; Desmet, G. *Journal of Chromatography A* **2010**, *1217*, 7074-7081.
- (7) Gritti, F.; Bell, D. S.; Guiochon, G. *Journal of Chromatography A* **2014**, *1355*, 179-192.
- (8) Gritti, F.; Guiochon, G. *Journal of Chromatography A* **2015**, *1384*, 76-87.
- (9) Armstrong, D. W.; Tang, Y.; Chen, S.; Zhou, Y.; Bagwill, C.; Chen, J.-R. *Analytical Chemistry* **1994**, *66*, 1473-1484.
- (10) Liu, Y.; Berthod, A.; Mitchell, C. R.; Xiao, T. L.; Zhang, B.; Armstrong, D. W. *Journal of Chromatography A* **2002**, *978*, 185-204.
- (11) Péter, A.; Török, G.; Armstrong, D. W.; Tóth, G.; Tourwé, D. *Journal of Chromatography A* **1998**, *828*, 177-190.
- (12) Sun, P.; Wang, C.; Breitbach, Z. S.; Zhang, Y.; Armstrong, D. W. *Analytical Chemistry* **2009**, *81*, 10215-10226.
- (13) Armstrong, D. W.; DeMond, W.; Alak, A.; Hinze, W. L.; Riehl, T. E.; Bui, K. H. *Analytical Chemistry* **1985**, *57*, 234-237.
- (14) Armstrong, D. W.; Demond, W.; Czech, B. P. *Analytical Chemistry* **1985**, *57*, 481-484.
- (15) Barhate, C. L.; Breitbach, Z. S.; Pinto, E. C.; Regalado, E. L.; Welch, C. J.; Armstrong, D. W. *Journal of Chromatography A* **2015**, *1426*, 241-247.
- (16) Stoll, D. R.; Li, X.; Wang, X.; Carr, P. W.; Porter, S. E.; Rutan, S. C. *Journal of Chromatography A* **2007**, *1168*, 3-43.
- (17) Stoll, D. R.; Cohen, J. D.; Carr, P. W. *Journal of Chromatography a* **2006**, *1122*, 123-137.
- (18) Stoll, D. R.; Carr, P. W. *Analytical Chemistry* **2017**, *89*, 519-531.
- (19) Stoll, D. R.; Harmes, D. C.; Danforth, J.; Wagner, E.; Guillarme, D.; Fekete, S.; Beck, A. *Analytical Chemistry* **2015**, *87*, 8307-8315.
- (20) Vaast, A.; Tyteca, E.; Desmet, G.; Schoenmakers, P. J.; Eeltink, S. *Journal of Chromatography A* **2014**, *1355*, 149-157.
- (21) León-González, M. E.; Rosales-Conrado, N.; Pérez-Arribas, L. V.; Guillén-Casla, V. *Biomedical Chromatography* **2014**, *28*, 59-83.
- (22) Cacciola, F.; Farnetti, S.; Dugo, P.; Marriotti, P. J.; Mondello, L. *Journal of Separation Science* **2017**, *40*, 7-24.

- (23) Uliyanchenko, E.; Cools, P. J. C. H.; van der Wal, S.; Schoenmakers, P. J. *Analytical Chemistry* **2012**, *84*, 7802-7809.
- (24) Stoll, D. R.; Talus, E. S.; Harmes, D. C.; Zhang, K. *Analytical and Bioanalytical Chemistry* **2015**, *407*, 265-277.
- (25) Chu, Y.-Q.; Wainer, I. W. *Pharmaceutical Research* **1988**, *5*, 680-683.
- (26) Davankov, V. A. R., S. V. *J. Chromatogr. A* **1971**, *60*, 280-283.
- (27) Mikes, F. E. B., G. *J. Chromatogr. A* **1978**, *149*, 455-464.
- (28) Pirkle, W. H. F., J. M. *J. Org. Chem.* **1981**, *46*, 2935-2938.
- (29) Okamoto, Y. H., S.; Okamoto, I.; Yuki, H.; Murata, S.; Noyori, R. T., H. *J. Am. Chem. Soc.* **1981**, *103*, 6971-6973.
- (30) Armstrong, D. W. W., T. J.; Armstrong, R. D.; Beesley, T. E. *Science* **1986**, *232*, 1132-1135.
- (31) Okamoto, Y. K., M.; Yamamoto, K.; Hatada, K. *Chem. Lett.* **1987**, 1857-1860.
- (32) Stalcup, A. M. C., S. C.; Armstrong, D. W.; Pitha, J. . *J. Chromatogr. A* **1990**, *513*, 181-194.
- (33) Armstrong, D. W. S., A. M.; Hilton, M. L.; Duncan, J. D.;; Faulkner, J. R., Jr.; Chang, S. C. *Anal. Chem.* **1990**, *62*, 1610-1615.
- (34) Pirkle, W. H. W., C. J.; Lamm, B. *J. Org. Chem.* **1992**, *57*, 3854-3860.
- (35) Allenmark, S. B., B.; Boreň, H. *J. Chromatogr. A* **1983**, *264*, 63-68.
- (36) Armstrong, D. W. D., W. . *J. Chromatogr. Sci.* **1984**, *22*, 411-415.
- (37) Okamoto, Y. K., M.; Yamamoto, K.; Hatada, K. *Chem. Lett.* **1984**, 739-742.
- (38) Armstrong, D. W. T., Y.; Chen, S.; Zhou, Y.; Bagwill, C.;; Chen, J.-R. *Anal. Chem.* **1994**, *66*, 1473-1484.
- (39) Lämmerhofer, M.; Lindner, W. *Journal of Chromatography A* **1996**, *741*, 33-48.
- (40) Maier, N. M.; Nicoletti, L.; Lämmerhofer, M.; Lindner, W. *Chirality* **1999**, *11*, 522-528.
- (41) Berthod, A.; Chen, X.; Kullman, J. P.; Armstrong, D. W.; Gasparrini, F.; D'Acquaric, I.; Villani, C.; Carotti, A. *Analytical Chemistry* **2000**, *72*, 1767-1780.
- (42) Gasparrini, F.; Misiti, D.; Rompietti, R.; Villani, C. *Journal of Chromatography A* **2005**, *1064*, 25-38.
- (43) Sun, P.; Armstrong, D. W. *Journal of Chromatography A* **2010**, *1217*, 4904-4918.
- (44) Han, X.; He, L.; Zhong, Q.; Beesley, T. E.; Armstrong, D. W. *Chromatographia* **2006**, *63*, 13-23.
- (45) Davankov, V. A. *Chirality* **1997**, *9*, 99-102.
- (46) Gasparrini, F.; Misiti, D.; Villani, C. *Chirality* **1992**, *4*, 447-458.
- (47) Oberleitner, W. R.; Maier, N. M.; Lindner, W. *Journal of Chromatography A* **2002**, *960*, 97-108.

- (48) Sajonz, P.; Schafer, W.; Gong, X.; Shultz, S.; Rosner, T.; Welch, C. J. *Journal of Chromatography A* **2007**, *1145*, 149-154.
- (49) Hamman, C.; Wong, M.; Aliagas, I.; Ortwine, D. F.; Pease, J.; Schmidt Jr, D. E.; Victorino, J. *Journal of Chromatography A* **2013**, *1305*, 310-319.
- (50) Ai, F.; Li, L.; Ng, S.-C.; Tan, T. T. Y. *Journal of Chromatography A* **2010**, *1217*, 7502-7506.
- (51) Cancelliere, G.; Ciogli, A.; D'Acquarica, I.; Gasparrini, F.; Kocergin, J.; Misiti, D.; Pierini, M.; Ritchie, H.; Simone, P.; Villani, C. *Journal of Chromatography A* **2010**, *1217*, 990-999.
- (52) Kotoni, D.; Ciogli, A.; Molinaro, C.; D'Acquarica, I.; Kocergin, J.; Szczerba, T.; Ritchie, H.; Villani, C.; Gasparrini, F. *Analytical Chemistry* **2012**, *84*, 6805-6813.
- (53) Cavazzini, A.; Marchetti, N.; Guzzinati, R.; Pierini, M.; Ciogli, A.; Kotoni, D.; D'Acquarica, I.; Villani, C.; Gasparrini, F. *TrAC Trends in Analytical Chemistry* **2014**, *63*, 95-103.
- (54) Gritti, F. G., G. *LC-GC N. Am.* **2012**, 586-597.
- (55) Omamogho, J. O. N., E.; Connolly, D.; Glennon, J. *LC-GC N. Am.* **2012**, 63-69.
- (56) DeStefano, J. J.; Langlois, T. J.; Kirkland, J. J. *Journal of Chromatographic Science* **2008**, *46*, 254-260.
- (57) Gritti, F. *LC-GC N. Am.* **2014**, 928-940.
- (58) Broeckhoven, K.; Cabooter, D.; Desmet, G. *Journal of Pharmaceutical Analysis* **2013**, *3*, 313-323.
- (59) Bruns, S.; Stoeckel, D.; Smarsly, B. M.; Tallarek, U. *Journal of Chromatography A* **2012**, *1268*, 53-63.
- (60) Gritti, F.; Farkas, T.; Heng, J.; Guiochon, G. *Journal of Chromatography A* **2011**, *1218*, 8209-8221.
- (61) Dolzan, M. D.; Spudeit, D. A.; Breitbach, Z. S.; Barber, W. E.; Micke, G. A.; Armstrong, D. W. *Journal of Chromatography A* **2014**, *1365*, 124-130.
- (62) Spudeit, D. A.; Dolzan, M. D.; Breitbach, Z. S.; Barber, W. E.; Micke, G. A.; Armstrong, D. W. *Journal of Chromatography A* **2014**, *1363*, 89-95.
- (63) Fanali, S.; D'Orazio, G.; Farkas, T.; Chankvetadze, B. *Journal of Chromatography A* **2012**, *1269*, 136-142.
- (64) Lomsadze, K.; Jibuti, G.; Farkas, T.; Chankvetadze, B. *Journal of Chromatography A* **2012**, *1234*, 50-55.
- (65) Gritti, F.; Guiochon, G. *Journal of Chromatography A* **2014**, *1348*, 87-96.
- (66) Weatherly, C. A.; Na, Y.-C.; Nanayakkara, Y. S.; Woods, R. M.; Sharma, A.; Lacour, J.; Armstrong, D. W. *Journal of Chromatography B* **2014**, *955-956*, 72-80.
- (67) Armstrong, D. W.; Li, W.; Chang, C. D.; Pitha, J. *Analytical Chemistry* **1990**, *62*, 914-923.

- (68) Jiang, C.; Tong, M.-Y.; Breitbach, Z. S.; Armstrong, D. W. *ELECTROPHORESIS* **2009**, *30*, 3897-3909.
- (69) Zhang, Y.; Breitbach, Z. S.; Wang, C.; Armstrong, D. W. *Analyst* **2010**, *135*, 1076-1083.
- (70) Perera, S.; Na, Y.-C.; Doundoulakis, T.; Ngo, V. J.; Feng, Q.; Breitbach, Z. S.; Lovely, C. J.; Armstrong, D. W. *Chirality* **2013**, *25*, 133-140.
- (71) Padivitage, N. L. T.; Dodbiba, E.; Breitbach, Z. S.; Armstrong, D. W. *Drug Testing and Analysis* **2014**, *6*, 542-551.
- (72) Woods, R. M.; Patel, D. C.; Lim, Y.; Breitbach, Z. S.; Gao, H.; Keene, C.; Li, G.; Kürti, L.; Armstrong, D. W. *Journal of Chromatography A* **2014**, *1357*, 172-181.
- (73) Woods, R. M. B., Z. S.; Armstrong, D. W. . *LC–GC N. Am.* **2014**, *32*, 742–751.
- (74) Fekete, S.; Kohler, I.; Rudaz, S.; Guillarme, D. *Journal of Pharmaceutical and Biomedical Analysis* **2014**, *87*, 105-119.
- (75) Wang, X. C., P. W.; Stoll, D. R. *LC–GC N. Am.* **2010**, *28*, 932-942.
- (76) Elgass, H.; Engelhardt, H.; Halász, I. *Fresenius' Zeitschrift für analytische Chemie* **1979**, *294*, 97-106.
- (77) Guiochon, G.; Sepaniak, M. J. *Analytical Chemistry* **1991**, *63*, 73-73.
- (78) Ma, Y.; Chassy, A. W.; Miyazaki, S.; Motokawa, M.; Morisato, K.; Uzu, H.; Ohira, M.; Furuno, M.; Nakanishi, K.; Minakuchi, H.; Mriziq, K.; Farkas, T.; Fiehn, O.; Tanaka, N. *Journal of Chromatography A* **2015**, *1383*, 47-57.
- (79) Usher, K. M.; Simmons, C. R.; Dorsey, J. G. *Journal of Chromatography A* **2008**, *1200*, 122-128.
- (80) de Villiers, A.; Lauer, H.; Szucs, R.; Goodall, S.; Sandra, P. *Journal of Chromatography A* **2006**, *1113*, 84-91.
- (81) Fountain, K. J.; Neue, U. D.; Grumbach, E. S.; Diehl, D. M. *Journal of Chromatography A* **2009**, *1216*, 5979-5988.
- (82) Gritti, F.; Guiochon, G. *Analytical Chemistry* **2008**, *80*, 5009-5020.
- (83) Gritti, F.; Martin, M.; Guiochon, G. *Analytical Chemistry* **2009**, *81*, 3365-3384.
- (84) Halász, I.; Endeke, R.; Asshauer, J. *Journal of Chromatography A* **1975**, *112*, 37-60.
- (85) Giddings, J. C. *Dynamics of Chromatography: Principles and Theory*, 1st ed.; CRC Press: Boca Raton: FL, 2002.
- (86) Boehm, R. E.; Martire, D. E.; Armstrong, D. W. *Analytical Chemistry* **1988**, *60*, 522-528.
- (87) Gritti, F.; Guiochon, G. *Journal of Chromatography A* **2010**, *1217*, 6350-6365.
- (88) Poppe, H.; Kraak, J. C.; Huber, J. F. K.; van den Berg, J. H. M. *Chromatographia* **1981**, *14*, 515-523.

- (89) Lin, J. H.; Lu, A. Y. *Pharmacological reviews* **1997**, *49*, 403-449.
- (90) Mena, F.; Mena, B.; Sharts, O. N. *Journal of Molecular Pharmaceutics & Organic Process Research* **2013**.
- (91) H. Zhang, Y. L., Z. Jiang. *J. Biomol. Res. Ther.* **2012**), *72*, 6905–6917.
- (92) R. Filler, R. S. *Future Med. Chem.* **2009**, *1* 777–791.
- (93) Filler, R.; Saha, R. *Future Medicinal Chemistry* **2009**, *1*, 777-791.
- (94) K. Köhler, K. W., A.S. Wirth. *Palladium-Catalyzed Cross-Coupling Reactions*; Wiley-VCH Verlag GmbH & Co. KGaA,: Weinheim, Germany, 2013.
- (95) Bellur Atici, E.; Karlığa, B. *Journal of Pharmaceutical Analysis* **2015**, *5*, 356-370.
- (96) Ertürk, S.; Sevinç Aktaş, E.; Ersoy, L.; Fıçıcıoğlu, S. *Journal of Pharmaceutical and Biomedical Analysis* **2003**, *33*, 1017-1023.
- (97) Turco, L.; Provera, S.; Curcuruto, O.; Bernabè, E.; Nicoletti, A.; Martini, L.; Castoldi, D.; Cimarosti, Z.; Papini, D.; Marchioro, C.; Dams, R. *Journal of Pharmaceutical and Biomedical Analysis* **2011**, *54*, 67-73.
- (98) Regalado, E. L.; Zhuang, P.; Chen, Y.; Makarov, A. A.; Schafer, W. A.; McGachy, N.; Welch, C. J. *Analytical Chemistry* **2014**, *86*, 805-813.
- (99) Regalado, E. L.; Dermenjian, R. K.; Joyce, L. A.; Welch, C. J. *Journal of Pharmaceutical and Biomedical Analysis* **2014**, *92*, 1-5.
- (100) Regalado, E. L.; Makarov, A. A.; McClain, R.; Przybyciel, M.; Welch, C. J. *Journal of Chromatography A* **2015**, *1380*, 45-54.
- (101) Zhang, W. *Journal of Fluorine Chemistry* **2008**, *129*, 910-919.
- (102) Przybyciel, M. *LC–GC Eur.* **2006**, *19*, 19-28.
- (103) Armstrong, D. W. *Journal of Liquid Chromatography* **1980**, *3*, 895-900.
- (104) Armstrong, D. W.; DeMond, W. *Journal of Chromatographic Science* **1984**, *22*, 411-415.
- (105) Maria Pawlowska, S. C., Daniel W. Armstrong. **1993**, *641*, 257–265.
- (106) Berthod, A.; Jin, H. L.; Beesley, T. E.; Duncan, J. D.; Armstrong, D. W. *Journal of Pharmaceutical and Biomedical Analysis* **1990**, *8*, 123-130.
- (107) Armstrong, D. W.; Stine, G. Y. *Journal of the American Chemical Society* **1983**, *105*, 2962-2964.
- (108) Seeman, J. I.; Secor, H. V.; Armstrong, D. W.; Ward, K. D.; Ward, T. J. *Journal of Chromatography A* **1989**, *483*, 169-177.
- (109) Karlsson, C.; Karlsson, L.; Armstrong, D. W.; Owens, P. K. *Analytical Chemistry* **2000**, *72*, 4394-4401.
- (110) Armstrong, D. W.; Liu, Y.; Ekborgott, K. H. *Chirality* **1995**, *7*, 474-497.
- (111) Zhang, B.; Soukup, R.; Armstrong, D. W. *Journal of Chromatography A* **2004**, *1053*, 89-99.
- (112) Soukup-Hein, R. J.; Schneiderheinze, J.; Mehelic, P.; Armstrong, D. W. *Chromatographia* **2007**, *66*, 461-468.

- (113) Patel, D. C.; Breitbach, Z. S.; Wahab, M. F.; Barhate, C. L.; Armstrong, D. W. *Analytical Chemistry* **2015**, *87*, 9137-9148.
- (114) Spudeit, D. A.; Breitbach, Z. S.; Dolzan, M. D.; Micke, G. A.; Armstrong, D. W. *Chirality* **2015**, *27*, 788-794.
- (115) Barhate, C. L.; Wahab, M. F.; Breitbach, Z. S.; Bell, D. S.; Armstrong, D. W. *Analytica Chimica Acta* **2015**, *898*, 128-137.
- (116) Allenmark, S. G.; Andersson, S.; Möller, P.; Sanchez, D. *Chirality* **1995**, *7*, 248-256.
- (117) Rosini, C.; Altemura, P.; Pini, D.; Bertucci, C.; Zullino, G.; Salvadori, P. *Journal of Chromatography A* **1985**, *348*, 79-87.
- (118) Stalcup, A. M.; Chang, S.-C.; Armstrong, D. W.; Pitha, J. *Journal of Chromatography A* **1990**, *513*, 181-194.
- (119) Okamoto, Y.; Kawashima, M.; Hatada, K. *Journal of Chromatography A* **1986**, *363*, 173-186.
- (120) Pawlowska, M.; Chen, S.; Armstrong, D. W. *Journal of Chromatography A* **1993**, *641*, 257-265.
- (121) Guillarme, D.; Bonvin, G.; Badoud, F.; Schappler, J.; Rudaz, S.; Veuthey, J.-L. *Chirality* **2010**, *22*, 320-330.
- (122) Kotoni, D.; Ciogli, A.; D'Acquarica, I.; Kocergin, J.; Szczerba, T.; Ritchie, H.; Villani, C.; Gasparrini, F. *Journal of Chromatography A* **2012**, *1269*, 226-241.
- (123) Thurmann, S.; Lotter, C.; Heiland, J. J.; Chankvetadze, B.; Belder, D. *Analytical Chemistry* **2015**, *87*, 5568-5576.
- (124) Regalado, E. L.; Welch, C. J. *Journal of Separation Science* **2015**, *38*, 2826-2832.
- (125) Sciascera, L.; Ismail, O.; Ciogli, A.; Kotoni, D.; Cavazzini, A.; Botta, L.; Szczerba, T.; Kocergin, J.; Villani, C.; Gasparrini, F. *Journal of Chromatography A* **2015**, *1383*, 160-168.
- (126) Yu, L.; Wang, S.; Zeng, S. In *Chiral Separations: Methods and Protocols*, Scriba, G. K. E., Ed.; Humana Press: Totowa, NJ, 2013, pp 221-231.
- (127) Biba, M.; Regalado, E. L.; Wu, N.; Welch, C. J. *Journal of Chromatography A* **2014**, *1363*, 250-256.
- (128) Min, Y.; Sui, Z.; Liang, Z.; Zhang, L.; Zhang, Y. *Journal of Pharmaceutical and Biomedical Analysis* **2015**, *114*, 247-253.
- (129) Wahab, M. F.; Pohl, C. A.; Lucy, C. A. *Journal of Chromatography A* **2012**, *1270*, 139-146.
- (130) Yew, B. G.; Ureta, J.; Shalliker, R. A.; Drumm, E. C.; Guiochon, G. *AIChE Journal* **2003**, *49*, 642-664.
- (131) Wong, V.; Shalliker, R. A.; Guiochon, G. *Analytical Chemistry* **2004**, *76*, 2601-2608.
- (132) Desmond, K. W.; Weeks, E. R. *Physical Review E* **2014**, *90*, 022204.

- (133) Wahab, M. F.; Dasgupta, P. K.; Kadjo, A. F.; Armstrong, D. W. *Analytica Chimica Acta* **2016**, *907*, 31-44.
- (134) Cavazzini, A.; Pasti, L.; Dondi, F.; Finessi, M.; Costa, V.; Gasparrini, F.; Ciogli, A.; Bedani, F. *Analytical Chemistry* **2009**, *81*, 6735-6743.
- (135) Berthod, A.; Liu, Y.; Bagwill, C.; Armstrong, D. W. *Journal of Chromatography A* **1996**, *731*, 123-137.
- (136) Gere, D. R.; Board, R.; McManigill, D. *Analytical Chemistry* **1982**, *54*, 736-740.
- (137) Wang, C.; Armstrong, D. W.; Risley, D. S. *Analytical Chemistry* **2007**, *79*, 8125-8135.
- (138) Payagala, T.; Wanigasekara, E.; Armstrong, D. W. *Analytical and Bioanalytical Chemistry* **2011**, *399*, 2445-2461.
- (139) Woods, R. M., Armstrong, D.W., Breitbach, Z.S. *LC-GC N. Am.* **2014**, *32*, 742-751.
- (140) van Wasen, U.; Swaid, I.; Schneider, G. M. *Angewandte Chemie International Edition in English* **1980**, *19*, 575-587.
- (141) Berthod, A.; Nair, U. B.; Bagwill, C.; Armstrong, D. W. *Talanta* **1996**, *43*, 1767-1782.
- (142) De Pauw, R.; Choikhet, K.; Desmet, G.; Broeckhoven, K. *Journal of Chromatography A* **2014**, *1361*, 277-285.
- (143) De Pauw, R.; Shoykhet, K.; Desmet, G.; Broeckhoven, K. *Journal of Chromatography A* **2015**, *1403*, 132-137.
- (144) Berger, T. A. *Chromatographia* **2010**, *72*, 597-602.
- (145) Nováková, L.; Chocholouš, P.; Solich, P. *Talanta* **2014**, *121*, 178-186.
- (146) Berger, T. A.; Berger, B. K. *Journal of Chromatography A* **2011**, *1218*, 2320-2326.
- (147) Berger, T. A.; Wilson, W. H. *Analytical Chemistry* **1993**, *65*, 1451-1455.
- (148) Berger, T. A. *Journal of Chromatography A* **2016**, *1444*, 129-144.
- (149) Berger, T. A. *Journal of Chromatography A* **2015**, *1421*, 171-183.
- (150) Liu, Y.; Rozhkov, R. V.; Larock, R. C.; Xiao, T. L.; Armstrong, D. W. *Chromatographia* **2003**, *58*, 775-779.
- (151) Pelletier, S.; Lucy, C. A. *Journal of Chromatography A* **2006**, *1125*, 189-194.
- (152) Sih, R.; Dehghani, F.; Foster, N. R. *The Journal of Supercritical Fluids* **2007**, *41*, 148-157.
- (153) Hupe, K. P.; Jonker, R. J.; Rozing, G. *Journal of Chromatography A* **1984**, *285*, 253-265.
- (154) Wang, C.; Zhang, Y. *Journal of Chromatography A* **2013**, *1281*, 127-134.
- (155) Peadar, P. A.; Lee, M. L. *Journal of Chromatography A* **1983**, *259*, 1-16.
- (156) Xu, Q. A. *Ultra-high performance liquid chromatography and its applications*; John Wiley & Sons, 2013.

- (157) Guiochon, G.; Tarafder, A. *Journal of Chromatography A* **2011**, *1218*, 1037-1114.
- (158) Cabooter, D.; Lynen, F.; Sandra, P.; Desmet, G. *Analytical Chemistry* **2008**, *80*, 1679-1688.
- (159) Berger, T. A. *Packed column SFC*; Royal society of chemistry, 1995; Vol. 2.
- (160) Rajendran, A.; Gilkison, T. S.; Mazzotti, M. *Journal of Separation Science* **2008**, *31*, 1279-1289.
- (161) Taylor, L. T. *The Journal of Supercritical Fluids* **2009**, *47*, 566-573.
- (162) Shannon, C. E. *Proceedings of the IRE* **1949**, *37*, 10-21.
- (163) Ismail, O. H.; Ciogli, A.; Villani, C.; De Martino, M.; Pierini, M.; Cavazzini, A.; Bell, D. S.; Gasparrini, F. *Journal of Chromatography A* **2016**, *1427*, 55-68.
- (164) Oppenheim, A. V. *Discrete-time signal processing*; Pearson Education India, 1999.
- (165) Horvath, C. G.; Preiss, B. A.; Lipsky, S. R. *Analytical Chemistry* **1967**, *39*, 1422-1428.
- (166) Barhate, C. L.; Wahab, M. F.; Tognarelli, D. J.; Berger, T. A.; Armstrong, D. W. *Analytical Chemistry* **2016**, *88*, 8664-8672.
- (167) Fekete, S.; Ganzler, K.; Fekete, J. *Journal of Pharmaceutical and Biomedical Analysis* **2011**, *54*, 482-490.
- (168) Jeong, E. S.; Kim, S.-H.; Cha, E.-J.; Lee, K. M.; Kim, H. J.; Lee, S.-W.; Kwon, O.-S.; Lee, J. *Rapid Communications in Mass Spectrometry* **2015**, *29*, 367-384.
- (169) D'Attoma, A.; Heinisch, S. *Journal of Chromatography A* **2013**, *1306*, 27-36.
- (170) Gargano, A. F. G.; Duffin, M.; Navarro, P.; Schoenmakers, P. J. *Analytical Chemistry* **2016**, *88*, 1785-1793.
- (171) Jacobson, S. C.; Culbertson, C. T.; Daler, J. E.; Ramsey, J. M. *Analytical Chemistry* **1998**, *70*, 3476-3480.
- (172) Moore, A. W.; Jorgenson, J. W. *Analytical Chemistry* **1995**, *67*, 3448-3455.
- (173) Piehl, N.; Ludwig, M.; Belder, D. *ELECTROPHORESIS* **2004**, *25*, 3848-3852.
- (174) Guetschow, E. D.; Steyer, D. J.; Kennedy, R. T. *Analytical Chemistry* **2014**, *86*, 10373-10379.
- (175) Umehara, R.; Harada, M.; Okada, T. *Journal of Separation Science* **2009**, *32*, 472-478.
- (176) Clicq, D.; Vervoort, N.; Vounckx, R.; Ottevaere, H.; Buijs, J.; Gooijer, C.; Ariese, F.; Baron, G. V.; Desmet, G. *Journal of Chromatography A* **2002**, *979*, 33-42.

- (177) Vankrunkelsven, S.; Clicq, D.; Cabooter, D.; De Malsche, W.; Gardeniers, J. G. E.; Desmet, G. *Journal of Chromatography A* **2006**, *1102*, 96-103.
- (178) Giddings, J. C. K., R. A. *Extracolumn Contributions to Chromatographic Band Broadening*; Marcel Dekker: New York, 1966.
- (179) Mandl, A.; Nicoletti, L.; Lämmerhofer, M.; Lindner, W. *Journal of Chromatography A* **1999**, *858*, 1-11.
- (180) McCalley, D. V.; Neue, U. D. *Journal of Chromatography A* **2008**, *1192*, 225-229.
- (181) Atwood, J. G.; Golay, M. J. E. *Journal of Chromatography A* **1981**, *218*, 97-122.
- (182) Grushka, E. *Analytical Chemistry* **1970**, *42*, 1142-1147.
- (183) Dasgupta, P. K.; Chen, Y.; Serrano, C. A.; Guiochon, G.; Liu, H.; Fairchild, J. N.; Shalliker, R. A. *Analytical Chemistry* **2010**, *82*, 10143-10150.
- (184) Shock, D.; Dennis, G. R.; Guiochon, G.; Dasgupta, P. K.; Shalliker, R. A. *Analytica Chimica Acta* **2011**, *703*, 245-249.
- (185) Wahab, M. F.; Wimalasinghe, R. M.; Wang, Y.; Barhate, C. L.; Patel, D. C.; Armstrong, D. W. *Analytical Chemistry* **2016**, *88*, 8821-8826.
- (186) Regalado, E. L.; Kozlowski, M. C.; Curto, J. M.; Ritter, T.; Campbell, M. G.; Mazzotti, A. R.; Hamper, B. C.; Spilling, C. D.; Mannino, M. P.; Wan, L.; Yu, J.-Q.; Liu, J.; Welch, C. J. *Organic & Biomolecular Chemistry* **2014**, *12*, 2161-2166.
- (187) Lorenz, H.; Seidel-Morgenstern, A. *Angewandte Chemie International Edition* **2014**, *53*, 1218-1250.
- (188) Patel, D. C.; Wahab, M. F.; Armstrong, D. W.; Breitbach, Z. S. *Journal of Chromatography A* **2016**, *1467*, 2-18.
- (189) Robbins, D. W.; Hartwig, J. F. *Science* **2011**, *333*, 1423.
- (190) Zhang, X.; Yin, J.; Yoon, J. *Chemical Reviews* **2014**, *114*, 4918-4959.
- (191) Welch, C. J.; Regalado, E. L. *Journal of Separation Science* **2014**, *37*, 2552-2558.
- (192) Pirzada, Z.; Personick, M.; Biba, M.; Gong, X.; Zhou, L.; Schafer, W.; Roussel, C.; Welch, C. J. *Journal of Chromatography A* **2010**, *1217*, 1134-1138.
- (193) Regalado, E. L.; Welch, C. J. *TrAC Trends in Analytical Chemistry* **2015**, *67*, 74-81.
- (194) Welch, C. J.; Gong, X.; Schafer, W.; Pratt, E. C.; Brkovic, T.; Pirzada, Z.; Cuff, J. F.; Kosjek, B. *Tetrahedron: Asymmetry* **2010**, *21*, 1674-1681.
- (195) Camenzuli, M.; Schoenmakers, P. J. *Analytica Chimica Acta* **2014**, *838*, 93-101.
- (196) Fekete, S.; Schappler, J.; Veuthey, J.-L.; Guillarme, D. *TrAC Trends in Analytical Chemistry* **2014**, *63*, 2-13.
- (197) Ortiz-Bolsico, C.; Torres-Lapasió, J. R.; García-Álvarez-Coque, M. C. *Journal of Chromatography A* **2012**, *1229*, 180-189.

- (198) Isaacman, G.; Wilson, K. R.; Chan, A. W. H.; Worton, D. R.; Kimmel, J. R.; Nah, T.; Hohaus, T.; Gonin, M.; Kroll, J. H.; Worsnop, D. R.; Goldstein, A. H. *Analytical Chemistry* **2012**, *84*, 2335-2342.
- (199) Stoll, D.; Danforth, J.; Zhang, K.; Beck, A. *Journal of Chromatography B* **2016**, *1032*, 51-60.
- (200) Donato, P.; Cacciola, F.; Tranchida, P. Q.; Dugo, P.; Mondello, L. *Mass Spectrometry Reviews* **2012**, *31*, 523-559.
- (201) Mohr, W.; Tang, T.; Sattin, S. R.; Bovee, R. J.; Pearson, A. *Analytical Chemistry* **2014**, *86*, 8514-8520.
- (202) Oliveira, R. V.; Henion, J.; Wickremsinhe, E. *Analytical Chemistry* **2014**, *86*, 1246-1253.
- (203) Horvatovich, P.; Hoekman, B.; Govorukhina, N.; Bischoff, R. *Journal of Separation Science* **2010**, *33*, 1421-1437.
- (204) Sarrut, M.; Corgier, A.; Fekete, S.; Guillarme, D.; Lascoux, D.; Janin-Bussat, M.-C.; Beck, A.; Heinisch, S. *Journal of Chromatography B* **2016**, *1032*, 103-111.
- (205) Wainer, I. W. *Journal of Pharmaceutical and Biomedical Analysis* **1989**, *7*, 1033-1038.
- (206) Miyoshi, Y.; Oyama, T.; Itoh, Y.; Hamase, K. *CHROMATOGRAPHY* **2014**, *35*, 49-57.
- (207) Ianni, F.; Sardella, R.; Lisanti, A.; Gioiello, A.; Cenci Goga, B. T.; Lindner, W.; Natalini, B. *Journal of Pharmaceutical and Biomedical Analysis* **2015**, *116*, 40-46.
- (208) Bester, K.; Vorkamp, K. *Analytical and Bioanalytical Chemistry* **2013**, *405*, 6519-6527.
- (209) Dugo, P.; Russo, M.; Sarò, M.; Carnovale, C.; Bonaccorsi, I.; Mondello, L. *Journal of Separation Science* **2012**, *35*, 1828-1836.
- (210) Liu, Q.; Jiang, X.; Zheng, H.; Su, W.; Chen, X.; Yang, H. *Journal of Separation Science* **2013**, *36*, 3158-3164.
- (211) Ma, S.; Grinberg, N.; Haddad, N.; Rodriguez, S.; Busacca, C. A.; Fandrick, K.; Lee, H.; Song, J. J.; Yee, N.; Krishnamurthy, D.; Senanayake, C. H.; Wang, J.; Trenck, J.; Mendonsa, S.; Claise, P. R.; Gilman, R. J.; Evers, T. H. *Organic Process Research & Development* **2013**, *17*, 806-810.
- (212) Ekborg-Ott, K. H.; Taylor, A.; Armstrong, D. W. *Journal of Agricultural and Food Chemistry* **1997**, *45*, 353-363.
- (213) Armstrong, D. W.; Zukowski, J.; Ercal, N.; Gasper, M. *Journal of Pharmaceutical and Biomedical Analysis* **1993**, *11*, 881-886.
- (214) Armstrong, D. W.; Duncan, J. D.; Lee, S. H. *Amino Acids* **1991**, *1*, 97-106.
- (215) Regalado, E. L.; Schariter, J. A.; Welch, C. J. *Journal of chromatography. A* **2014**, *1363*, 200-206.

- (216) Koga, R.; Miyoshi, Y.; Sato, Y.; Mita, M.; Konno, R.; Lindner, W.; Hamase, K. *Journal of Chromatography A* **2016**, *1467*, 312-317.
- (217) Hamase, K.; Miyoshi, Y.; Ueno, K.; Han, H.; Hirano, J.; Morikawa, A.; Mita, M.; Kaneko, T.; Lindner, W.; Zaitso, K. *Journal of Chromatography A* **2010**, *1217*, 1056-1062.
- (218) Venkatramani, C. J.; Al-Sayah, M.; Li, G.; Goel, M.; Girotti, J.; Zang, L.; Wigman, L.; Yehl, P.; Chetwyn, N. *Talanta* **2016**, *148*, 548-555.
- (219) Welsch, T.; Schmidtkunz, C.; Müller, B.; Meier, F.; Chlup, M.; Köhne, A.; Lämmerhofer, M.; Lindner, W. *Analytical and Bioanalytical Chemistry* **2007**, *388*, 1717-1724.
- (220) Venkatramani, C. J.; Wigman, L.; Mistry, K.; Chetwyn, N. *Journal of Separation Science* **2012**, *35*, 1748-1754.
- (221) Stevenson, P. G.; Tarafder, A.; Guiochon, G. *Journal of Chromatography A* **2012**, *1220*, 175-178.
- (222) Cortes, H. J.; Campbell, R. M.; Himes, R. P.; Pfeiffer, C. D. *Journal of Microcolumn Separations* **1992**, *4*, 239-244.
- (223) Moaddel, R.; Venkata, S. L. V.; Tanga, M. J.; Bupp, J. E.; Green, C. E.; Iyer, L.; Furimsky, A.; Goldberg, M. E.; Torjman, M. C.; Wainer, I. W. *Talanta* **2010**, *82*, 1892-1904.
- (224) Regalado, E. L.; Sherer, E. C.; Green, M. D.; Hendersonl, D. W.; Thomas Williamson, R.; Joyce, L. A.; Welch, C. J. *Chirality* **2014**, *26*, 95-101.
- (225) Murphy, R. E.; Schure, M. R.; Foley, J. P. *Analytical Chemistry* **1998**, *70*, 1585-1594.
- (226) Potts, L. W.; Stoll, D. R.; Li, X.; Carr, P. W. *Journal of Chromatography A* **2010**, *1217*, 5700-5709.
- (227) Thekkudan, D. F.; Rutan, S. C.; Carr, P. W. *Journal of Chromatography A* **2010**, *1217*, 4313-4327.
- (228) Filgueira, M. R.; Huang, Y.; Witt, K.; Castells, C.; Carr, P. W. *Analytical Chemistry* **2011**, *83*, 9531-9539.
- (229) Jeong, L. N.; Sajulga, R.; Forte, S. G.; Stoll, D. R.; Rutan, S. C. *Journal of Chromatography A* **2016**, *1457*, 41-49.
- (230) Stoll, D. R.; O'Neill, K.; Harnes, D. C. *Journal of Chromatography A* **2015**, *1383*, 25-34.
- (231) Stoll, D. R. *Bioanalysis* **2015**, *7*, 3125-3142.
- (232) Groskreutz, S. R.; Swenson, M. M.; Secor, L. B.; Stoll, D. R. *Journal of Chromatography A* **2012**, *1228*, 31-40.
- (233) Larson, E. D.; Groskreutz, S. R.; Harnes, D. C.; Gibbs-Hall, I. C.; Trudo, S. P.; Allen, R. C.; Rutan, S. C.; Stoll, D. R. *Analytical and Bioanalytical Chemistry* **2013**, *405*, 4639-4653.

BIOGRAPHICAL INFORMATION

Chandan Laxman Barhate obtained his Master of Technology (Integrated) degree in Biotechnology from D.Y. Patil University at Pune, India in 2009. His master's thesis work was based on the isolation and structural determination of biologically active compounds from marine bacteria and fungi under the guidance of Dr. Lisette D'Souza at the National Institute of Oceanography (Goa, India). After a brief stint at the University of South Florida, he joined Prof. Daniel W. Armstrong's research group at the University of Texas at Arlington where he conducted research on ultrafast liquid and sub/supercritical fluid chromatography. He has presented his work in Pittcon, HPLC and received California Society of Separation Sciences (CASSS) travel grant for attending the HPLC 2016 conference. Chandan is married with Priyanka who is an IT professional.